

In compliance with the
Canadian Privacy Legislation
some supporting forms
may have been removed from
this dissertation.

While these forms may be included
in the document page count,
their removal does not represent
any loss of content from the dissertation.

**Intracaldera geology of the Ilopango Caldera,
El Salvador, Central America**

By

Crystal P. MANN

**Department of Earth and Planetary Sciences
McGill University
Montréal, Québec, Canada**

March 2003

**A thesis submitted to the Faculty of Graduate Studies and Research in
partial fulfilment of the requirements of the degree of
Master of Science**

© C.P. Mann 2003



National Library
of Canada

Bibliothèque nationale
du Canada

Acquisitions and
Bibliographic Services

Acquisitons et
services bibliographiques

395 Wellington Street
Ottawa ON K1A 0N4
Canada

395, rue Wellington
Ottawa ON K1A 0N4
Canada

Your file *Votre référence*
ISBN: 0-612-88259-4
Our file *Notre référence*
ISBN: 0-612-88259-4

The author has granted a non-exclusive licence allowing the National Library of Canada to reproduce, loan, distribute or sell copies of this thesis in microform, paper or electronic formats.

L'auteur a accordé une licence non exclusive permettant à la Bibliothèque nationale du Canada de reproduire, prêter, distribuer ou vendre des copies de cette thèse sous la forme de microfiche/film, de reproduction sur papier ou sur format électronique.

The author retains ownership of the copyright in this thesis. Neither the thesis nor substantial extracts from it may be printed or otherwise reproduced without the author's permission.

L'auteur conserve la propriété du droit d'auteur qui protège cette thèse. Ni la thèse ni des extraits substantiels de celle-ci ne doivent être imprimés ou autrement reproduits sans son autorisation.

Canada

Abstract

Calderas are surface expressions of long-lived magmatic systems, which typically erupt voluminous amounts of pyroclastic material with devastating consequences both globally and locally. These depressions are often filled with water, thus increasing the probability of explosive eruption. Understanding the eruption mechanisms and the role of water can aid scientists in mitigating volcanic disasters. Ilopango Caldera, which is part of the Central American volcanic arc in El Salvador, is a lake-filled caldera located approximately 10 km east of the capital city of San Salvador. Ilopango has an eventful history of eruption; the most recent pyroclastic eruption, known as the Tierra Blanca Joven (TBJ), took place ~1600 years ago. The eruption ejected 18 km³ DRE (dense rock equivalent) of pyroclastic debris and devastated the Early Classic Mayan civilization. In 1880 a lava dome was erupted into the center of the caldera lake. The aim of this study is to understand the nature of Ilopango eruptions, the magmatic evolution of Ilopango through time and attempt to place Ilopango into a regional context. Field relationships, thorough unit descriptions and ¹⁴C age determinations are used to establish a portion of the intracaldera stratigraphy and the depositional environment. Physical volcanology and glass geochemistry, combined with secondary electron imaging and textures indicative of cooling, are used to establish the explosive to effusive emplacement of the San Agustín Block unit. Whole-rock geochemistry, combined with Ar-Ar age determinations, are then used to establish the magmatic evolution of Ilopango through time. I conclude that the intracaldera stratigraphy is mostly subaqueously emplaced

and that the caldera was occupied by a lake > 53,000 years ago during formation of the San Agustín Block unit. The eruption which formed the San Agustín Block unit began with a phreatomagmatic phase and progressed to a more degassed phase, spalling pumices from the quenched carapace of the lava dome. The magmatic evolution of Ilopango is not a progressive magmatic process related to a time factor, but rather reflected by a reservoir that experiences replenishment of a more mafic composition causing fluctuations in magma composition over time. Ilopango is less evolved than other Central American silicic centers such as Atitlán, Amatitlán and Zúñil, but is similar in composition to Santa María, Santiaguito and Acantenango.

Résumé

Les caldeiras sont l'expression superficielle des systèmes magmatiques rémanents, qui sont souvent à l'origine de volumineuses éruptions de matériel pyroclastique aux conséquences dévastatrices tant localement qu'à échelle globale. Ces depressions sont souvent remplies d'eau, ce qui accroît la probabilité d'éruption explosive. La compréhension des mécanismes éruptifs et du rôle de l'eau peut aider les scientifiques à réduire les désastres volcaniques. La caldeira d'Ilopango, dans l'arc volcanique d'Amérique Centrale, au Salvador, est une caldeira remplie par un lac située à environ 10 km à l'Est de la capitale San Salvador. Ilopango a une histoire éruptive complexe ; l'éruption pyroclastique la plus récente, l'éruption de Tierra Blanca Joven (TBJ), a eu lieu il y a environ 1600 ans. Cette éruption a produit 18 km³ DRE (équivalent roche dense) de débris pyroclastiques et a détruit la civilisation Maya Classique Précoce. En 1880 un dôme de lave s'est mis en place au centre du lac caldeirique. Le but de cette étude est de comprendre la nature des éruptions d'Ilopango et l'évolution magmatique d'Ilopango au cours du temps, et d'essayer de replacer Ilopango dans un contexte régional. Les relations de terrain, des descriptions détaillées des unités et des datations au ¹⁴C permettent de décrire une partie de la stratigraphie intra-caldeirique et le contexte de dépôt. La volcanologie physique et l'observation de textures de refroidissement, combinées à la géochimie des verres et à une observation d'images de microscopie électronique indiquent une mise en place explosive puis effusive de l'unité de San Agustín Block. La géochimie sur roche totale, combinée avec des datations Ar-Ar est ensuite utilisée pour décrire l'évolution magmatique d'Ilopango au cours du temps. Nous en concluons que la stratigraphie

intra-caldeirique est essentiellement subaquatique et que la caldeira était occupée par un lac il y a plus de 53000 ans lors de la formation de l'unité de San Agustín Block. L'éruption qui a formé l'unité de San Agustín Block a débuté par une phase phréatomagmatique et a évolué vers une phase plus dégazée, arrachant des ponces à la carapace vitrifiée du dôme de lave. L'évolution magmatique d'Ilopango n'est pas un processus progressif lié à un phénomène temporel, mais correspond plutôt à la réalimentation d'un réservoir en magma plus mafique, à l'origine de fluctuations dans la composition du magma au cours du temps. Ilopango est moins évolué que d'autres centres siliciques d'Amérique Centrale comme Atitlán, Amatitlán et Zuñil, mais a une composition similaire à Santa María, Santiaguito et Acantenango.

Preface

This thesis consists of 4 chapters. The second chapter has been accepted and is scheduled to be published in the Geological Society of America Special Paper concerning Natural Hazards in El Salvador, edited by W.I. Rose, J.J. Bommer, D.L. López, M.J. Carr, and J.J. Major. The third chapter is also in manuscript format, and is intended for submission to a refereed journal. Both manuscripts have been integrated as chapters formatted to the general layout of the thesis.

The following is excerpted from Guidelines for Thesis Preparation, Faculty of Graduate Studies and Research, McGill University:

“Candidates have the option of including, as part of the thesis, the text of one or more papers submitted, or to be submitted, for publication, or the clearly-duplicated text (not the reprints) of one or more published papers. These texts must conform to the "Guidelines for Thesis Preparation" with respect to font size, line spacing and margin sizes and must be bound together as an integral part of the thesis.

The thesis must be more than a collection of manuscripts. All components must be integrated into a cohesive unit with a logical progression from one chapter to the next. In order to ensure that the thesis has continuity, connecting texts that provide logical bridges preceding and following each manuscript are mandatory.

The thesis must conform to all other requirements of the "Guidelines for Thesis Preparation" in addition to the manuscripts. The thesis must include the following: a table of contents, a brief abstract in both English and French, an introduction which clearly states the rationale and objectives of the research, a comprehensive review of the literature (in addition to that covered in the introduction to each paper), a final conclusion and summary, and a thorough bibliography.

As manuscripts for publication are frequently very concise documents, where appropriate, additional material must be provided (e.g., in appendices) in sufficient detail to allow a clear and precise judgement to be made of the importance and originality of the research reported in the thesis.

In general, when co-authored papers are included in a thesis the candidate must have made a substantial contribution to all papers included in the thesis. In addition, the candidate is required to make an explicit statement in the thesis as to who contributed to such work and to what extent. This statement should appear in a single section entitled "Contributions of Authors" as a preface to the thesis. The supervisor must attest to the accuracy of this statement at the doctoral oral defence. Since the task of the examiners is made more difficult in these cases, it is in the candidate's interest to clearly specify the responsibilities of all the authors of the co-authored papers."

Fieldwork, sampling, petrography, sieving of volcanic ash, porosity experiments, scanning electron imaging, preparation of electron microprobe disks, partial electron microprobe analyses and the grinding and crushing for XRF whole-rock analyses were performed by the author. XRF whole-rock analyses were performed by T. Ahmedali and G. Keating at the Department of Earth and Planetary Sciences, McGill University. $^{40}\text{Ar}/^{39}\text{Ar}$ age determinations were performed by A. Calvert of the United States Geological Survey, Menlo Park, California. ^{14}C age determinations were performed at Beta Analytic and the United States Geological Survey, Eastern Earth Surface Process Team, and were facilitated by J. Vallance of the United States Geological Survey, Vancouver, Washington.

Contributions of Authors

Funding for this project was provided by an NSERC operating grant to Dr. J. Stix, NSF Grant EAR-9903291 to J. Vallance and a CIDA Innovative Research Award to C. P. Mann. The thesis author, C. P. Mann, is responsible for all new scientific data on the intracaldera deposits, pyroclastic units and lavas of the Ilopango Caldera. Dr. J. Stix acted as research supervisor and Dr. J. Vallance acted as co-supervisor, advising the author during the critical evaluation of data and logical

development of the scientific concepts expressed in the thesis. Mathieu Richer provided field support during the field work component.

Thesis Format

The thesis is comprised of four chapters. The first chapter offers a general introduction to calderas, caldera formation, background on problems addressed in the thesis and previous studies conducted at Ilopango. The second chapter develops the intracaldera stratigraphy and presents evidence for subaqueous eruption and emplacement of the San Agustín Block unit. The third chapter addresses the magmatic and chemical evolution of the caldera through time and compares Ilopango to other Central American silicic centers. The fourth chapter contains overall conclusions.

Acknowledgements

This is most likely the most important section of this entire thesis. Without a lot of help from a lot of people this study wouldn't have been possible. First and foremost I thank the all the students in the Earth and Planetary Sciences at McGill for their support and interest in my work. To the graduate students, whom I now consider my friends and colleagues, I consider myself lucky to have been part of this group and look forward to the future. I thank my great roommate, Annick Chouinard, for not turning the coffee grinder on until noon as I was putting the finishing touches on my thesis. I thank Oliver Schatz, for just being Oliver and being with me "every step" of the way. I thank Don Francis for always helping me to look at things from the "other" side, his help is greatly appreciated. Many, many thanks to Mathieu Richer for all his hard work in the field and incredible patience. I thank Abby Peterson for all her help with last minute tables and diagrams. I thank Guillaume Girard for his help with translation of the abstract into French. Many thanks to George Panagiotidis for speedy thin sections, to Glenna Keating for infinite patience and great explanations of XRF procedures and Shi Lang for his help with the microprobe. From the bottom of my heart I thank our computer expert, Brigitte Dionne, for her ability to solve the problem of the temperamental computers in 129. I also thank Anne Kosowski and Carol Matthews for help with unravelling the confusing McGill procedures. I thank Andy Calvert for helping me understand Ar-Ar age determinations and openness to questions. I thank Mike Carr for his willingness to share data.

I thank my supervisor John Stix for his enthusiasm for volcanology, support as I developed my project and complete tolerance. I thank my co-supervisor Jim Vallance for his ideas and interest in Ilopango. I thank the people of the Amigos del Lago de Ilopango for all their help and continuing support for this project, especially Fred Thill and Jeanette Monterrosa for continued updates. I thank Carlos Pullinger for escapades into the field and look forward to more. Lastly, I thank my MOM for all her patience and understanding and my friend Cesar Escobar for his support and help with my black lab, Guy.

Table of Contents

<i>Abstract</i>	<i>ii</i>
<i>Résumé</i>	<i>iv</i>
<i>Preface</i>	<i>vi</i>
<i>Acknowledgements</i>	<i>x</i>
<i>Table of Contents</i>	<i>xii</i>
<i>List of Figures</i>	<i>xv</i>
<i>List of Tables</i>	<i>xvii</i>
<i>List of Appendices</i>	<i>xviii</i>
Chapter 1	
General Introduction	
<i>General Statement</i>	<i>1</i>
<i>Previous Studies of Ilopango</i>	<i>4</i>
<i>Objectives of this Thesis</i>	<i>6</i>
<i>References</i>	<i>8</i>
Chapter 2	
Subaqueous intracaldera volcanism, Ilopango Caldera, El Salvador, Central America	
<i>Abstract</i>	<i>13</i>
<i>Resumen</i>	<i>15</i>
<i>Keywords</i>	<i>16</i>
<i>Introduction</i>	<i>17</i>
<i>Geological setting</i>	<i>22</i>
Regional geology	22
Ilopango Caldera and the intracaldera setting	22
Eruptive history of Ilopango	23
<i>Sample Preparation and Analytical Techniques</i>	<i>23</i>
<i>Observations and results</i>	<i>24</i>
Terminology	24
Field description, petrology and composition of intracaldera units	24
<i>Discussion</i>	<i>38</i>

Intracaldera framework.....	38
Depositional setting.....	38
Subaqueous eruption and emplacement of the San Agustín Block Unit.....	41
Model of eruption and emplacement of the San Agustín Block Unit.....	48
<i>Conclusions.....</i>	<i>50</i>
<i>Acknowledgements.....</i>	<i>51</i>
<i>References.....</i>	<i>52</i>
<i>Appendix 2.1.....</i>	<i>60</i>
 <i>Bridge to Chapter 3.....</i>	 <i>61</i>
 Chapter 3	
Magmatic evolution of the Ilopango Caldera, El Salvador, Central America	
<i>Abstract.....</i>	<i>62</i>
<i>Keywords.....</i>	<i>63</i>
<i>Introduction.....</i>	<i>63</i>
<i>Previous Work.....</i>	<i>67</i>
<i>Sample Preparation and Analytical Techniques.....</i>	<i>68</i>
<i>Rock Descriptions.....</i>	<i>72</i>
Lava domes and intracaldera lavas.....	72
Pyroclastic units.....	93
<i>Results.....</i>	<i>96</i>
Geochronology.....	96
Major and Trace Element Data.....	96
Interpretation of the data.....	105
<i>Discussion.....</i>	<i>114</i>
Comparison of Ilopango with other Central American silicic centers.....	118
<i>Conclusions.....</i>	<i>123</i>
<i>Acknowledgements.....</i>	<i>124</i>
<i>References.....</i>	<i>125</i>
<i>Appendix 3.1.....</i>	<i>132</i>
<i>Appendix 3.2.....</i>	<i>133</i>
<i>Appendix 3.3.....</i>	<i>134</i>
<i>Appendix 3.4.....</i>	<i>135</i>

Chapter 4

Conclusions.....137

List of Figures

Chapter 2

Figure 2.1	Location map of the Central American volcanic arc in El Salvador.....	18
Figure 2.2	Intracaldera topographic map of Ilopango showing area of study.....	21
Figure 2.3	Schematic stratigraphic section of Ilopango intracaldera units.....	25
Figure 2.4	Whole-rock and glass compositions from selected units erupted from Ilopango caldera on a SiO_2 vs. $\text{Na}_2\text{O} + \text{K}_2\text{O}$ classification diagram.....	28
Figure 2.5	Examples of sedimentary structures in the Lacustrine Unit.....	30
Figure 2.6	Contact between the Lacustrine Unit and the San Agustín Block Unit.....	32
Figure 2.7	Secondary electron imaging (SEI) of the Fine Ash facies grain morphology.....	33
Figure 2.8	Pumice Breccia facies grain morphology and cooling textures.....	35
Figure 2.9	Glass analyses of major elements for two intracaldera units and TB2.....	42
Figure 2.10	Schematic diagram of model for the San Agustín Block Unit eruption and emplacement.....	49

Chapter 3

Figure 3.1	Map of Central America and the Central American volcanic arc.....	64
Figure 3.2	Intracaldera topographic map of Ilopango showing the area of study.....	72
Figure 3.3	Photomicrograph of plagioclase phenocrysts from the northeast lava dome demonstrating LAC texture.....	75
Figure 3.4	Photomicrograph of phenocryst textures represented by the northeast lava dome.....	76
Figure 3.5	Photographs of the Northwest Lava Dome.....	79
Figure 3.6	Photograph of the South Lava Domes.....	82
Figure 3.7	Photomicrographs of phenocryst textures found in Cerro Cuyultepe.....	85
Figure 3.8	Photographs of Cerro Los Patos.....	87
Figure 3.9	Photographs of Islas Quemadas.....	88
Figure 3.10	Photomicrographs of phenocryst textures found in the Islas Quemadas mafic enclave and the TB4 pyroclastic unit.....	90

Figure 3.11	Whole-rock compositions from selected lavas and pyroclastic units erupted from Ilopango caldera on a SiO_2 vs. $\text{Na}_2\text{O} + \text{K}_2\text{O}$ classification diagram.....	96
Figure 3.12	AFM diagram of selected lavas and pyroclastic units erupted from the Ilopango caldera demonstrating a calc-alkaline trend.....	98
Figure 3.13	Major element Harker variation diagrams of selected Ilopango lavas and pyroclastic units.....	99
Figure 3.14	Minor element Harker variation diagrams of selected Ilopango lavas and pyroclastic units.....	103
Figure 3.15	Compiled modal phenocryst percentages observed in selected Ilopango lavas and pyroclastic units.....	106
Figure 3.16	Variation diagrams compared to modal phenocryst percentages (Fig. 15).....	107
Figure 3.17	Variation diagrams testing plagioclase fractionation.....	109
Figure 3.18	Hypothetical model for evolution of the mafic phases based on the modal mineralogy and the normative mineralogy using Fe vs. Mg cation%.....	111
Figure 3.19	Ilopango lavas and pyroclastic units represented on a Time vs. SiO_2 variation diagram.....	115
Figure 3.20	Major element Harker variation diagrams representing major silicic centers in Central America.....	118
Figure 3.21	Trace element Harker variation diagrams representing major silicic centers in Central America.....	120

List of Tables

Chapter 2

Table 2.1.	Electron Microprobe data of glass compositions.....	27
Table 2.2.	Whole - rock geochemistry of the Pumice Breccia from the San Agustín Block unit.....	37

Chapter 3

Table 3.1	Whole - rock geochemistry replicates.....	69
Table 3.2	Whole - rock geochemistry of Ilopango lavas and pyroclastic units.....	100
Table 3.3	Whole - rock geochemistry of Ilopango lavas and pyroclastic units.....	101

List of Appendices

Chapter 2

Appendix 2.1 Vesicularity calculations.....	60
---	----

Chapter 3

Appendix 3.1 Ilopango Dome $^{40}\text{Ar}/^{39}\text{Ar}$ Summary.....	131
Appendix 3.2 Whole-rock geochemistry from J. Vallance.....	132
Appendix 3.3 Mesonorm calculation of mineral phases.....	133
Appendix 3.4 Rayleigh fractionation calculations.....	134

Chapter 1

General Introduction

General Statement

Caldera eruptions have proven to be some of the most catastrophic eruptions in Earth's history. Calderas are typically a manifestation of long-lived silicic systems, which erupt repeatedly producing voluminous amounts of pyroclastic material. Understanding the mechanisms which influence eruptions, the dynamics between the magmatic material and surrounding environment and pre-eruption warning signs, can aid scientists in predicting these types of volcanic eruptions and their effects, both globally and locally.

Calderas are large volcanic depressions formed by the collapse of overlying rock due to evacuation of a magma reservoir (Williams, 1941). Based on various caldera systems, Smith and Bailey (1968) have defined a caldera cycle, which describes the general evolution of a caldera system. The caldera cycle starts with doming of the overlying rock due to increasing pressure within the magma reservoir and subsequently the generation of ring fractures. The ring fractures provide the underlying magma with a simple path to the surface which leads to the next step a caldera-forming eruption. Once the pathway has been established the magma migrates up the faults, erupting violently at the surface. As the magma is erupted the overlying rock subsides and the caldera depression forms. Typically, the size of the resulting depression is used as a proxy for the size of the reservoir (Lipman, 1997). After the depression has formed, erosion and landsliding of the caldera wall takes

place, and post-caldera volcanism in the form of lava domes typically occurs. The next stage may involve resurgent doming and major ring-fracture volcanism.

Mechanisms that trigger such eruptions have been attributed to a buildup of pressure in a closed-system magma reservoir (Cox, 1979). One such mechanism is crystal fractionation. As crystal fractionation takes place, the concentration of water in the melt increases and subsequently causes overpressure within the magma reservoir (Tait *et al.*, 1989). Another mechanism is the influx of new magma into the magma reservoir, termed magma replenishment (Eichelberger, 1975). The new magma is typically of a less evolved composition, and when this more mafic magma intrudes the system, conditions within the magma reservoir change, the temperature rises and the P_{H_2O} increases. Both crystal fractionation and magma replenishment processes can lead to caldera forming eruptions, but these two processes can be distinguished based on rock textures, phenocryst textures and crystal fractionation trends.

The ratio of external water (e.g. groundwater, lake water, meteoric water, etc.) to magma surface area plays a key role in determining the explosivity of volcanic eruptions (Wohletz, 1983). With a water/magma ratio of ~ 0.3 the explosivity of volcanic eruptions increases compared to a volcanic setting such as Hawaii (water/magma ~ 1) where basaltic magma generally flows into the Pacific Ocean fairly quietly. Studies have shown that phreatomagmatic eruptions produce glass shards which display a distinct glass morphology which can be distinguished from glass shards produced by a magmatic eruption (Heiken and Wohletz, 1985). In many caldera systems, the depression becomes filled with water, thus enhancing the

explosivity of subsequent volcanic eruptions. Therefore, understanding the role of external water in caldera systems is important to understanding their evolution and their associated hazards.

Caldera-forming eruptions are catastrophic events. Caldera eruptions are frequently associated with evacuation of tens of cubic kilometers of pyroclastic material, leaving behind depressions of similar size. Hazards associated with these eruptions include ash fallout which blankets both proximal and distal sites, pyroclastic flows and the emission of volcanic gases. These eruptions also have been associated with climate change and the devastation of civilizations throughout history (Free and Angel, 2002; Roscoe, 2001; Espindola *et al.*, 2000; Hildreth and Fierstein, 2000; Stothers, 2000; Knesel and Davidson, 1997; Wilson *et al.*, 1995; Krueger *et al.*, 1990; Woolley, 1983; Sheets, 1979). Ilopango Caldera is among these catastrophic Quaternary eruptions, yet has received little attention.

The Ilopango Caldera is located 10 km east of San Salvador, the capital city of El Salvador. It is a lake filled caldera which has experienced at least four voluminous pyroclastic eruptions in the last 57,000 years. The most recent large event was a pyroclastic eruption, termed the Tierra Blanca Joven (TBJ), which took place approximately 1600 years ago, devastating the Early Classic Mayan civilization (Hart, 1981, Dull *et al.*, 2001). Olivine crystals and mafic bands observed in the pumices of this eruption and mafic enclaves from a lava dome erupted in the center of the lake in AD 1880 are suggestive of mafic replenishment and mingling/mixing processes (Hart, 1981; Richer *et al.* in press). Deposit characteristics of the TBJ eruption indicate that part of the eruption was phreatomagmatic in nature, (Hart,

1981; Vallance, personal communication, 2001) suggesting that a lake was present at that time. The present study investigates the evolution of this silicic caldera center over time and attempts to place it in a regional context.

Previous Studies of Ilopango

Theories of the formation of Lake Ilopango, also known as Lake Cojutepec, have been evolving for over a century, although the local people hold it with superstitious reverence. Four voluminous eruptions are known to be associated with the Ilopango Caldera. The four eruptions have been informally named, from youngest to oldest, Tierra Blanca Joven (TBJ), Tierra Blanca 2 (TB2), Tierra Blanca 3 (TB3) and Tierra Blanca 4 (TB4). The two events that Ilopango is best known for are the eruption of the TBJ unit which devastated the Early Classic Maya 1600 years ago, and dome growth of the Islas Quemadas in 1880.

The first descriptive account of Lake Ilopango came from archeologists. E.G. Squier (1850) believed that the depression occupied by the lake formed by collapse after up - arching of surrounding rock. Dollfus and Mont-Serrat (1868) believed that a river, blocked by volcanic pyroclasts, backed up and formed the lake. Montessus de Ballore (1884) disagreed and thought the lake depression was the result of a huge explosion. Lardé (1924) and Lothrop (1927), who were interested in the Mayan artifacts below the TBJ horizon, were the first to realize that Ilopango was the source of the TBJ unit which they had informally named Panchimalco. Based on outward dipping basement rock, they believed the Panchimalco tephra was produced by an explosion from a large volcano, which left behind a scoured-out basin which

subsequently filled with water. Sapper (1925) was the first to suggest the lake lies in a collapse basin. Williams and Meyer-Abich (1955) produced the first geologic report of the region and suggested that Lake Ilopango occupied a deep graben which had formed at the end of the Pliocene or beginning of the Pleistocene. They suggested that after the initial collapse there were two caldera collapses, each preceded by volcanic activity.

Recognition of the Tierra Blanca units has aided in developing a stratigraphy for the volcano. Weyl (1955) was the first to recognize the caldera of Ilopango to be the source of all the Tierra Blanca units. A team of German geologists, in collaboration with the Ministry of Public Works of El Salvador, produced a geologic map of El Salvador (Weber and Weisemann, 1978), restricting the Tierra Blanca units to the Holocene period. While doing a development assessment of the capital city, San Salvador, Schmidt-Thomé (1975) recognized black soil horizons in the Tierra Blanca tephra and suggested the mapped Tierra Blanca unit encompasses products of more than one event separated by time. Sheets (1976) contributed a ^{14}C date of A.D. 260 ± 114 on a piece of charred wood in the uppermost Tierra Blanca unit, while Steen-McIntyre (1976) did preliminary petrographic and grain size work on the same unit. Hart and Steen-McIntyre (1978) and Hart (1981) studied the TBJ eruption in detail, determining that Ilopango was the source and had erupted $\sim 18 \text{ km}^3$ DRE (dense rock equivalent) of volcanic material from a stratified magma chamber. During geothermal exploration projects, CEL (1992) refined the stratigraphy and defined three additional units stratigraphically below TBJ, informally naming them TB2, TB3 and TB4. These eruptions have been temporally constrained to the last

56.9 +2.8/-2.1 ka (Rose *et al.*, 1999). Dull *et al.* (2001) reported AMS ages on new samples of wood found in the TBJ and reassessed the previously dated samples to determine an updated age of A.D. 420 ± 20 for this unit.

In 1880, a lava dome named Islas Quemadas was erupted in the center of the caldera lake. The state geologist of El Salvador, W.A. Goodyear (1880), witnessed the birth of the Islas Quemadas and wrote in detail about the erupting volcano and the associated seismic activity. M.J. Laferrière also witnessed the birth of Islas Quemadas and supports the story of Goodyear (Anonymous, 1880). Montessus de Ballore (1884) witnessed the birth of Islas Quemadas and was the first to comment on the mafic enclaves or “concretions within the rhyolite lava.” Hague and Iddings (1886) described rocks sampled in El Salvador by Goodyear, concluding the Islas Quemadas rock is a vesicular, hornblende-pyroxene andesite. Weyl (1955) concluded that Islas Quemadas rock is a hornblende-hypersthene dacite, while Williams and Meyer-Abich (1955) concluded the rock is a hornblende dacite with olivine-rich clots torn from the roof, conduit or reservoir by the rising dacite magma. Golombeck and Carr (1978) correlated seismic shocks and volcanic activity associated with the 1879-1880 activity with solid-earth tides.

Objectives of this Thesis

This study comprises a detailed investigation of the intracaldera deposits and lava domes within the Ilopango Caldera. Data collected from the intracaldera pyroclastic deposits include petrography, pumice porosity values, scanning electron imaging (SEI), major element glass compositions and ¹⁴C age determinations. Data

collected from the intracaldera lava domes include petrography, XRF whole-rock analyses and $^{40}\text{Ar}/^{39}\text{Ar}$ age determinations. There are two objectives to this study. The first objective was to establish a working intracaldera stratigraphy and establish the subaqueous eruption and emplacement mechanisms of specific intracaldera units, with particular reference to the San Agustín Block unit. The second objective was to use data collected from the intracaldera domes to establish the magmatic evolution of Ilopango through time and then to compare Ilopango to other Central American silicic centers on a regional scale.

References

- Anonymous, 1880, A lacustrine volcano: *Nature*, v. 22, p. 129.
- CEL, 1992, Desarrollo de los recursos geotérmicos del area centro-occidental de El Salvador. Prefactibilidad geotérmica del area de Coatepeque: Comisión Ejecutiva Hidroelectrica del Rio Lempa Reconocimiento Geotérmico, Internal Report, p. 1-104.
- Cox, K.G., Bell, J.D., and Pankhurst, R.J., 1979, The interpretation of igneous rocks: Beecles and London, London, 450 p.
- Dollfus, A., and de Montserrat, E., 1868, Voyage geologique dans les republicues de Guatemala et de Salvador; France, Mission Scientifique au Mexique et dans l’Amerique centrale, *Geologie: France*, 539 p.
- Dull, R., Southon, J., and Sheets, P., 2001, Volcanism, ecology and culture: a reassessment of the Volcán Ilopango TBJ eruption in the southern Maya realm: *Latin American Antiquity*, v. 12, p. 25-44.
- Eichelberger, J. C., 1975, Origin of andesite and dacite: evidence of mixing at Glass Mountain in California and at other circum-Pacific volcanoes: *Geological Society of America Bulletin*: v. 86, p. 1381–1391.
- Espindola, J.M., Macias, J.L., Tilling, R.I., and Sheridan, M.F., 2000, Volcanic history of El Chichon Volcano (Chiapas, Mexico) during the Holocene, and its impact on human activity: *Bulletin of Volcanology*, v. 62, n. 2, p. 90-104.

- Free, M., and Angell, J.K., 2002, Effect of volcanoes on the vertical temperature profile in radiosonde data: *Journal of Geophysical Research D, Atmospheres* 107, n. 9-10, p. 16-11.
- Golombek, M.P., and Carr, M.J., 1978, Tidal triggering of seismic and volcanic phenomena during the 1879-1880 eruption of Islas Quemadas volcano in El Salvador, Central America: *Journal of Volcanology and Geothermal Research*, v. 3, p. 299-307.
- Goodyear, W.A., 1880, Earthquake and volcanic phenomena. December 1879 and January 1880 in the Republic of Salvador, Central America, *Star and Herald*, p. 56.
- Hart, W.J.E, 1981, The Panchimalco tephra, El Salvador, Central America [unpublished M.Sc. thesis]: Rutgers University, New Brunswick, New Jersey.
- Hart, W.J., and Steen-McIntyre, V, 1983, Tierra Blanca Joven tephra from the AD 260 eruption of Ilopango Caldera: *in* Sheets, P.D. ed., *Archeology and volcanism in Central America; the Zapotitan Valley of El Salvador*, University of Texas Press, Austin, p. 14-34.
- Hauge, A, and Iddings, J.P., 1886, Notes on the volcanic rocks of the republic of Salvador, Central America: *American Journal of Science*, v. 32, p. 26-31.
- Heiken, G., and Wohletz, K., 1985, *Volcanic ash*: Berkeley, University of California Press, 246 p.
- Hildreth, W., Fierstein, J., 2000, Katmai volcanic cluster and the great eruption of 1912: *Bulletin of the Geological Society of America*, v. 112, n. 10, p. 1594-1620.

- Knesel, K.M. and Davidson, J.P., 1997, The origin and evolution of large-volume silicic magma systems: Long Valley Caldera: *International Geology Review*, v. 39, n. 11, p. 1033-1052.
- Krueger, A.J., Walter, L.S., Schnetzler, C.C., and Doiron, S.D., 1990, TOMS measurements of the sulfur dioxide emitted during the 1985 Nevado del Ruiz eruptions: *Journal of Volcanology and Geothermal Research*, v. 41, n. 1-4, p. 7-15.
- Lipman, P.W., 1997, Subsidence of ash-flow calderas: Relationship to caldera size and magma-chamber geometry: *Bulletin of Volcanology*, v. 49, o, 198-218.
- Larde, J., 1924, *Geologia general de Centro America y especial de El Salvador*: San Salvador, 83 p.
- Lothrop, S.K., 1927, Pottery types and their sequence in El Salvador: *Indian Notes and Monographs*, v. 1, p. 165-220.
- Montessus de Ballore, F., 1884, *Tremblores y erupciones volcánicas en Centro-América con un apendice meteorológico*: Imprenta Del Doctor Francisco Sagrini, San Salvador, 246 p.
- Richer, M., Mann, C., and Stix, J., *in press*, Mafic magma injection triggers eruption at Ilopango Caldera, El Salvador, Central America, in Rose, W.I., Bommer, J.J., López, D.L, Carr, M.J., and Major, J.J., eds., *Natural Hazards in El Salvador*: Geological Society of America Special Paper.
- Roscoe, H.K, 2001, The risk of large volcanic eruption and the impact of this risk on future ozone depletion: *Natural Hazards*, v. 23, n. 2-3, p. 231-246.

- Rose, W.I., Conway, F.M., Pullinger, C.R., Deino, A., and McIntosh, W.C., 1999, An improved age framework for late Quaternary silicic eruptions in northern Central America: *Bulletin of Volcanology*, v. 61, p. 106-120.
- Sapper, K., 1925, *Los volcanes de la America Central: Estudios sobre America y Espana*, Extraserie, 116 p.
- Schmidt-Thóme, M., 1975, The geology in the San Salvador area (El Salvador, Central America), a basis for city development and planning: *Geologisches Jahrbuch, Reihe B, Regionale Geologie Ausland*, n. 13, p. 207-225.
- Sheets, P.D., 1979, Environmental and cultural effects of the Ilopango eruption in Central America, *in* Sheets, P.D., and Grayson, D.K., eds., *Volcanic activity and Human Ecology*, Academic Press, p. 525-564.
- Smith, R.L., and Bailey, R.A., 1968, Resurgent caldrons, *Geological Society of America Memoir*, v. 116, p. 613-662.
- Squier, E.G., 1850, *The volcanoes of Central America*, 20 p.
- Steen-McIntyre, V., 1976, Petrography and particle size analysis of selected tephra samples from western El Salvador: A preliminary report: *in* Sheets, P., ed., *Ilopango volcano and Maya Protoclassic: University Museum Studies #9*, Southern Illinois University, p 68-79.
- Stothers, R.B., 2000, Climatic and demograhic consequences of the massive volcanic eruption of 1258: *Climatic Change*, v. 45, n. 2, p. 361-374.
- Tait, S., Jaupart, C., and Vergnolle, S, 1989, Pressure, gas content and eruption periodicity of a shallow, crystallising magma chamber: *Earth and Planetary Science Letters*, v.92, no.1, p.107-123.

- Weber, H.S., and Wieseemann, G., 1978, Mapa geológico general de El Salvador: Instituto eográfico Nacional de El Salvador, map San Salvador, scale 1:100,000, 1 sheet.
- Weyl, R., 1955, Beiträge zur Geologie El Salvadors: Neues Jahrbuch Geologie und Paläontologie, v 101, p. 12-38.
- Williams, H., 1941, Caldera and their origin: California University Publications, Geological Science, v. 25, no.6, p. 239-346.
- Williams, H., and Meyer-Abich, H., 1955, Volcanism in the southern part of El Salvador with particular reference to the collapse basins of Lakes Coatepeque and Ilopango: University of California Publications in the Geological Sciences, v. 32, p. 1-64.
- Wilson, C.J.N., Weaver, S.D., Briggs, R.M., Houghton, B.F., McWilliams, M.O. and Lanphere, M.A., Volcanic and structural evolution of Taupo Volcanic Zone, New Zealand: a review: Journal of Volcanology and Geothermal Research, v. 68, n. 1-3, p. 1-28.
- Wohletz, K.H., 1983, Mechanism of hydrovolcanic pyroclastic formation: Grain size, scanning electron microscopy, and experimental results: Journal of Volcanology and Geothermal Research, v. 17, p. 31-63.
- Woolley, A.R., 1983, What really happened at Krakatoa?: Open Earth, v. 20, p. 17-19.

Chapter 2

Subaqueous intracaldera volcanism, Ilopango Caldera, El Salvador, Central America

Crystal P. Mann, John Stix and Mathieu Richer

Department of Earth and Planetary Sciences,

McGill University

James Vallance¹

Department of Civil Engineering and Applied Mechanics

McGill University

**To be published in: Natural Hazards in El Salvador: Geological Society of America
Special Paper, Rose, W.I., Bommer, J.J., López, D.L, Carr, M.J., and Major, J.J., eds.**

¹ Present address: US Geological Survey, 1300 SE Cardinal Court, Bldg. 10, Suite 100, Vancouver,
WA, 98638 U.S.A.

Abstract

The Ilopango Caldera, located 10 km east of San Salvador, has erupted voluminous silicic pyroclastics four times in the last 57,000 years. The present caldera has a quasi-rectangular shape and is filled by Lake Ilopango. This paper provides a detailed description of a segment of the intracaldera stratigraphy at Ilopango caldera, with emphasis on the San Agustín Block Unit. Physical volcanology, petrology and geochemistry establish the depositional environment and eruptive conditions of the intracaldera sequence and help to model the emplacement of the San Agustín Block Unit. The intracaldera sequence comprises a sequence of pyroclastic density currents, unconformably overlain by lacustrine sediments and conformably overlain by the San Agustín Block Unit. A new radiocarbon age on wood near the top of the lacustrine unit indicates that a lake was present $\geq 43,670$ years ago. The intracaldera sequence displays abundant evidence of emplacement in a subaqueous environment.

The San Agustín Block Unit comprises a basal fine ash facies and an overlying pumice breccia facies. The basal fine ash facies is a hydromagmatic layer containing pumiceous and blocky angular glass shards, aggregates of fine ash and phenocryst fragments, and phenocrysts with a fine ash coating. The overlying pumice breccia facies is comprised of pumice clasts up to three meters in length. The pumice clasts display a series of jointing textures indicative of hot emplacement and rapid cooling. These two facies suggest an initial subaqueous explosive eruption in which a vesiculated silicic melt fragmented upon contact with the water. When the magma

had degassed sufficiently, the eruption style evolved to subaqueous dome growth that spalled quenched pumice clasts from a moderately vesiculated carapace.

Resumen

La Caldera de Ilopango se encuentra a 10 km al este de San Salvador. Ilopango ha tenido cuatro grandes erupciones de piroclastos ricos en sílice durante los últimos 57,000 años. La caldera actualmente tiene forma rectangular y el Lago de Ilopango se encuentra dentro de ella. Este artículo proporciona una descripción detallada de un segmento de la estratigrafía en el interior de la caldera de Ilopango con énfasis en una unidad que se llama “Unidad de Bloque San Agustín.” La volcanología física, petrología y geoquímica describen el medio ambiente deposicional y las condiciones eruptivas de la secuencia en el interior de la caldera y ayudan a modelar el emplazamiento de la “Unidad de Bloque San Agustín.” La secuencia en el interior de la caldera es constituida de flujos piroclásticos discordantes sobre ella yacen sedimentos lacustres y sobre estos últimos yace de manera concordante la “Unidad de Bloque San Agustín”. Una datación reciente con el método de radiocarbón de madera encontrada cerca del techo de la secuencia lacustre indica que un lago ya existía hace $\geq 43,670$ años. La secuencia en el interior de la caldera muestra evidencia de un emplazamiento en un medio ambiente subacuático.

La “Unidad de Bloque San Agustín” constituye una facie basal de ceniza fina y una facie superpuesta de pómez brecha. La facie basal de ceniza fina es un estrato hidromagmático conteniendo pedazos de vidrio, algunos en forma de bloque y otros vesiculares con textura de pómez. Contiene además un agregado de ceniza fina con fragmentos fenocristales y fenocristales con una recubierta de ceniza fina. La pómez

brecha está compuesta de pómez con una elongación a trece metros. Los clastos pómez muestran diaclasas radiales, diaclasas concéntricas y diaclasas perpendiculares a la superficie que indican una deposición caliente y un enfriamiento rápido. Las dos facies sugieren una erupción inicialmente explosiva donde un magma sílice vesiculado es fragmentado cuando se pone en contacto con el agua. Cuando el magma está lo suficientemente desgasificado, la erupción desarrolla un domo subacuático desboronando clastos templados de pómez proveniente de una caparazón vesiculada.

Keywords

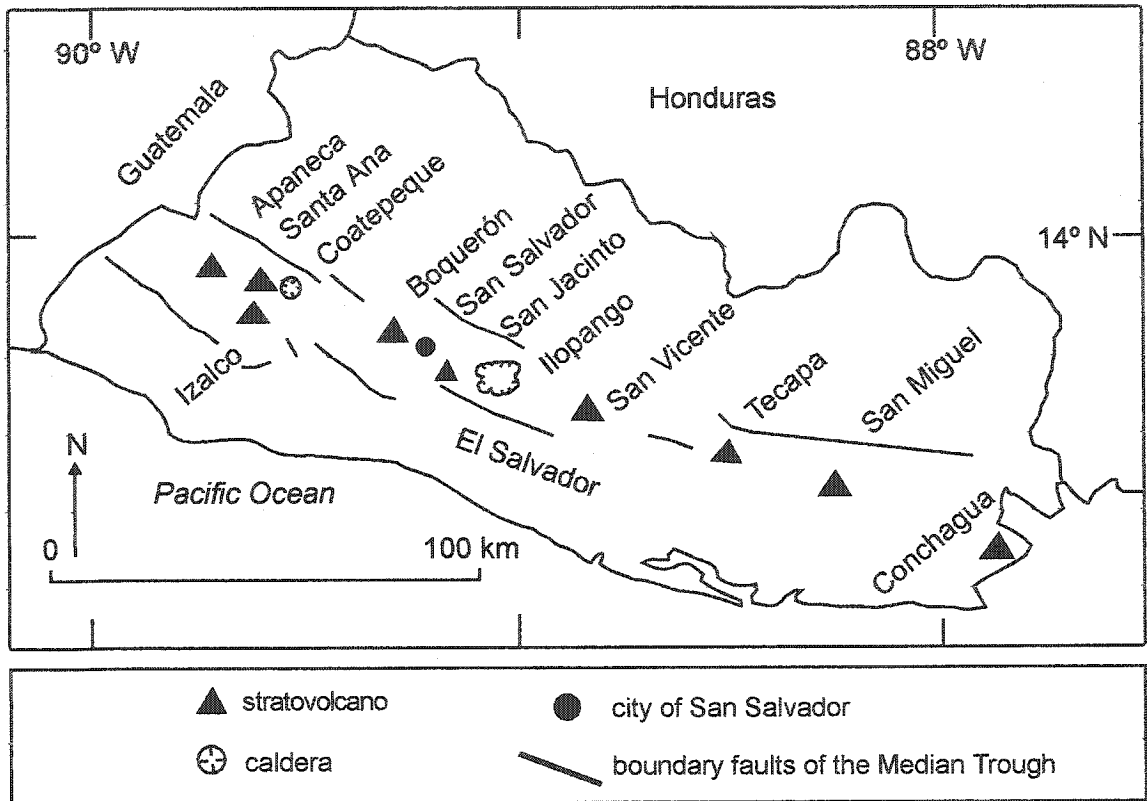
Ilopango Caldera; El Salvador; subaqueous intracaldera volcanism; hydromagmatic fragmentation; subaqueous lava dome

Introduction

Caldera-forming eruptions are among the most devastating volcanic eruptions on Earth. Well-known examples include Krakatau, Indonesia (1883), Taupo, New Zealand (AD 186), Toba, Sumatra (75 ka), and Long Valley, USA (~760 ka). Once a caldera forms, the depression may fill with water, increasing the probability of explosive eruptions. Ilopango Caldera in El Salvador contains Lago de Ilopango, an 8 x 11 km lake located approximately 10 km east of San Salvador, the capital city (Fig. 2.1). At least four large silicic explosive eruptions have occurred in the past 57,000 years (Rose *et al.*, 1999). The last violent eruption in AD 429 contributed to the devastation of Early Classic Mayan civilization in El Salvador and eastern Guatemala (Lothrop, 1927; Sheets, 1979; Hart, 1981; Dull *et al.*, 2001). In AD 1879 and 1880, dome growth formed the Islas Quemadas (Goodyear, 1880; Richer *et al.*, this volume). This recent activity strongly indicates that a body of magma still exists below the Ilopango caldera. These eruptions demonstrate that Ilopango is still active and clearly capable of explosive and effusive eruptions in the future.

In order to fully understand the effects of water during subaqueous eruptions in a caldera lake and the subsequent depositional processes, a comparison of subaerial and subaqueous deposits is necessary. In this regard, Ilopango provides an unsurpassed opportunity to compare intracaldera and extracaldera deposits, since the pyroclastic facies found outside the caldera are all emplaced subaerially, whereas many deposits within the caldera appear to be emplaced subaqueously. Until now, studies of Ilopango have focused primarily on the extracaldera deposits. In reconnaissance studies, Williams and Meyer-Abich (1955) divided the intracaldera

Figure 2.1 Location map of the Central American volcanic arc in El Salvador. Structural failure at the end of the Pliocene or early Pleistocene resulted in a tectonic depression called the Median Trough, which includes the volcanic chain (Williams and Meyer-Abich, 1955). Ilopango is bordered by three large volcanic structures. Boquerón, a large composite volcano, borders Ilopango to the west-northwest. San Jacinto, a cluster of andesitic domes, borders Ilopango to the west. San Vicente, a large composite volcano, borders Ilopango to the southeast. Modified from Carr *et al.* (1981).

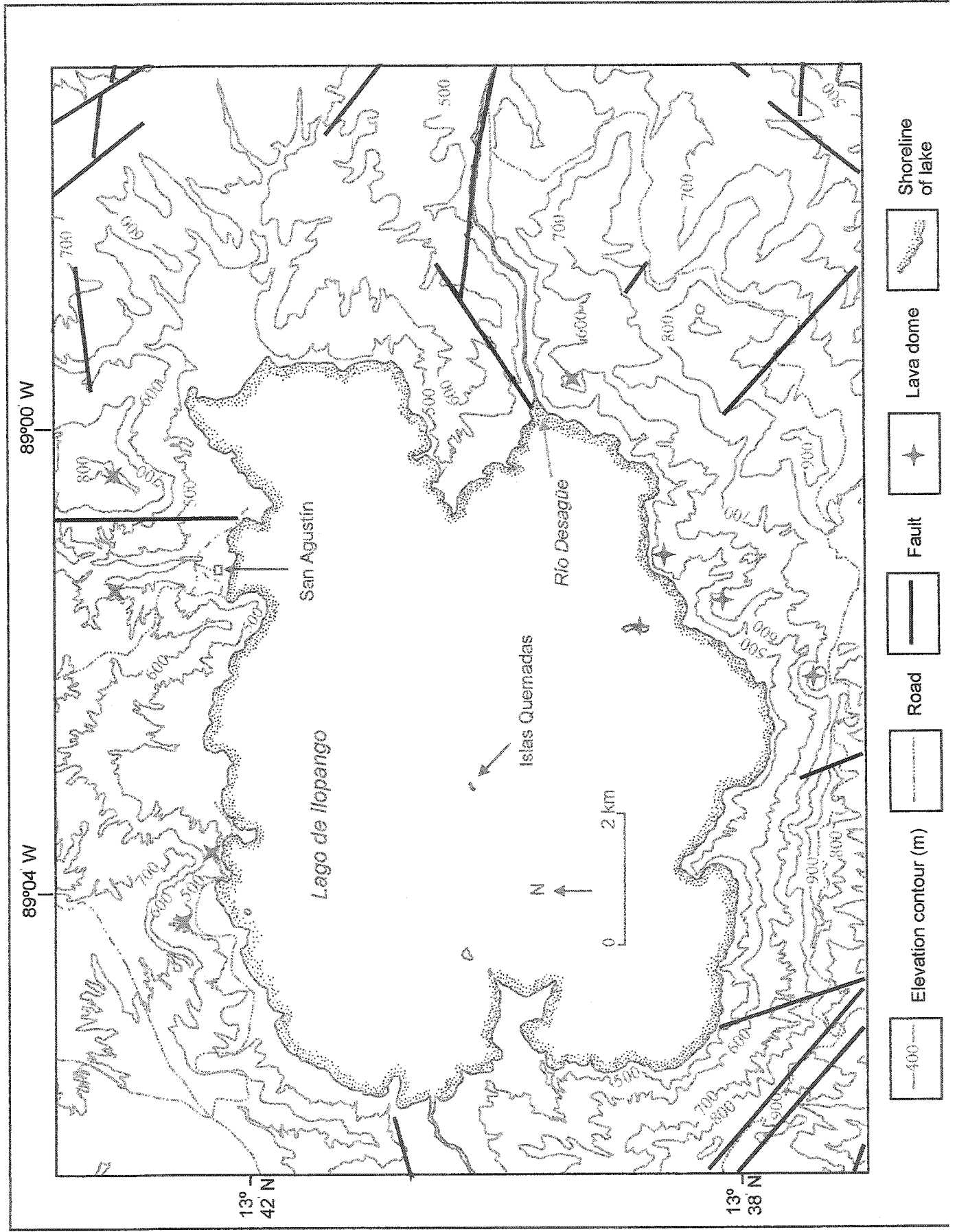


deposits into (1) older fluvial and lacustrine deposits with interbedded “pyroclastic avalanche” deposits on the southern and northeastern walls of the caldera and (2) younger dacite pumice and ash deposits emplaced in water, and “pyroclastic avalanches, pyroclastic falls and lahars” on the northern, western and upper parts of the eastern caldera walls. Weber and Wiesemann (1978) mapped the intracaldera deposits in the north to northwest and north-northeast part of the caldera as epiclastic rocks, and deposits in the south to southeast and south-southwest parts as ignimbrite. Hart (1981) described the intracaldera deposits on the northern caldera wall as “undifferentiated Ilopango-derived pyroclastic and epiclastic deposits with the occasional lahar deposit”.

In this paper, we provide a detailed description of a segment of the intracaldera stratigraphy at Ilopango caldera and focus on a sequence informally named the San Agustín Block Unit, which is well exposed to the east and west of the northern lakeshore village of San Agustín (Fig. 2.2). Found only inside the caldera, the San Agustín Block Unit comprises a thin, basal fine-grained ash and a thick, overlying pumice breccia. The pumice breccia is a spectacular facies with pumice clasts up to 3.0 m across, bed thicknesses up to 15 m, and abundant cooling-induced textures. These features make the Pumice Breccia facies a key intracaldera marker horizon. In this report, we use physical volcanology, petrology and geochemistry to establish the depositional environment, eruptive conditions and mode of emplacement of the intracaldera sequence. We first describe the associated intracaldera units and present evidence that a lake occupied Ilopango at the time these units were emplaced.

We then demonstrate that the San Agustín Block Unit was both subaqueously erupted and subaqueously emplaced, and discuss a plausible model of formation.

Figure 2.2. Intracaldera topographic map of Ilopango showing area of study. Modified from Instituto Geográfico Nacional (1981, 1984) and Weber and Wieseemann (1978).



Geological Setting

Regional geology

El Salvador is part of the Central American volcanic arc that extends 1100 km from the Guatemala-Mexico border to northern Panama (Carr and Stoiber, 1990). Tectonism and volcanism largely shape the regional geology of El Salvador. The volcanic chain occurs in a tectonic depression bounded to the south by fault blocks consisting of, from west to east, the Tacuba, Balsam and Jucuarán mountain ranges (Williams and Meyer-Abich, 1955; Wiesemann, 1975; Carr and Stoiber, 1981). The volcanic chain includes composite volcanoes, dacitic domes and two calderas, Coatepeque and Ilopango (Fig. 2.1).

Ilopango Caldera and the intracaldera setting

The Ilopango Caldera is located at the junction of the east-west, north-south and northeast-southwest fault zones (Wiesemann, 1975). The present caldera has a quasi-rectangular shape measuring 16 km east-west and 13 km north-south, and its morphology seems to be controlled by tectonics and mass-wasting processes. The southern wall of the caldera is defined by the upthrown Balsam mountain range. The youngest dome, Islas Quemadas, is located in the approximate center of the caldera and may lie along east-west fault structures (Williams and Meyer-Abich, 1955). The Río Desagüe drains the lake to the east along an east-west fault (Fig. 2.2). Many domes ranging in composition from andesite to dacite occur within the caldera (Weber and Wiesemann, 1978). These domes also may lie along established faults.

The upthrown southern wall of the caldera (elevations of 500 to 1000 m) is 100 to 200 m higher above lake level than the northern wall (elevations of 500 to 800 m).

Eruptive history of Ilopango

Since the initial structural failure at the end of the Pliocene or early Pleistocene that formed the Ilopango depression, a series of large explosive eruptions from the caldera have formed voluminous deposits of pyroclastic material. The four pyroclastic events from oldest to youngest are informally named Tierra Blanca 4 (TB4), Tierra Blanca 3 (TB3), Tierra Blanca 2 (TB2) and Tierra Blanca Joven (TBJ) (CEL, 1992). These eruptions have been temporally constrained to the last 56.9 ± 2.8 – 2.1 ka (Rose *et al.*, 1999). TB4, TB3, and TB2 are recognized as eruptions from Ilopango, but detailed studies have not yet been done. The youngest pyroclastic eruption, TBJ, is well established at AD 429 ± 20 years (Dull *et al.*, 2001).

Sample Preparation and Analytical Techniques

Electron microprobe analyses of volcanic glass were performed with a JEOL JXA-8900R at McGill University, Canada. Analyses were performed with an accelerating voltage of 15 kV, a beam current of 20 nA and a beam diameter of 15 μm . These parameters provided the best conditions to minimize Na loss. Following the methods of Sheridan and Marshal (1983) volcanic ash samples were prepared for secondary electron imaging. Pumice clasts used for porosity measurements were sprayed with a silicone-based spray to seal the vesicles, and left overnight to dry.

This technique developed by R.P. Hoblitt (U.S. Geological Survey, Vancouver), is assumed to contribute negligible mass and volume to the clast. The porosity calculations were then performed following Houghton and Wilson (1989).

Observations and Results

Terminology

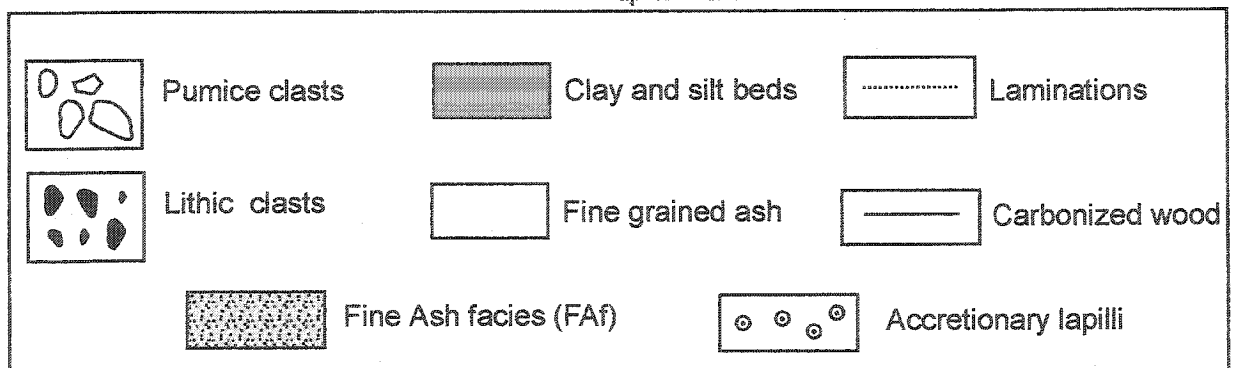
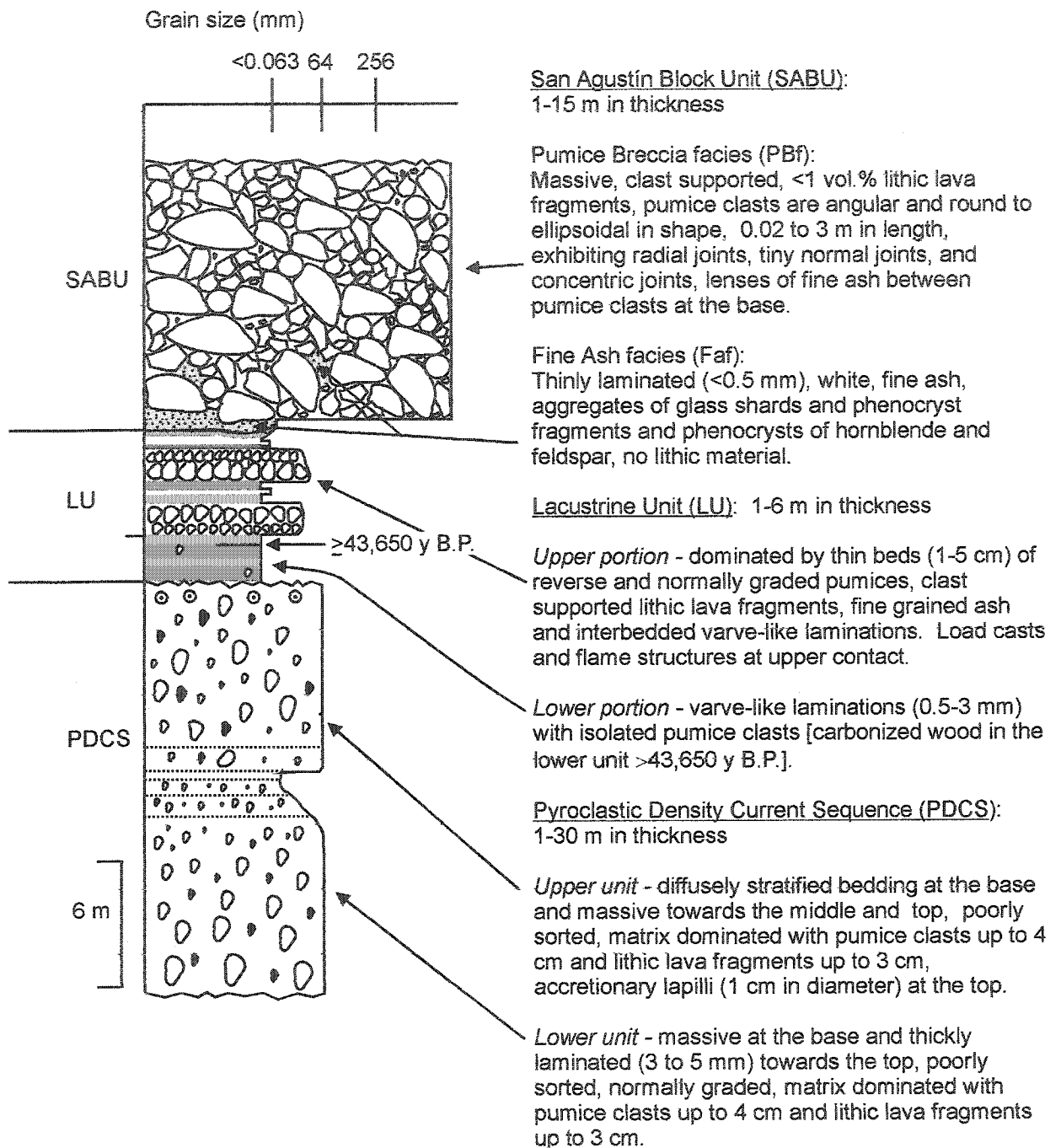
Pyroclastic terms used here are based on the size classification of volcanoclastic fragments by Fisher (1961) in conjunction with a constituent compositional classification established by Cook (1965). Nomenclature and stratigraphic thicknesses are based on the recommendations of Ingram (1954). The various units described below are named informally for convenience.

Field description, petrology and composition of intracaldera units

The stratigraphic sequence was traceable around the lake, but laterally discontinuous (Fig. 2.3). Not all units are observed at each locality, and in some instances, the lowermost unit extends beneath the lake. For this reason, absolute thicknesses could not be established, and the thicknesses reported here are considered minimum values.

Pyroclastic Density Current Sequence (PDCS) With an overall thickness of 1 to 30 m, this sequence is the lowermost unit of the intracaldera stratigraphy. The Pyroclastic Density Current Sequence comprises two lithified, moderately sorted

Figure 2.3. Schematic stratigraphic section of Ilopango intracaldera units. See text for details.



subunits made up of lithic fragments of lava, pumice and fine ash (Fig. 2.3). There is an absence of paleosols and lacustrine layers throughout the sequence. No welding textures, cooling joints, elutriation pipes or charcoal were observed. This sequence or parts of this sequence may be present outside the caldera, but at this time it is not recognized.

The lower unit and the upper unit display distinct textures. The lower unit is massive at its base and middle, and thickly laminated (3 to 5 mm) toward the top; pumice and lithic material are normally graded, with a decrease in grain size upward. The contact between the lower unit and upper unit is sharp, with the upper unit directly conformable above the lower unit. The upper unit is laminated on a cm scale at its base, and becomes more massive toward the middle and top, with no apparent grading. At the top of the upper unit, accretionary lapilli up to 1 cm in diameter and rounded to subrounded clots of friable, brown silt are observed.

In both units, approximately 85 to 90 % of the volume is matrix, which is made up of fine ash and phenocrysts of hornblende, feldspar and Fe-Ti oxides. Pumice clasts comprise 5-10 vol.% of each unit and are subangular to subrounded, ranging in size from 0.5-4 cm, with phenocrysts of 1-2 vol.% hornblende, <1 vol.% feldspar and traces of Fe-Ti oxides. Three types of lithic fragments are present: (1) black obsidian, (2) altered reddish/brown, fragments of porphyritic lava with feldspar needles, and (3) grey, porphyritic lava fragments with hornblende needles and a glassy groundmass. Lithic fragments comprise <7 vol.% of each unit; they are

TABLE 2.1. ELECTRON MICROPROBE DATA ON GLASS COMPOSITIONS

Unit Clast type Analysis*	PDCS Pumice 30	SABU-FAf Fine ash 32	SABU-PBf Pumice 29	TB2 Pumice 11
Wt. %				
SiO ₂	73.38 ± 0.62	70.50 ± 0.89	71.40 ± 0.69	72.41 ± 0.29
TiO ₂	0.18 ± 0.02	0.27 ± 0.03	0.26 ± 0.03	0.23 ± 0.02
Al ₂ O ₃	12.13 ± 0.18	13.36 ± 0.25	13.45 ± 0.29	12.51 ± 0.08
FeO	1.25 ± 0.08	1.69 ± 0.12	1.69 ± 0.14	1.38 ± 0.05
MnO	0.07 ± 0.02	0.11 ± 0.02	0.10 ± 0.03	0.07 ± 0.03
MgO	0.24 ± 0.03	0.46 ± 0.11	0.43 ± 0.05	0.27 ± 0.01
CaO	1.38 ± 0.06	2.03 ± 0.12	2.05 ± 0.18	1.51 ± 0.03
Na ₂ O	3.96 ± 0.28	4.22 ± 0.23	4.51 ± 0.17	4.13 ± 0.14
K ₂ O	2.48 ± 0.09	2.20 ± 0.06	2.21 ± 0.07	2.54 ± 0.05
P ₂ O ₅	0.03 ± 0.01	0.06 ± 0.01	0.06 ± 0.01	0.03 ± 0.01
Total	95.10 ± 0.94	94.89 ± 0.91	98.15 ± 0.54	95.08 ± 0.31
Cl	0.18 ± 0.02	0.14 ± 0.04	0.14 ± 0.01	0.16 ± 0.01
O	-0.04 ± 0.00	-0.03 ± 0.01	-0.02 ± 0.00	-0.04 ± 0.00

Notes: PDCS = Pyroclastic Density Current Sequence; SABU = San Agustín Block unit; FAf = Fine Ash facies; PBf = Pumice Breccia facies; TB2 = Tierra Blanca 2.

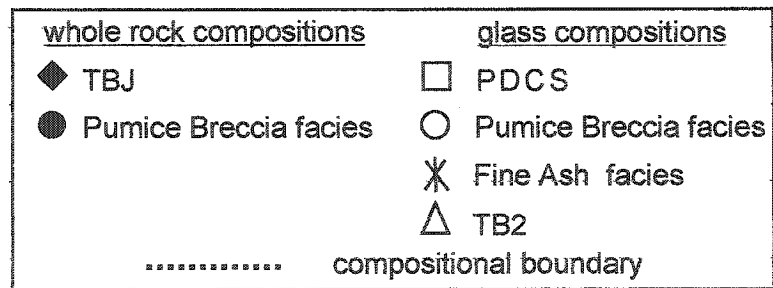
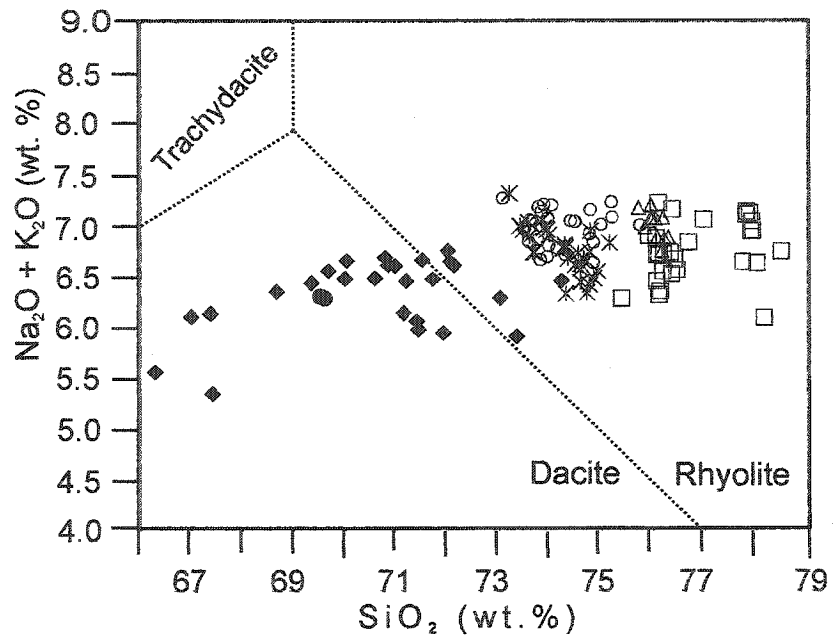
*Total number of analyses of representative unit. Compositions are displayed as mean ± 1σ.

subangular to subrounded in shape, ranging in size from 0.2 to 3 cm. Electron-microprobe analysis of glass shards from the pumice clasts indicates a rhyolitic composition, with 75.5-78.7 wt.% SiO₂ and 6.4-7.4 wt.% Na₂O + K₂O (Fig. 2.4; Table 2.1).

The Pyroclastic Density Current Sequence is unconformably overlain by the Lacustrine Unit, as indicated by an erosional contact between the top of the upper unit of the Pyroclastic Density Current Sequence and the base of the Lacustrine Unit.

Lacustrine Unit (LU) This unit ranges from 1 to 6 m in thickness and is characterized by an upward transition of finely laminated (0.5-3 mm) to thin beds (1-5 cm) (Fig. 2.3). There are no paleosols, fossils or evidence of bioturbation in the unit. The lower portion of the sequence displays abundant fine horizontal laminations (0.5-3 mm) of fine ash, silt and clay beds. The laminated beds are usually flat and horizontal, but occasionally are deformed and exhibit irregular

Figure 2.4. Whole-rock and glass compositions from selected units erupted from Ilopango caldera on a SiO_2 vs. $\text{Na}_2\text{O} + \text{K}_2\text{O}$ classification diagram. All values are normalized to 100 wt.% anhydrous. The compositions of TBJ are from Carr and Rose (1987). In general, glass compositions of the Pumice Breccia facies are rhyolitic in composition, whereas whole-rock compositions are dacitic.

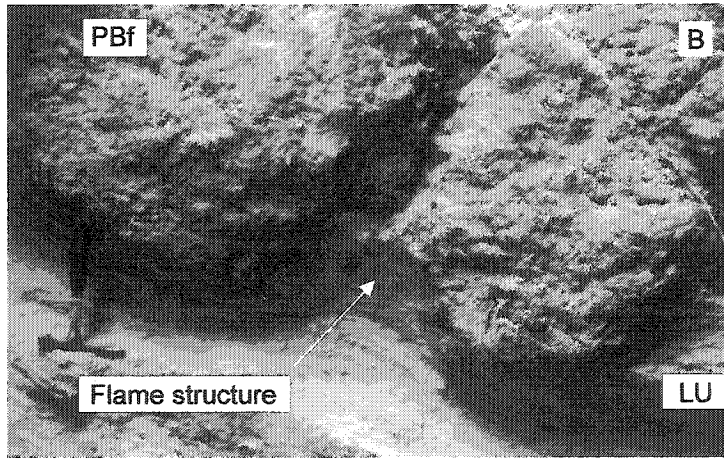
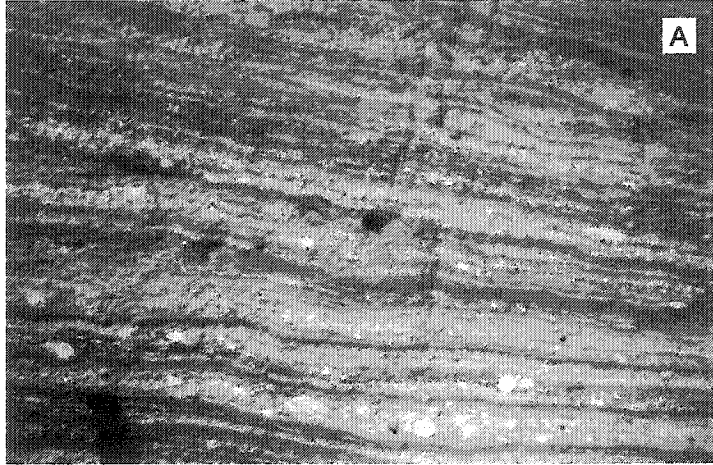


patterns. Isolated round to subrounded sand to pebble-sized pumice clasts are found throughout the lower portion (Fig. 2.5A).

A single sample of charred wood collected near the top of the lower portion of the Lacustrine Unit was found in a canyon 1.5 km northeast of the village of San Agustín. The sample (Beta 166558) was collected with tweezers, wrapped in aluminum foil and submitted to Beta Analytic Inc. for ^{14}C dating. The radiocarbon contained in this sample was statistically indistinguishable from radiocarbon background standards yielding a result of $\geq 43,670$ y. B.P.

The upper portion of the sequence is very thin to thinly bedded (1–5 cm), alternating between rounded to subrounded, clast-supported pumice beds that are both reversely and normally graded with pumice up to 2 cm in diameter, and well sorted, subrounded to subangular clast-supported beds rich in lithic fragments with clasts up to 1 cm in diameter. These beds are typically separated by fine ash beds and units consisting of moderately sorted pumice and lithic fragments in a fine-grained matrix (or both). Lenticular clots of fine white ash ranging in length from 3 to 6 cm are observed close to the top of the unit. These clots are associated with thin beds containing both lithic fragments and pumice. The contact of the Lacustrine Unit and the overlying San Agustín Block Unit is sharp, and soft-sediment deformation is indicated by the presence of flame structures and load casts compacting sediment up to 20 cm in depth (Fig. 2.5B). No paleosols are observed at the contact.

Figure 2.5. Examples of sedimentary structures in the Lacustrine Unit. A) Laminated beds of the lower portion of the Lacustrine Unit. Machete handle for scale is 6 cm long. B) Lacustrine Unit (LU) overlain by the Pumice Breccia facies (PBf). Flame structures indicated by the white arrow. Hammer for scale is 20 cm long.



San Agustín Block Unit (SABU) The San Agustín Block Unit is found only inside the caldera and is traceable discontinuously around the lake. This unit drapes the pre-existing topography, with thicknesses ranging from 1 to 15 m. Two distinct facies define the San Agustín Block Unit: a basal fine layer of ash and an overlying pumice breccia (Figs. 2.3, 2.6).

Fine Ash facies (FAf) The fine-grained ash layer at the base and in lenses within the basal portion of the overlying pumice breccia is a white, friable, moderately sorted, vitric-crystal fine ash that lacks lithic fragments (Fig. 2.6). No diatoms are observed. This layer is laterally discontinuous and has a maximum thickness of 30 cm. It is characterized by thin (< 0.5 mm) yellowish orange lamellae comprised of juvenile material such as coarse pumice shards (vesicular glass), fine ash, and phenocryst fragments.

The coarse pumice shards (0.063 to 1 mm) display two dominant morphologies. The first type is thin and fibrous looking with elongate parallel vesicles displaying both ragged and blunt edges. Some of these grains are delicately twisted, with occasional ruptured circular vesicles (Fig. 2.7A). The second type is equant in shape, with ovoid to circular vesicles enclosed by glass walls (Fig. 2.7B). Both types of shards are colorless, with no visible microlites. No quench-crack structures are observed. Electron-microprobe analysis of the glass shards indicates a rhyolitic composition, with 73.2– 75.3 wt.% SiO₂ and 6.4-7.4 wt.% Na₂O + K₂O (Fig. 2.4; Table 2.1).

Figure 2.6. Contact between the Lacustrine Unit and the San Agustín Block Unit. Symbols: Pumice Breccia facies (PBf), Fine Ash facies (Faf) and upper portion of the Lacustrine Unit (Upper LU). A discontinuous lens of white volcanic ash, which is the Fine Ash facies, is observed at the base of the Pumice Breccia facies.

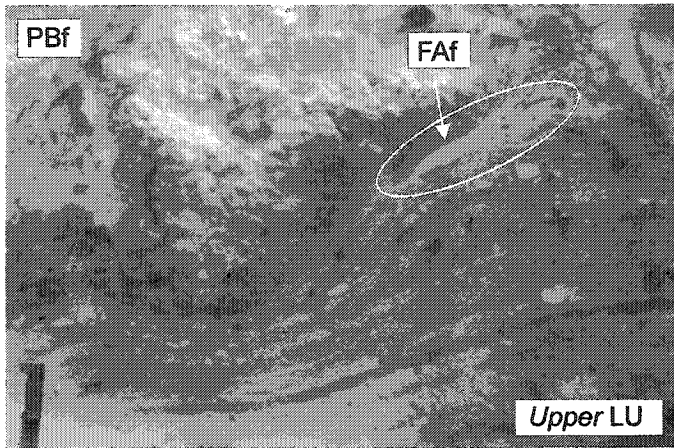
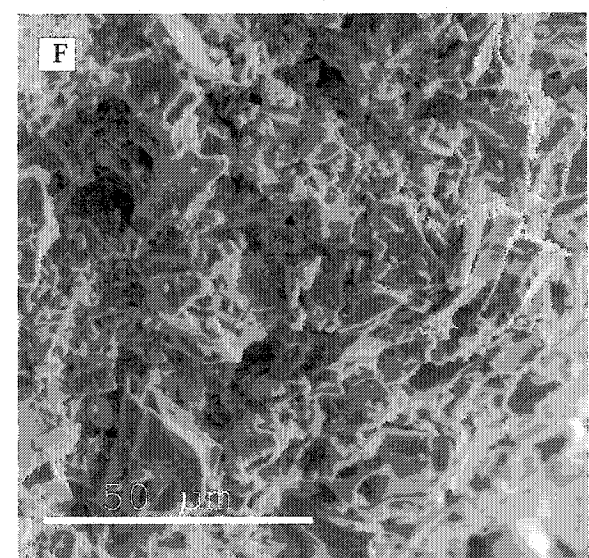
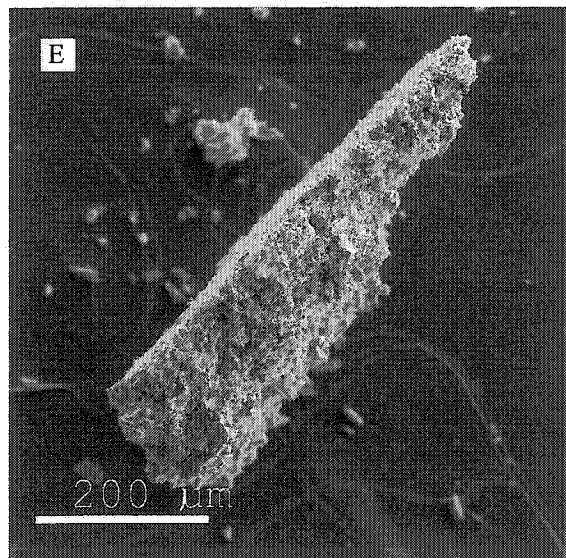
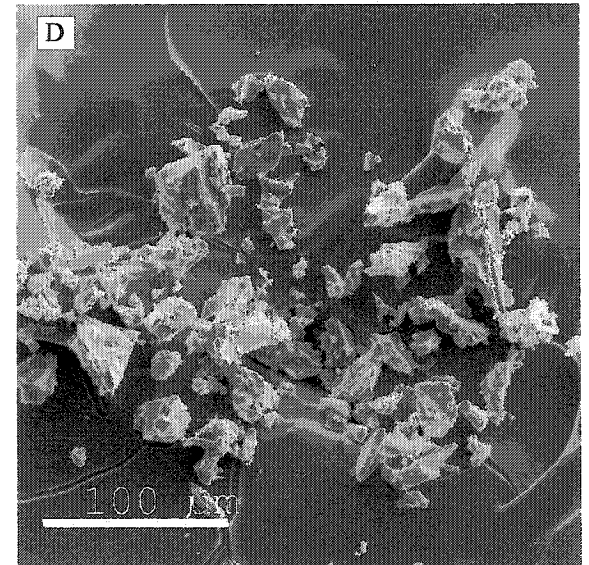
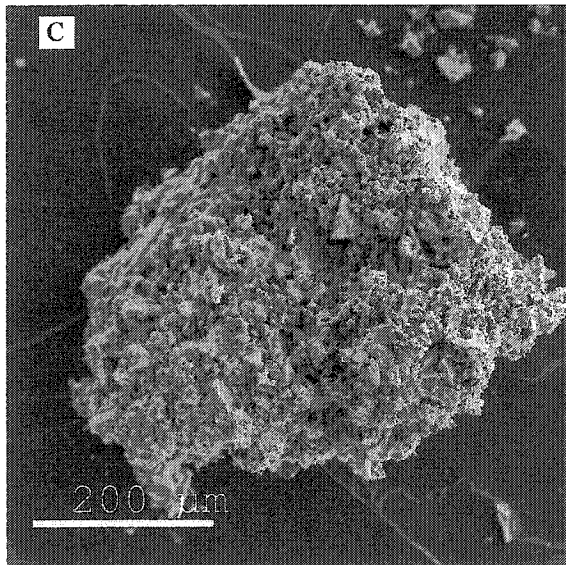
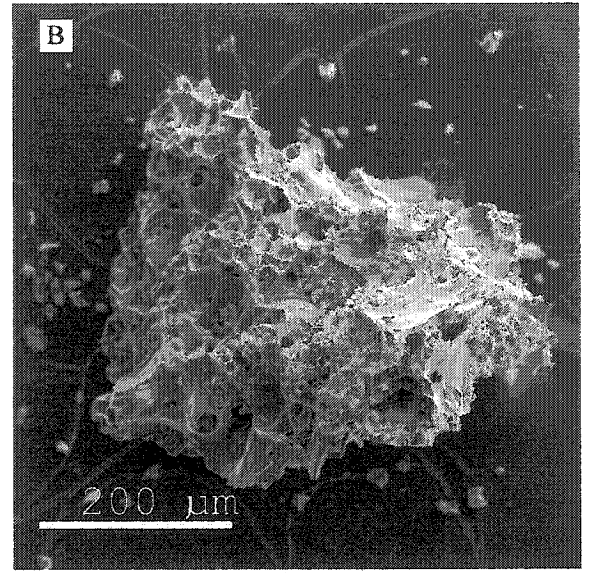
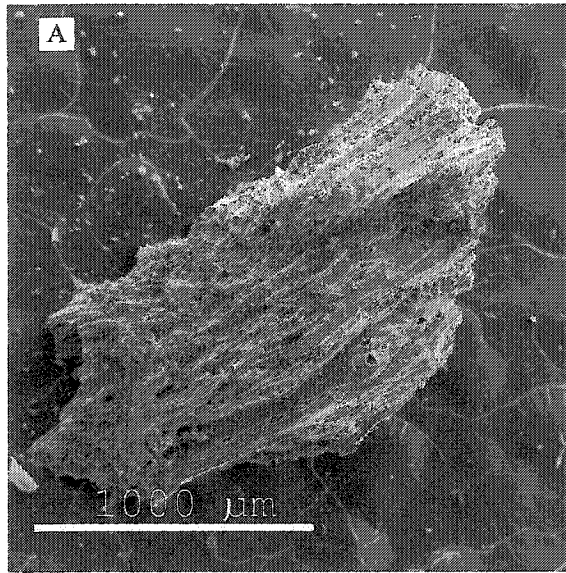


Figure 2.7. Secondary electron imaging (SEI) of the Fine Ash facies grain morphology. A: Fibrous pumice shards with parallel elongate vesicles. B: Equant pumice shards with ovoid to spherical vesicles. C: Aggregate of fine ash, phenocryst fragments and larger glass shards. D: Angular, blocky glass shards with planar and curvilinear fractures across bubble junctions. E: Hornblende with adhering dust. F: Dust adhering to hornblende in image (E). Note that scales are different in each photo. SEI images were taken using a JEOL JXA-8900L electron-microprobe.

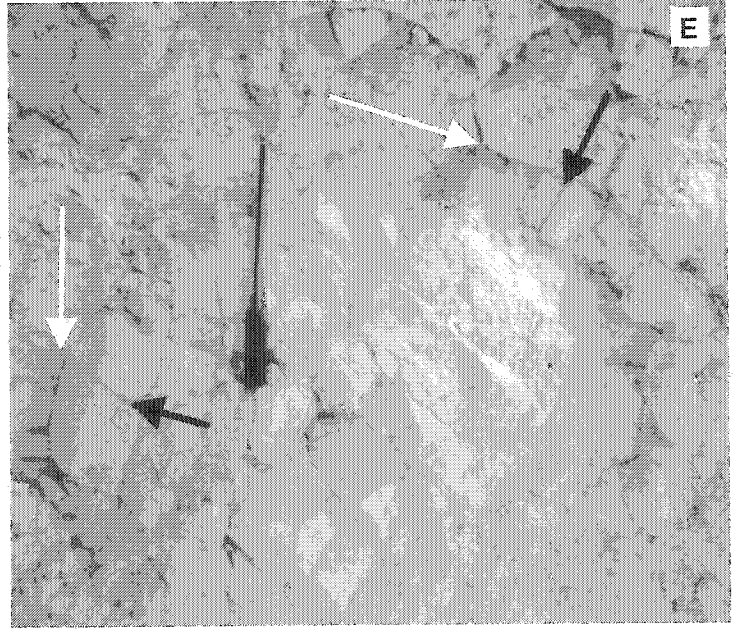
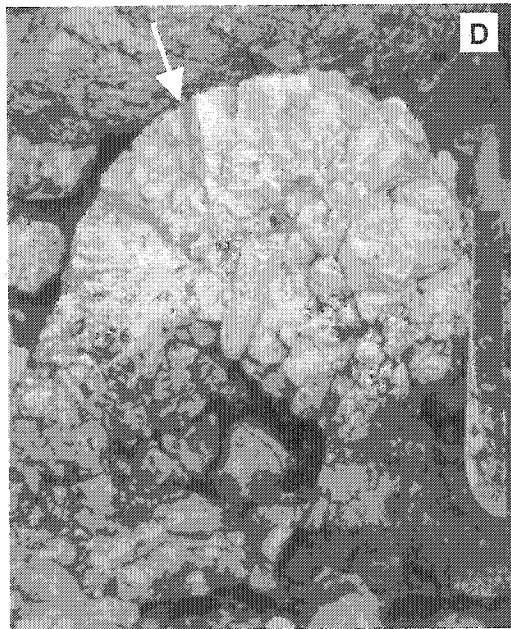
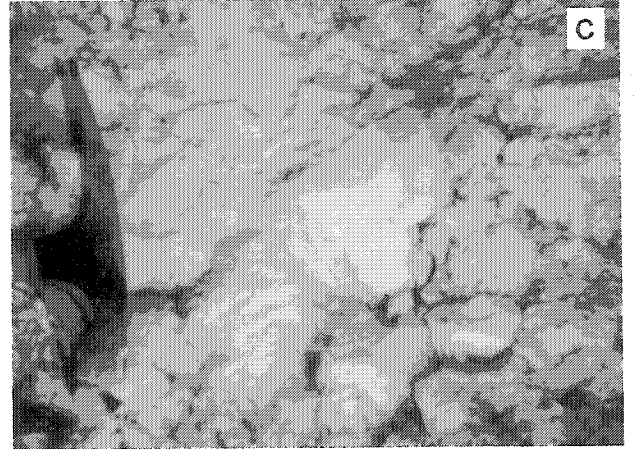
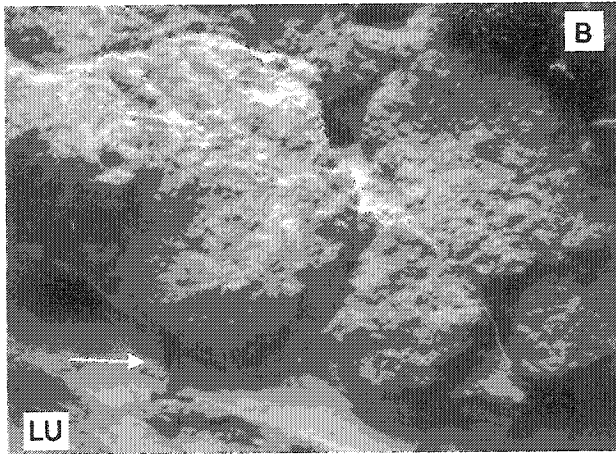
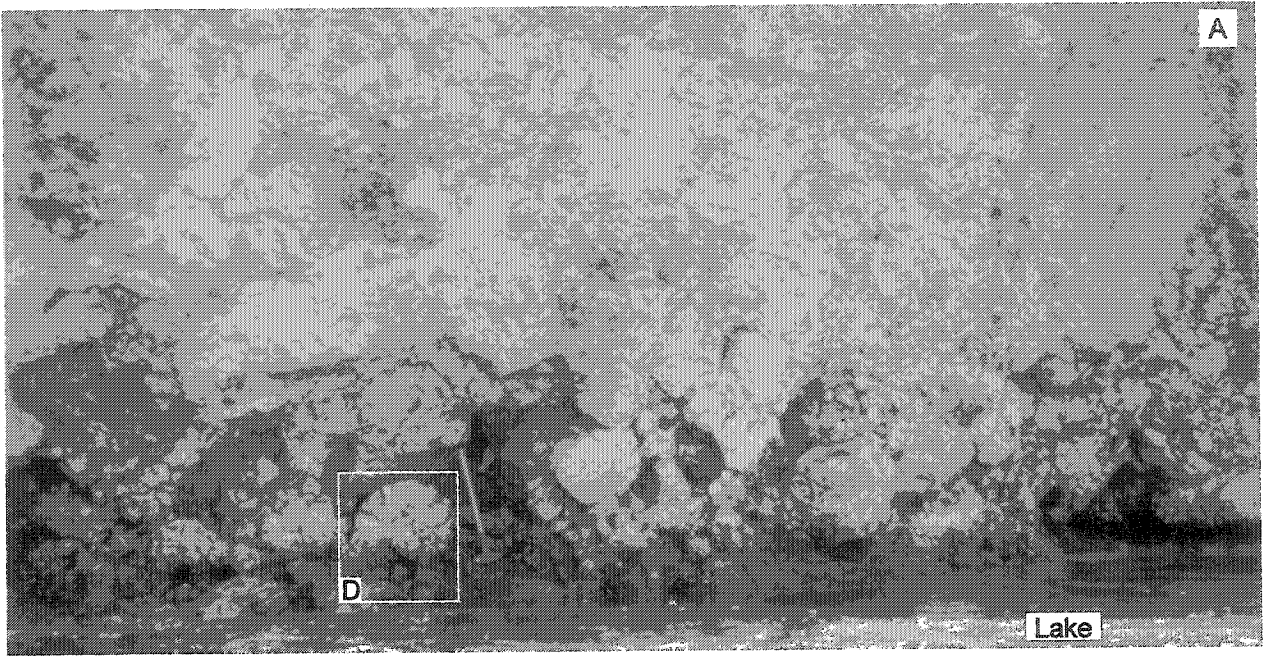


The fine ash is present as aggregates, glass shards and adhering dust, and comprises 60 vol.% of the bed. The aggregates are rounded to subrounded clusters of tiny fragmented phenocrysts and angular shards of glass (Fig. 2.7C). Some of the aggregates are slightly altered to a dirty orange color. The glass shards comprising the fine fraction (<0.063 mm) display two principal morphologies: (1) angular and blocky, with planar to curvilinear fractures and a scarcity of ovoid vesicles (Fig. 2.7D), and (2) Y-shaped forms representing bubble-wall junctions.

Phenocrysts and phenocryst fragments of hornblende and plagioclase also are present. The phenocrysts are subhedral and range in size from 0.063 to 1 mm (Fig. 2.7E). Phenocryst fragments are <0.063 mm. Fine ash adheres to many phenocrysts, as observed on the hornblende in Figure 2.7E-F.

Pumice Breccia facies (PBf) This facies is a massive, well-sorted, clast-supported bed with thicknesses ranging from 1 to 15 m (Fig. 2.8A). The pumice clasts display angular to spherical to ellipsoidal shapes, with aspect ratios (vertical axis/horizontal axis) of 0.2 to 1, ranging in length from 0.02 to 3 m (Fig. 2.8B-C). Pumice clasts up to 60 cm in length tend to be quite well rounded and have aspect ratios of 1. Pumice clasts > 60 cm are subangular to subrounded in shape with an aspect ratio of 0.2 to 0.9. The larger pumice clasts (>20 cm in length) are heavily fractured and readily break into smaller fragments when disturbed. The pumice clasts 2 to 20 cm in length are prismatic in shape. The bulk of the pumice clasts are between 60 and 90 cm in length. This facies loads the underlying Lacustrine Unit,

Figure 2.8. Pumice Breccia facies grain morphology and cooling textures. A: Massive, clast-supported pumice clasts, note large round clasts at the base. White box is magnified in D below. Hammer for scale is 80 cm long. B: Larger pumice clasts displaying subangular to subrounded clast morphology. White arrow points to a hammer for scale which is 20 cm high. C: Smaller angular pumice clasts. These clasts represent the fractured surface of a larger pumice. Hammer head for scale is 13 cm long. D: Radially jointed pumice (indicated with white arrow) with fragmented core, machete for scale is 45 cm long. E: Concentric joints (indicated with the white arrows) with radial joints (indicated with black arrows) normal to concentric joints, pen for scale is 14 cm long.



forcing sediment and the basal fine ash layer to be pushed up between the pumice clasts in the form of flame structures. Lenses of the fine ash are observed toward the base of this facies as isolated pockets between pumice clasts.

Three types of jointing structures dominate the pumice clasts. (1) Radial columnar joints up to 3-4 cm in width and 8-10 cm in length form fan-shaped structures perpendicular to the curving clast surface (Fig. 2.8D) and are also perpendicular to concentric joints defined below. (2) Tiny normal joints 1 cm in width and up to 2 cm in length are observed at the edges of the pumice clasts. (3) Concentric joints are curved and concentric to the pumice core (Fig. 2.8E).

The pumice clasts range in vesicularity from 49-87 vol.% (Appendix 2.1) and are comprised of phenocrysts of hornblende, plagioclase and ilmenite. Two main variants of the vesicular texture dominate: (1) irregular shapes range from round to more elongate, up to 3.5 mm in length, and (2) smaller round vesicles as small as 0.020 mm.

Phenocrysts range in size from 0.8 mm to 1.2 cm. The larger phenocrysts mostly appear as glomeroporphyritic clusters of plagioclase, hornblende and ilmenite and clusters of plagioclase with hornblende. Bubbles radiate from many of the large phenocrysts and glomeroporphyritic clusters.

Lithic fragments comprise <1 vol.% of this facies, consisting of grey fragments of porphyritic lava with hornblende and feldspar needles in a glassy matrix. The fragments are 1 to 2 cm in size and subangular to subrounded in shape.

Electron-microprobe analysis of the pumice glass shards indicates a rhyolitic composition of 73-75.9 wt.% SiO₂ and 6.6-7.4 wt.% Na₂O + K₂O (Fig. 2.4; Table

2.1), whereas whole rock powders analyzed by XRF have a dacitic composition with 69.5 wt.% SiO₂ and 6.3 wt.% Na₂O + K₂O (Fig. 2.4; Table 2.2).

Mingling textures occur as rounded clots of more mafic compositions surrounded by the dacite and as planar dark bands alternating with the dacitic host. These textures indicate that the mafic material was sufficiently fluid to flow and mingle with the dacitic host.

TABLE 2.2. WHOLE ROCK GEOCHEMISTRY

Unit Clast type Sample	SABU-PBf Pumice CM261-01	SABU-PBf Pumice CM262-01
Wt. %		
SiO ₂	66.49	66.31
TiO ₂	0.38	0.39
Al ₂ O ₃	15.22	15.23
Fe ₂ O ₃	3.47	3.33
MnO	0.13	0.13
MgO	1.15	1.19
CaO	3.66	3.55
Na ₂ O	4.03	3.98
K ₂ O	1.95	1.97
P ₂ O ₅	0.14	0.13
LOI	3.44	3.73
Total	100.06	99.94
ppm		
BaO	1059	1053
Ce	0	26
Co	0	11
Cr	0	0
La	13	0
Ni	0	0
Sc	0	0
V	46	39
Ga	14.4	14.9
Nb	5.1	5.8
Pb	2.9	2.1
Rb	43.4	44.9
Sr	325.6	325.4
Th	3.9	3.5
U	1.8	1.9
Y	19.7	20.0
Zr	159.1	158.1

Notes: SABU = San Agustín Block Unit; PBf = Pumice Breccia facies. X-ray fluorescence whole rock analyses were performed with a Philips PW2440 4 kW automated XRF spectrometer system at the Geochemical Laboratories, McGill University, Canada, by Tariq Ahmedali and Glenna Keating. Major elements (Si, Ti, Al, Fe, Mn, Ca, Na, K and P) were determined using 32 mm diameter fused beads composed of 5 parts lithium tetraborate and 1 part sample and trace elements (Ba, Ce, Co, Cr, La, Ni, Sc, V, Ga, Nb, Pb, Rb, Sr, Th, U, Y, Zr) were determined using 40 mm diameter pressed pellets.

Discussion

Intracaldera framework

Constrained by the age of the lower unit of the overlying Lacustrine Unit, the Pyroclastic Density Current Sequence may be the intracaldera expression of one of the older Tierra Blanca eruptions. A minimum limiting ^{14}C age of $\geq 43,670$ years has been established on the lower portion of the Lacustrine Unit. The presence of lacustrine sediments suggests that a lake, possibly a water-filled caldera, occupied Ilopango at this time. Rose *et al.* (1999) established a ^{14}C age of 57,000 years on the Congo pyroclastic flow from Coatepeque Caldera. The Congo pyroclastic flow underlies Tierra Blanca 4 (TB4), a fall-out deposit from the oldest of the documented Ilopango eruptions. Therefore the TB4 eruption is younger than 57,000 years.

Depositional setting

The sharp contact and the absence of paleosols and lacustrine layers between the two Pyroclastic Density Current subunits indicate that these two units were deposited in rapid succession. In the lower unit, the normally graded pumice and lithic material and the gradation from a massive base to a finely laminated top suggest a single depositional unit with a change in depositional energy. The more massive lower portion suggests a dense concentrated flow, whereas the laminations at the top suggest gradual sorting of dilute suspended ash as observed in the subaqueous environment (Fiske and Matsuda, 1964).

The sharp contact between the lower and upper units indicates a change in depositional conditions. The upper unit is characterized by a massive, moderately sorted, non-graded texture, whereas the laminations at its base are moderately sorted. The laminated layers may represent initial pulses as the pyroclastic density current gradually became more sustained.

It is difficult to determine the temperature of the Pyroclastic Density Current Sequence at the time of emplacement. Key indicators for hot emplacement in the Pyroclastic Density Current Sequence are absent which may suggest that this sequence was emplaced at lower temperatures.

The presence of accretionary lapilli at the top of the upper unit suggests a water vapor-rich environment (Fisher and Schmincke, 1984). Accretionary lapilli do form in the subaerial environment during magmatic eruptions through clouds (Alvarado and Soto, 2002) and during phreatomagmatic eruptions, when lake water is vaporized, such as during the 1965 eruption of Taal Volcano (Moore *et al.*, 1966).

On the basis of evidence available, we conclude that water was present during eruption. The lower unit and the upper unit are clearly temporally related. The normally graded beds and sedimentary structures of the lower unit suggest deposition in a subaqueous environment. Although the temperature of the unit is undetermined, the absence of indicators of hot emplacement is consistent with deposition in a subaqueous environment. The textures and sedimentary structures of the upper unit could be indicative of a subaerial or subaqueous environment, but the presence of accretionary lapilli in the upper unit could indicate that the eruption column was partly emergent in a humid subaerial environment.

The unit overlying the Pyroclastic Density Current Sequence is lacustrine in origin; a lake thus was present after emplacement of the Pyroclastic Density Current Sequence. The lower part of the Lacustrine Unit is marked by finely laminated beds of volcanic ash, silt and clay scattered with sand-sized pumice and intermittent deformed beds. The varve-like laminations are structures indicative of a quiet environment below wave base such as a lake (Pettijohn and Potter, 1964). Similar sedimentary structures, well documented at Laguna de Ayarza in Guatemala, have been interpreted to result from the sedimentary infilling of a caldera lake (Peppe *et al.*, 1985). Sedimentation of the fine-grained material was the result of suspension settling, with the isolated, larger pumice clasts representing intermittent waterlogging and sinking of floating pumice (Manville *et al.*, 1998). The subtle deformation of the laminations could be due to tectonic activity such as earthquakes causing the disturbance, but the calm environment continued, as shown by the fine horizontal laminations above.

Clast-supported, reversely and normally graded pumice beds with load casts and accompanying flame structures characterize the uppermost portion of the unit. Pumice which is erupted subaerially and then emplaced subaqueously, becomes water-saturated as a function of its surface area (Whitham and Sparks, 1986); therefore, the larger the pumice fragment, the longer it takes to sink (e.g., the AD 181 Taupo eruption: White *et al.*, 2001). Evidence of such a process are the reversely graded accumulations of pumice clasts observed in the field. In the upper portion of the unit, the clast-supported layers of pumice alternate between reversely graded and normally graded. Once pumice becomes saturated with water, the weight of the

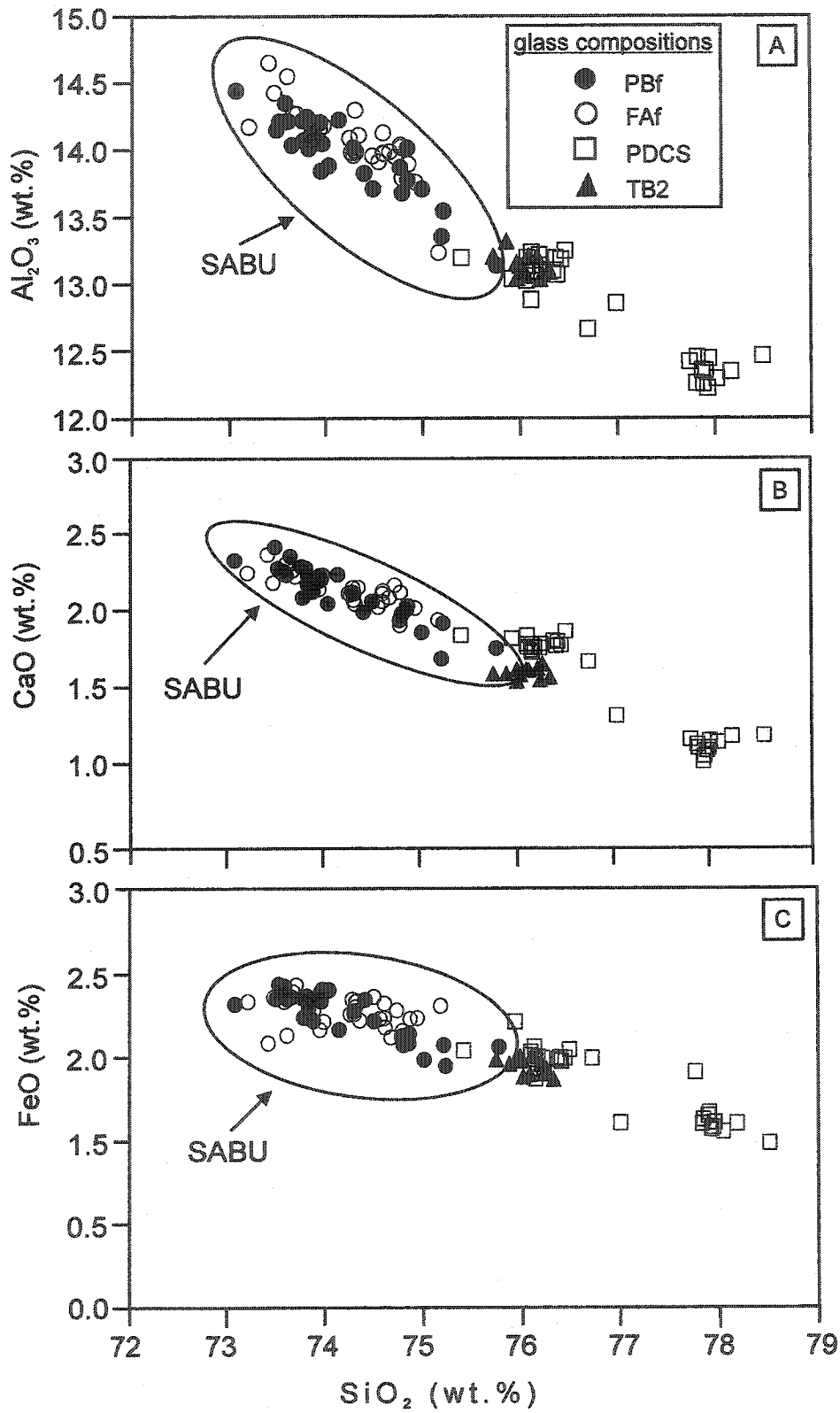
larger pumice is greater. If remobilized, the redeposited bed would then be normally graded.

The load casts and flame structures observed at the uppermost part of the unit indicate soft-sediment deformation. For plastic deformation to occur in fine-grained sediments instead of brittle faulting requires the sediment to be saturated with at least 15 to 20 wt.% water (Heiken, 1971). In the subaerial environment, the deposition of such finely laminated beds is difficult because the environment is not quiet for a sufficiently long period.

Subaqueous eruption and emplacement of the San Agustín Block Unit

Relationship between the Fine Ash facies and the Pumice Breccia facies On the basis of stratigraphic relationships and chemical similarities, we conclude that the basal Fine Ash facies and the overlying Pumice Breccia facies are coeval. The Fine Ash facies is found at the base of the unit, directly overlain by the Pumice Breccia facies, with an absence of paleosols and lacustrine beds between them. Electron-microprobe analysis shows that the glass shards from the Fine Ash facies and glass from the Pumice Breccia facies are rhyolitic in composition, with values of 73-75.5 wt.% SiO₂ and 6.3 -7.5 wt.% Na₂O + K₂O (Fig. 2.4; Table 2.1). Assuming that the glass is a quenched record of the evolved magma the geochemical data of the glasses show that the Fine Ash facies and Pumice Breccia facies are chemically similar (Figs. 2.9A-C).

Figure 2.9. Glass analyses of major elements for two intracaldera units and TB2. A: Al_2O_3 vs. SiO_2 . B: CaO vs. SiO_2 . C: FeO vs. SiO_2 . SABU is the San Agustín Block Unit, white ellipse encompasses the compositional field of the San Agustín Block Unit, Pbf is the Pumice Breccia facies, Faf is the Fine Ash facies, PDCS is the Pyroclastic Density Current Sequence and TB2 is Tierra Blanca 2. All values are normalized to 100 wt.% anhydrous, and total Fe is calculated as FeO^* .



Fragmentation of the Fine Ash To determine the eruptive environment of the basal Fine Ash facies, it is important to understand the fragmentation processes taking place by evaluating the grain morphology of the juvenile material and grain-size distribution of the bed.

During magmatic fragmentation, bubbles rupture in response to large differences between internal pressure and ambient pressure (Sparks, 1978). Controlled by bubble morphology, tephra produced by magmatic fragmentation records the vesicularity of the melt, and the glass shards reflect the thinned walls or bubble junctions at the time of eruption (Heiken and Wohletz, 1991).

Hydromagmatic fragmentation takes place when magma interacts with external water causing the quenched melt to shatter (Wohletz, 1983). Therefore, the juvenile products of a phreatomagmatic eruption are not primarily controlled by bubble morphology but instead display angular, blocky grains with low vesicularity, whereas thicker plate-like fragments are representative of the bubble walls (Wohletz, 1983).

In the Fine Ash facies, the coarse pumice shard morphology indicates magmatic fragmentation, whereas the finer-grained shards indicate hydromagmatic fragmentation. The coarser-grained (>0.063 mm) pumice shards are elongate with pipe vesicles and equant with ovoid vesicles, the shard margins being clearly controlled by vesicle shape (Fig. 2.7A-B). However, the finer-grained glass shards (<0.063 mm) are dominated by fracture-bounded grains, giving rise to blocky, angular shards with curvilinear and planar surfaces (Fig. 2.7C).

Ash aggregates in the Fine Ash facies The presence of angular, blocky fragments of glass argues for the involvement of water during fragmentation, whereas aggregates of ash and abundance of adhering dust are evidence for humid atmospheric conditions or water vaporized from the lake at the time of eruption. Secondary electron images (SEI) of the fine ash reveal abundant dust adhering to phenocrysts and glass shards, as well as rounded to subrounded aggregates of juvenile material consisting of fragmented phenocrysts, blocky glass shards and fine ash. These textures are not a product of fragmentation, but instead are indicators of conditions in and surrounding the eruption column. Similar aggregates have been observed in deposits from subaerial plinian, phreatic, phreatomagmatic and vulcanian eruptions of varying compositions (Clanton *et al.*, 1983; Heiken and Wohletz, 1985). The mechanism of aggregate formation is poorly understood, but Sorem (1982) reported ash clusters in the distal fall deposit of the 1980 Mt. St. Helens eruption and interpreted the morphology as a result of both mechanical interlocking of the grains and electrostatic attraction. Houghton *et al.* (2000) expanded on this theme and attributed aggregate formation to many variables, including the amount of liquid (water and dissolved gas species) present.

We have previously presented evidence for the presence of a lake at the time of eruption. Thus, we can make three important inferences. (1) The lake was the source of the water that contributed to fragmentation of the magma. (2) The lake was the source of the water that caused ash aggregates to form. (3) The eruption column was partly subaqueous and partly subaerial.

The occurrence of both magmatic and hydromagmatic shards illustrates magma interaction with external water, whereas the absence of lithic material indicates little erosion of the surrounding country-rock. Fragmentation may have occurred near the top of the conduit in shallow water. Fragmentation in the upper portions of the conduit would reduce the amount of lithic material entrained, whereas shallow depths would promote both substantial vesiculation of the magma and hydromagmatic fragmentation.

Eruption and emplacement of the Pumice Breccia facies The clasts of dacitic pumice are brecciated and display textures indicative of hot emplacement and rapid cooling. The original pumice clasts have been fractured, and many have brecciated into smaller fragments ranging in size from 2 to 20 cm. Such brecciation is associated with the rapid cooling of lavas and is common in both the subaerial and subaqueous environment (Pichler, 1965; Fink, 1983).

Abundant textures attributed to cooling occur in the large pumice breccia clasts (> 20 cm) as radial joints, columnar joints, tiny normal joints and concentric joints. Although cooling joints are observed in both the subaqueous and subaerial environment, the diversity of joint types and patterns at Ilopango is associated with subaqueous eruptions elsewhere (Furnes *et al.*, 1980; Kano *et al.*, 1991; McPhie *et al.*, 1993; Sakamoto and Tanimoto, 1996; Allen and McPhie, 2000). For example, radial joints are observed in subaqueous lobes of rhyolitic lava perpendicular to the lobe surface (Furnes *et al.*, 1980; Kano *et al.*, 1991), whereas tiny normal joints are observed perpendicular to quenched margins in the subaqueously erupted and

emplaced cobble-boulder facies of the rhyolitic Yali pumice breccia (Allen and McPhie, 2000). There is also an absence of microlites in the glass of the pumice clasts, suggesting rapid quenching of the clasts.

The efficiency of brecciation, the abundance and morphology of the different joints, and the absence of microlites throughout the clasts, together argue for hot clasts that were rapidly quenched. We have shown that a lake was present at the time of emplacement of the San Agustín Block Unit; based on textures attributed to cooling, we infer that the Pumice Breccia facies was rapidly quenched in the lake.

Extremely large clasts of pumice are documented in lake-filled intracaldera environments and in lake environments proximal to volcanic activity. In both cases, lava domes are present within the lake and at the lakeshore. Clasts of pumice up to 12 m are observed at Sierra La Primavera Caldera, México (Mahood, 1980) and are observed up to 17 m from the AD 186 Taupo eruption, New Zealand (Wilson and Walker, 1985; von Lichten *et al.*, 2002). At Mono Lake, eastern California, U.S.A., Stine (1984) recorded pumice clasts at the lakeshore ≤ 2 m. Floating rafts of pumice have been documented during the 1953-1957 marine eruption of the Tulumán volcano, Papua New Guinea (Reynolds and Best, 1976). On the basis of the similar geochemistry of pumice clasts and dome material, the large pumice clasts at Sierra La Primavera and Taupo were interpreted as pumice clasts spalled from the carapace of a growing subaqueous lava dome (Mahood, 1980; Wilson and Walker, 1985). At Mono Lake, chemical analyses have not been performed on the pumice blocks to test the link with the dome material, but (Stine, 1984) proposed that they formed during a sublacustrine eruption and rose to the surface.

The cooling-induced textures found at Sierra La Primavera and Taupo resemble those at Ilopango, although some of the depositional characteristics are quite different. At Sierra La Primavera laminated layers intermittently drape the large fragments of pumice, whereas at Ilopango, the pumice breccia bed is massive and clast-supported, without intermittent laminated layers. At Sierra La Primavera, the large pumice clasts became waterlogged at different rates and thus sank at different times (Mahood, 1980). At Taupo, the large pumice clasts occur as isolated blocks around the lake and appear to be the youngest products of the AD 186 eruption (Wilson and Walker, 1985). At Mono Lake, the pumice blocks also are isolated blocks concentrated mostly on the western and northern shores of the lake (Stine, 1984). At Ilopango, the unit is massive and discontinuous owing to erosion, although it is also traceable around the lake. From field observations and comparison to other studies we infer that (1) the pumice clasts at Ilopango sank rapidly, not allowing time for the deposition of lacustrine layers, and (2) the pumice clasts at Ilopango also may record the level of the lake at the time they were deposited.

Considering the evidence for rapid cooling and rapid deposition, we suggest that the pumice clasts became quickly waterlogged after eruption. The massive, clast-supported nature of the Pumice Breccia facies indicates rapid deposition. When immersed in water, hot pumice will rapidly ingest the surrounding water, increase in density and sink (Whitham and Sparks, 1986; Cashman and Fiske, 1991; Kano, 1996). The presence of lithic fragments 1-2 cm in size that coexist with pumice clasts ranging up to 3 m in length indicates that both materials were deposited at the same time. Once sufficiently waterlogged, the pumice clasts will settle out of the water

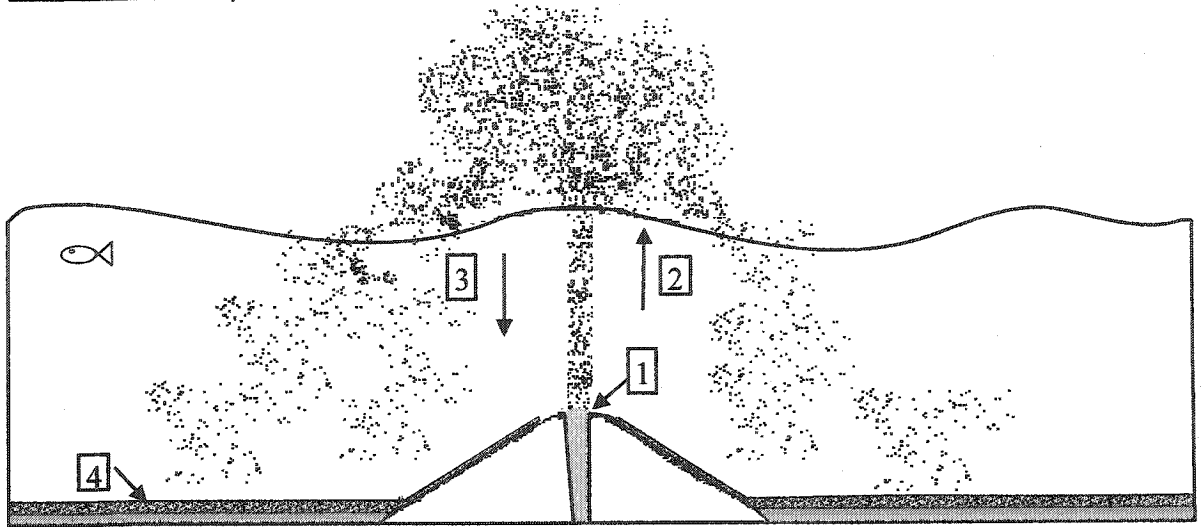
column at the same rate as a smaller clast with a much higher initial density (Cashman and Fiske, 1991), suggesting they are hydraulically equivalent. The range of vesicularity of the pumice clasts also suggests that some were comparatively dense and sank immediately.

Model of eruption and emplacement of the San Agustín Block Unit

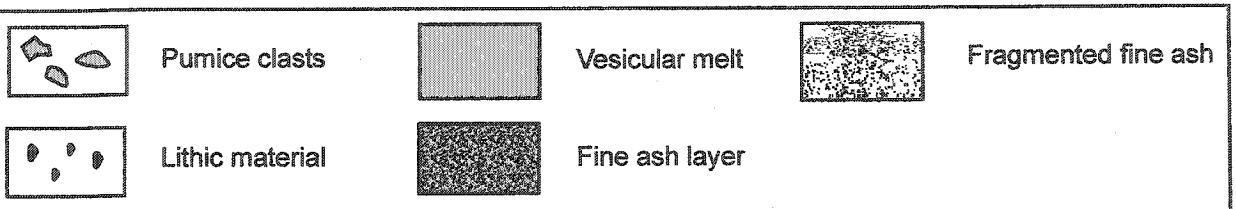
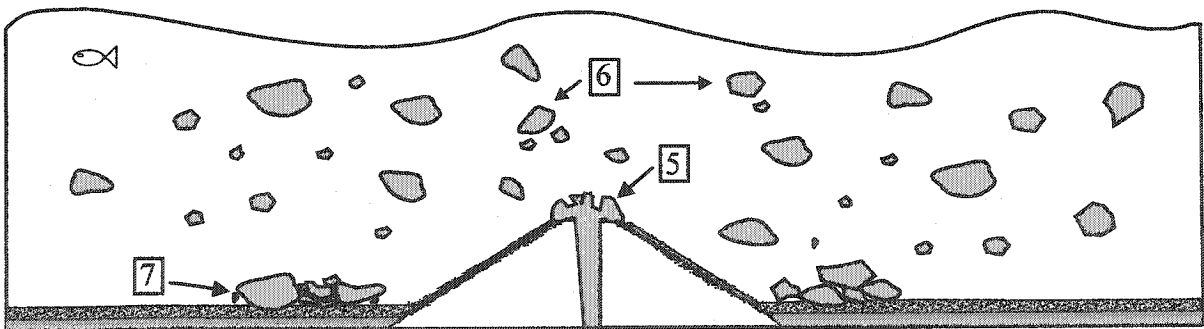
We propose a sequence of magmatic and phreatomagmatic eruptions that formed the San Agustín Block Unit (Fig. 2.10). Inside the caldera, a shallow subaqueous eruption began, and vesiculating rhyolitic melt fragmented explosively. The eruption column progressed from subaqueous to subaerial. In the subaerial environment, the moist particles in the eruption plume aggregated, and fine ash adhered to the phenocrysts and pumice shards. The larger and denser material fell out of the eruption plume and settled through lake water to be deposited on the bottom. Some ash may have been carried away by wind. This explosive phase was followed by construction of a subaqueous dome. As the hot silicic magma was extruded from the vent, it cooled rapidly and brecciated upon contact with the lake water. Quenched pumice clasts spalled from the vesiculated carapace of the growing dome. The denser clasts sank immediately, whereas others ingested water and sank when sufficiently waterlogged. Some pumice clasts sank close to the source, whereas other clasts floated to the edge of the lake. The first pumice clasts to sink made contact with the layer of fine ash, disrupting it and causing the fine sediment to become caught up between depositing pumice clasts.

Figure 2.10. Schematic diagram of model for the San Agustín Block Unit eruption and emplacement. A. Phase 1: 1) Vesiculating rhyolitic melt erupts in water, fragmenting explosively upon contact. 2) Plume begins subaqueously and progresses to the subaerial environment. Once subaerial, the fine ash and phenocryst fragments cluster together, and fine ash adheres to phenocrysts. 3) The denser particles fall back into the lake. 4) The basal fine-ash facies is deposited onto the lake bottom overlying lacustrine sediments. B. Phase 2: 5) A more degassed dacitic melt extrudes from the vent, cooling rapidly upon contact with lake water. 6) The quenched pumice clasts are spalled from the carapace of the dome. The dense pumice clasts sink immediately; others sink when sufficiently waterlogged, and some float to the lake edge. 7) Accumulating pumice clasts on the lake bottom form the Pumice Breccia facies which directly overlies the fine ash layer, disturbing it and causing the fine sediment to become caught up among the pumice clasts.

a. Phase 1: Explosive



b. Phase 2: Effusive



Conclusions

1. We have investigated a portion of the intracaldera stratigraphy at Ilopango caldera consisting of a sequence of pyroclastic density currents followed by a lacustrine deposit, in turn followed by the San Agustín Block Unit. The lacustrine sequence, containing driftwood, indicates that a lake occupied Ilopango caldera at $\geq 43,670$ y. B.P.

2. The San Agustín Block Unit comprises a basal fine ash facies and an overlying pumice breccia facies found only within the caldera. The fine ash consists of coarse pumiceous glass shards and fine blocky glass shards, aggregates of fine ash with phenocryst fragments, and phenocrysts with abundant adhering dust. The blocky shards are hydromagmatic in origin, whereas the aggregates and phenocrysts with adhering dust support a water-rich environment. The pumice breccia facies contains pumice clasts whose shapes are angular to ellipsoidal, with aspect ratios of 0.2 to 1 and sizes ranging up to 3 m in length. The pumice clasts display radial joints, tiny normal joints and concentric jointing, all indicative of hot emplacement and rapid quenching. The distinguishable characteristics of the Pumice Breccia facies, such as pumice diameter, thickness, and jointing textures, indicate that this unit is a key stratigraphic marker horizon with which to conduct further intracaldera studies.

3. Through observation of the individual intracaldera stratigraphic units, we infer that a lake occupied the caldera, at least periodically, for an extended length of time and has played an active role in explosive volcanism at Ilopango.

Acknowledgements

We extend our gratitude to the Fundación de Amigos del Lago de Ilopango, especially Ernesto Freund, Jeannette Monterrosa and Fred Thill, for their help with logistics and incredible support while in El Salvador. Many thanks to Carlos Pullinger of the Servicio Geológico division of the Servicio Nacional de Estudios Territoriales, for taking the time to familiarize us with the outer caldera deposits and for his ongoing enthusiasm to understand the San Agustín Block Unit. We are forever indebted to our new friends at San Agustín, especially Natividad Rauda and his family, for their patience while in the field and acceptance of C.P.M and M.R. into their village and homes. We thank Chris Harpel of the Cascades Volcano Observatory for his help tracking down elusive references, and Sergio Espinosa for his help with translation of the abstract to Spanish. We also thank Guillermo Alvarado and Barry Cameron for their reviews, which significantly improved this manuscript. We are most grateful to Mike Carr for his input and suggestions to the paper. This project was funded by a bursary awarded through the Canadian Bureau of International Education by the Canadian International Development Agency to C.P.M., by a research grant from the Natural Sciences and Engineering Research Council of Canada to J.S., and by National Science Foundation Grant EAR-9903291 to J.V.

References

- Allen, S.R., and McPhie, J., 2000, Water-settling and resedimentation of submarine rhyolitic pumice at Yali, eastern Aegean, Greece: *Journal of Volcanology and Geothermal Research*, v. 95, p. 285-307.
- Alvarado, G.E., and Soto, G. J., 2002, Pyroclastic flow generated by crater-wall collapse and outpouring of the lava pool of Arenal Volcano, Costa Rica: *Bulletin of Volcanology*, v. 63, p. 557-568.
- Carr, M.J., Mayfield, D.G., and Walker, J.A., 1981, Relation of lava compositions to volcano size and structure in El Salvador: *Journal of Volcanology and Geothermal Research*, v. 10, p. 35-48.
- Carr, M.J., and Rose, W.I., 1987, CENTAM-a database of analyses of Central American volcanic rocks: *Journal of Volcanology and Geothermal Research*, v. 33, p. 231-252.
- Carr M.J., and Stoiber, R.E., 1981, Lavas and faults characterize El Salvador: *Geotimes*, v. 26, no. 7, p. 20-21.
- Carr, M.J., and Stoiber, R.E., 1990, Volcanism, *in* Dengo, G., and Case, J.E., eds., *The Geology of North America: the Caribbean Region*, Geological Society of America Bulletin H, p. 375-391.
- Cashman, K.V., and Fiske, R.S., 1991, Fallout of pyroclastic debris from submarine volcanic eruptions: *Science*, v. 253, p. 275-280.

- CEL, 1992, Desarrollo de los recursos geotérmicos del area centro-occidental de El Salvador. Prefactibilidad geotérmica del area de Coatepeque: Comisión Ejecutiva Hidroelectrica del Rio Lempa Reconocimiento Geotérmico, Internal Report, p. 1-104.
- Clanton, U.S., Gooding, J.L., and Blanchard, D.P., 1983, Volcanic ash "clusters" in the stratosphere after the El Chichon, Mexico, eruption [abs.]: Eos (Transactions, American Geophysical Union), v. 64, no. 5, p. 1139.
- Cook, E. F., 1965, Stratigraphy of Tertiary volcanic rocks in eastern Nevada: Nevada Bureau of Mines Rept. 11, 66 p.
- Dull, R., Southon, J., and Sheets, P., 2001, Volcanism, ecology and culture: a reassessment of the Volcán Ilopango TBJ eruption in the southern Maya realm: Latin American Antiquity, v. 12, p. 25-44.
- Fink, J.H., 1983, Structure and emplacement of a rhyolitic obsidian flow: Little Glass Mountain, Medicine Lake Highland, northern California: Geological Society of America Bulletin, v. 94, p. 362-380.
- Fisher, R.V., 1961, Proposed classification of volcanoclastic sediments and rocks: Geological Society of America Bulletin, v. 72, p. 1409-1414.
- Fisher, R.V., and Schmincke, H.-U., 1984, Pyroclastic rocks: Berlin, Springer-Verlag, 472 p.
- Fiske, R.S., and Matsuda, T., 1964, Submarine equivalents of ash flows in the Tokiwa Formation, Japan: American Journal of Science, v. 262, p. 76-106.

- Furnes, H., Fridleifsson, I.B., and Atkins, F.B., 1980, Subglacial volcanics - on the formation of acid hyaloclastites: *Journal of Volcanology and Geothermal Research*, v. 8, p. 95-110.
- Goodyear, W.A., 1880, Earthquake and volcanic phenomena. December 1879 and January 1880 in the Republic of Salvador, Central America, *Star and Herald*, p. 56.
- Hart, W.J.E, 1981, The Panchimalco tephra, El Salvador, Central America [unpublished M.Sc. thesis]: Rutgers University, New Brunswick, New Jersey.
- Heiken, G.H., 1971, Tuff rings: examples from the Fort Rock - Christmas Lake Valley Basin, south-central Oregon: *Journal of Geophysical Research*, v. 76, p. 5615-5626.
- Heiken, G., and Wohletz, K., 1985, *Volcanic ash*: Berkeley, University of California Press, 246 p.
- Heiken, G., and Wohletz, K., 1991, Fragmentation processes in explosive volcanic eruptions: *Sedimentation in Volcanic Settings*, SEPM Special Publication No. 45, p. 19-26.
- Houghton, B.F., and Wilson, C.J.N., 1989, A vesicularity index for pyroclastic deposits: *Bulletin of Volcanology*, v. 51, p. 451-462.
- Houghton, B.F., Wilson, C.J.N., Smith, R.T., and Gilbert, J.S., 2000, Phreatoplinian eruptions, *in* Sigurdsson, H., Houghton, B., McNutt, S., Rymer, H., and Stix, J., eds., *Encyclopedia of Volcanoes*, Academic Press, p. 513-525.
- Ingram, R.L., 1954, Terminology for the thickness of stratification and parting units in sedimentary rocks: *Geological Society of America Bulletin*, v. 65, p. 937-938.

Instituto Geográfico Nacional "Ingeniero Pablo Arnoldo Guzmán", 1981, América Central República de El Salvador Lago de Ilopango: map SAL-LL1, scale 1:20,000, 1 sheet.

Instituto Geográfico Nacional "Ingeniero Pablo Arnoldo Guzmán", 1984, República de El Salvador: maps 2356 I, 2357 II, 2457 III, 2456 IV scale 1:50,000, 4 sheets.

Kano, K., 1996, A Miocene coarse volcanoclastic mass-flow deposit in the Shimane Peninsula, SW Japan: product of a deep submarine eruption?: *Bulletin of Volcanology*, v. 58, p. 131-143.

Kano, K., Takeuchi, K., Yamamoto, T., and Hoshizumi, H., 1991, Subaqueous rhyolite block lavas in the Miocene Ushikiri Formation, Shimane Peninsula, SW Japan: *Journal of Volcanology and Geothermal Research*, v. 46, p. 214-253.

LeBas, M.J., LeMaitre, R.W., Streckeisen, A.L., and Zanettin, B., 1986, A chemical classification of volcanic rocks based on the total alkali-silica diagram: *Journal of Petrology*, v. 27, p. 247-250.

Lothrop, S.K., 1927, Pottery types and their sequence in El Salvador: *Indian Notes and Monographs*, v. 1, p. 165-220.

Mahood, G.A., 1980, Geological evolution of a Pleistocene rhyolitic center - Sierra La Primavera, Jalisco, Mexico: *Journal of Volcanology and Geothermal Research*, v. 8, p. 199-230.

- Manville, V., White, J.D.L., Houghton, B.F., and Wilson, C.J.N., 1998, The saturation behavior of pumice and some sedimentological implications: *Sedimentary Geology*, v. 119, p. 5-16.
- McPhie, J., Doyle, M., and Allen, R., 1993, *Volcanic textures: a guide to the interpretation of textures in volcanic rocks*: Tasmania, CODES Key Centre, 198 p.
- Moore, J.G., Nakamura, K., and Alcaraz, A., 1966, The 1965 eruption of Taal volcano: *Science*, v. 151, p. 955-960.
- Pettijohn, F.J., and Potter, P.E., 1964, *Atlas and glossary of primary sedimentary structures*: New York, Springer-Verlag, 370 p.
- Pichler, H., 1965, Acid hyaloclastites: *Bulletin Volcanologique*, v. 28, p. 293-310.
- Poppe, L.J., Paull, C.K., Newhall, C.G., Bradbury, J.P., and Ziagos, J., 1985, A geophysical and geological study of Laguna de Ayarza, a Guatemalan caldera lake: *Journal of Volcanology and Geothermal Research*, v. 25, p. 125-144.
- Reynolds, M.A., and Best, J.G., 1976, Summary of the 1953-1957 eruption of Tulumán Volcano, Papua New Guinea, *Volcanism in Australasia*, New York, Elsevier Scientific Publishing, p. 287-296.
- Richer, M., Mann, C., and Stix, J., *in press*, Mafic magma injection triggers eruption at Ilopango Caldera, El Salvador, Central America, in Rose, W.I., Bommer, J.J., López, D.L., Carr, M.J., and Major, J.J., eds., *Natural Hazards in El Salvador*: Geological Society of America Special Paper.

- Rose, W.I., Conway, F.M., Pullinger, C.R., Deino, A., and McIntosh, W.C., 1999, An improved age framework for late Quaternary silicic eruptions in northern Central America: *Bulletin of Volcanology*, v. 61, p. 106-120.
- Sakamoto, I., and Tanimoto, H., 1996, Rhyolitic pumice dredged from the bank located between Hachijyoshima and Aogashima Is: *Journal of the Faculty of Marine Science and Technology, Tokai University*, v. 41, p. 139-156.
- Sheets, P.D., 1979, Environmental and cultural effects of the Ilopango eruption in Central America, *in* Sheets, P.D., and Grayson, D.K., eds., *Volcanic activity and Human Ecology*, Academic Press, p. 525-564.
- Sheridan, M.F., and Marshall, J.R., 1983, SEM examination of pyroclastic materials: basic considerations: *in* *Scanning Electron Microscopy 1983*, SEM, Chicago, p. 113-118.
- Sorem, R., 1982, Volcanic ash clusters: tephra rafts and scavengers: *Journal of Volcanology and Geothermal Research*, v. 13, p. 63-71.
- Sparks, R.S.J., 1978, The dynamics of bubble formation and growth in magmas: a review and analysis: *Journal of Volcanology and Geothermal Research*, v. 3, p. 1-37.
- Stine, S., 1984, Late Holocene lake level fluctuations and island volcanism at Mono Lake, California, *in* Stine, S., Wood, S., Sieh, K., and Miller, C.D., eds., *Holocene paleoclimateology and tephrochronology east and west of the Central Sierra Crest*, Friends of the Pleistocene, Guidebook, p. 21-49.

- von Lichten, I.J., White, J.D.L., and Manville, V., 2002, Giant rafted pumice around Lake Taupo from the 1.8 ka eruption [abs.]: Eos (Transactions, Western Pacific Geophysical Meeting, American Geophysical Union), v. 83, no. 22, p. WP110.
- Weber, H.S., and Wiesemann, G., 1978, Mapa geológico general de El Salvador: Instituto eográfico Nacional de El Salvador, map San Salvador, scale 1:100,000, 1 sheet.
- White, J.D.L., Manville, V., Wilson, C.J.N., Houghton, B.F., Riggs, N.R., and Ort, M., 2001, Settling and deposition of AD 181 Taupo pumice in lacustrine and associated environments, *in* White, J.D.L., and Riggs, N.R., eds., Volcaniclastic Sedimentation in Lacustrine Settings: International Association of Sedimentologists Special Paper, p. 141-150.
- Whitham, A., and Sparks, R., 1986, Pumice: Bulletin of Volcanology, v. 48, p. 209-223.
- Wiesemann, G., 1975, Remarks on the geologic structure of the Republic of El Salvador, Central America: Mitteilungen Aus Den Geologische - Palaeontologische Institute Der Universität Hamburg, v. 44, p. 557-574.
- Williams, H., and Meyer-Abich, H., 1955, Volcanism in the southern part of El Salvador with particular reference to the collapse basins of Lakes Coatepeque and Ilopango: University of California Publications in the Geological Sciences, v. 32, p. 1-64.

Wilson, C.J.N., and Walker, G.P.L., 1985, The Taupo eruption, New Zealand. 1.

General aspects: Philosophical Transactions of the Royal Society of London,
v. 314, p. 199-226.

Wohletz, K.H., 1983, Mechanisms of hydrovolcanic pyroclast formation: grain-size,
scanning electron microscopy, and experimental studies: Journal of
Volcanology and Geothermal Research, v. 17, p. 31-63.

Appendix 2.1

VESICULARITY CALCULATIONS (*Houghton and Wilson, 1989*)

Sample	W_c^{air} (g)	W_c^{water} (g)	S.G.	Vesicularity
202-01	32.09	5.76	1.22	49.22
202-01	20.91	-1.42	0.94	60.98
202-01	8.88	-11.15	0.44	81.52
202-01	8.83	-9.82	0.47	80.27
202-01	9.61	-11.82	0.45	81.32
202-01	7.39	-9.72	0.43	82.01
202-01	9.62	-7.85	0.55	77.06
202-01	9.55	-6.13	0.61	74.62
202-01	8.57	-9.77	0.47	80.52
202-01	8.57	-9.77	0.47	80.52
202-01	6.85	-12.84	0.35	85.51
202-01	9.40	-12.63	0.43	82.22
202-01	11.59	-10.41	0.53	78.06
202-01	9.38	-6.60	0.59	75.55
202-01	5.42	-11.67	0.32	86.80
261-01	6.38	-11.78	0.35	85.37
261-01	8.04	-12.19	0.40	83.44
252-01	13.69	-10.64	0.56	76.55
252-01	8.87	-9.24	0.49	79.60
290-01	12.39	-4.80	0.72	69.96
290-01	16.09	-6.57	0.71	70.41
280-01	5.73	-12.19	0.32	86.67
280-01	13.53	-9.08	0.60	75.07
280-01	10.27	-11.23	0.48	70.10
288-01	9.06	-13.32	0.40	83.13
288-01	15.26	-0.86	0.95	60.55
288-01	17.67	-2.43	0.88	63.37
290-01	10.06	-8.60	0.54	77.54
290-01	11.27	-6.43	0.64	73.46
290-01	8.74	-6.75	0.56	76.48
290-01	17.33	-9.86	0.64	73.44
290-01	8.91	-6.68	0.57	76.18
206-01	13.20	-9.72	0.58	76.00
206-01	8.13	-10.87	0.43	82.17
206-01	10.25	-8.79	0.54	77.57
206-01	10.99	-9.51	0.54	77.66
261-01	8.39	-3.34	0.72	70.20
261-01	7.39	-1.37	0.84	64.85

Notes: W_c^{air} = weight of clast in air; W_c^{water} = weight of clast in water; S.G. = Specific Gravity; Non-vesicular dacite was taken as 2.4 g/cm³.

Bridge to Chapter 3

In the previous chapter, the intracaldera stratigraphy of Ilopango was established and determined to be emplaced mostly subaqueously. The San Agustín Block unit was shown to be a key marker horizon. A model was proposed in which an eruption begins with a phreatomagmatic phase and evolves into a more effusive phase in which the pumice clasts are spalled from a subaqueously growing lava dome.

Chapter 3 examines the magmatic evolution of the Ilopango Caldera by considering all the intracaldera domes and pyroclastic units. Geochemistry, radiometric age dates and a new ^{14}C , date which further constrains emplacement of the San Agustín Block unit, are presented. The data are integrated in a working model of magmatic evolution for the Ilopango Caldera through time and then placed into a regional context by comparison to other Central American silicic centers.

Chapter 3

Magmatic evolution of the Ilopango Caldera, El Salvador, Central America

C.P. Mann and J. Stix

Department of Earth and Planetary Sciences

McGill University

J. Vallance¹

Department of Civil Engineering and Applied Mechanics

McGill University

¹ Present address: US Geological Survey, 1300 SE Cardinal Court, Bldg. 10, Suite 100
Vancouver, WA. 98638 USA

Abstract

Volcanism along the volcanic front of the Central American volcanic arc is the Quaternary expression of active subduction processes. The volcanic front is comprised of stratovolcanoes, caldera systems, cinder cones and dome complexes. The Ilopango Caldera, located along this front in El Salvador, has experienced frequent activity as recently as AD 1880 when a lava dome formed in the middle of the caldera lake, and previously in AD 429 when $\sim 18 \text{ km}^3$ DRE of pyroclastic material devastated the Early Classic Mayan civilization. This aim of this paper is to 1) understand the magmatic evolution of the Ilopango caldera and 2) gain a general perspective of where Ilopango sits chemically relative to other major Central American silicic centers. Petrography and geochemistry are combined with new radiometric and radiocarbon age determinations to establish the magmatic evolution of Ilopango over time. We show that the evolution of Ilopango is not a progressive process directly related to a time factor, such as progressive magma differentiation by closed-system crystallization. Based on mafic mixing/mingling textures and phenocryst disequilibrium textures observed in the intracaldera lavas and pyroclastic units, we conclude that Ilopango is underlain by a shallow level reservoir which experiences replenishment of a more mafic magma, undergoes fractional crystallization and periodically erupts. Based on major and trace element geochemistry, Ilopango is less evolved than other Central American silicic centers such as Atitlán, Amatitlán, Ixtepeque and Zúñil, but is chemically similar to the less evolved Santa María, Santiaguito and Acantenango centers.

Keywords

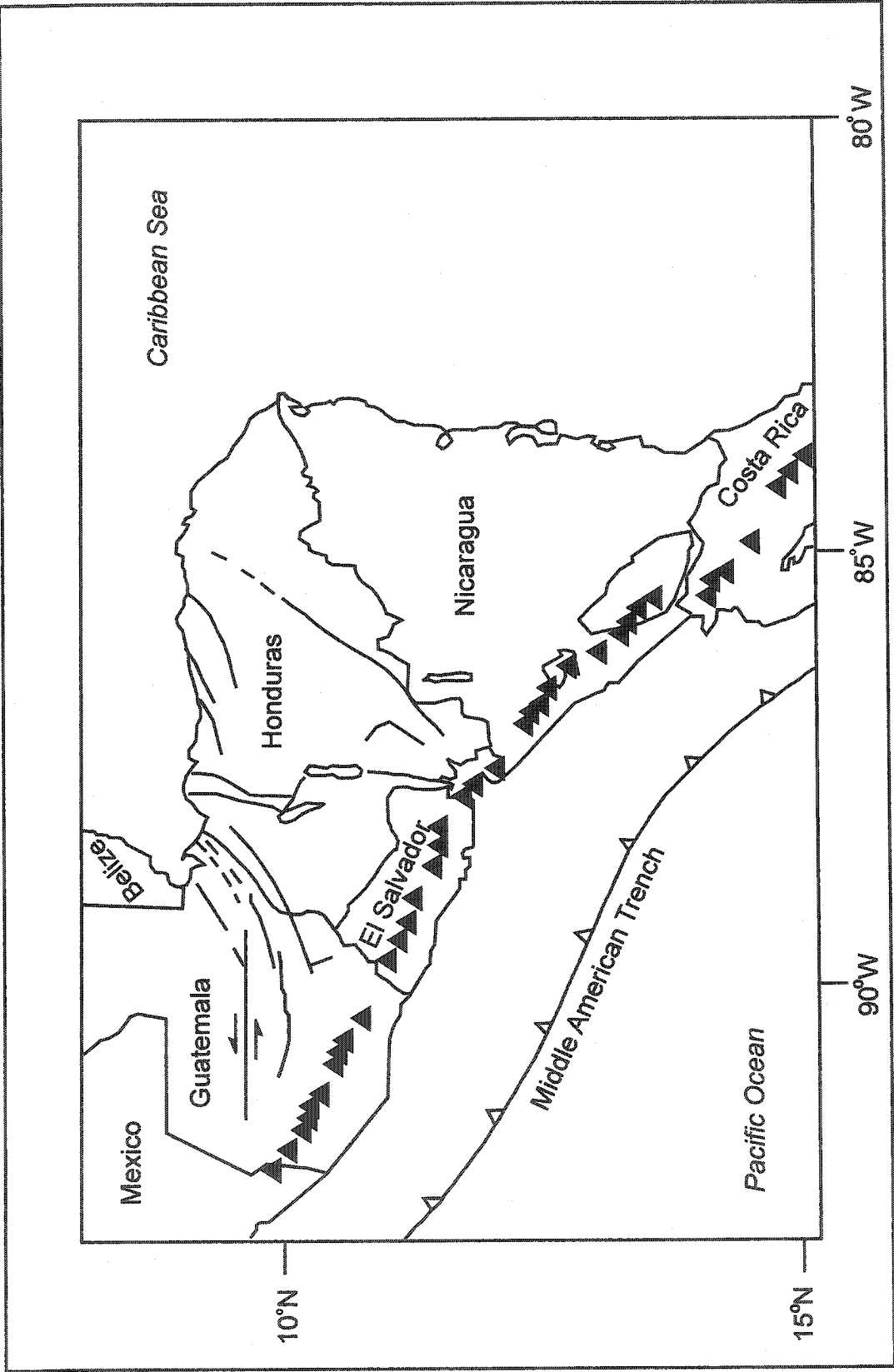
Central America, Ilopango Caldera, plagioclase textures, magma mixing

Introduction

Quaternary volcanism in Central America is a direct reflection of subduction processes (Stoiber and Carr, 1973; Carr and Stoiber, 1990; Patino *et al.*, 2000). Extending approximately 1100 km, the Central American volcanic arc reaches from the Guatemala-Mexico border to northern Panama. The Quaternary volcanoes lie parallel to the Middle American Trench, where the Cocos plate subducts underneath the Caribbean plate at a convergence rate of 9.6 cm/yr (Fig. 3.1; Molnar and Sykes, 1969; Dengo *et al.*, 1970; DeMets *et al.*, 1990). Divided into eight distinct segments, the Central American volcanic arc is separated by offsets believed to be tears in the subducting slab (Stoiber and Carr, 1973; Carr and Stoiber, 1977). Two sources have been identified as contributors to Central American volcanism, an EMORB source and a modified mantle source comprised of MORB and marine sediment input (Carr *et al.* 1990). The volcanic front, comprised of stratovolcanoes, dome complexes, caldera systems and cinder cones, offers scientists an opportunity to understand active tectonic-magmatic processes.

To understand the role subduction processes play in caldera systems, it is important to understand the magmatic evolution of these systems. Carr *et al.* (1982) suggest that a thicker crust beneath Guatemala and El Salvador increases fractional

Figure 3.1 Map of Central America. Black triangles represent the volcanic front. Black dashed lines and lines with arrows represent faults. Modified from Patino *et al.* (2000).



crystallization, giving rise to the presence of silicic volcanism. Calderas in Guatemala have been relatively well documented, but the calderas located in El Salvador have received little attention.

The silicic centers in Guatemala are lake filled calderas with histories of catastrophic eruptions located close to major cities and are strikingly unique in terms of magmatic evolution. Amatitlán caldera is an evolving silicic system, with a history of nine pyroclastic eruptions, decreasing in volume over the last 300,000 years (Wunderman and Rose, 1984). Activity began at Atitlán caldera at about 1.4 Ma entailing four episodes of caldera collapse, with the youngest occurring 84,000 years ago. The lake filled caldera is currently occupied by three andesite stratovolcanoes, two of which exhibit phenocryst textures suggesting magma mixing (Newhall, 1987; Halsor and Rose, 1991). Ayarza is believed to be two coalescing calderas underlain by two separate evolving systems, with one system more mafic than the other (Peterson and Rose, 1985).

In El Salvador the volcanic chain extends 220 km in length striking N74W (Stoiber and Carr, 1973). Two calderas exist in El Salvador, Coatepeque and Ilopango, both lake-filled and close to major cities. Coatepeque, estimated to have formed approximately 70 ka, has experienced at least two major collapses associated with catastrophic eruption of biotite bearing rhyodacitic tephra. The last eruption was followed by emplacement of cinder cones and silicic domes, the last dome growth occurring 10,000 years ago (CEL, 1992). Ilopango has an eventful history of catastrophic, explosive eruptions associated with caldera collapse, as well as dome growth events. Ilopango is most famous for its AD 429 eruption in which 18 km^3

DRE (dense rock equivalent) of dacitic to rhyolitic ash and pumice were erupted, alternating from phreatomagmatic to magmatic activity (Hart, 1981; Dull *et al.*, 2001) and devastating the Early Classic Mayan civilization (Sheets, 1979). More recently in 1880, Ilopango experienced dome growth in the center of the caldera lake initiated by injection of more mafic material (Richer *et al.*, *in press*) destroying the lakeshore village of Atuscatla (Goodyear, 1880).

This study reports new field, petrographic, mineralogical and chemical data from intracaldera lavas and pyroclastic rocks of Ilopango Caldera. The data are placed into a stratigraphy, allowing changes in magma composition over time to be evaluated. The geochemical data are then compared with other selected silicic volcanic centers along the Central American arc, to establish a regional perspective of Ilopango in relation to the other centers.

Previous Work

Williams and Meyer-Abich (1955) conducted reconnaissance in Central America, reporting formation of the Ilopango depression in the Plio-Pleistocene followed by two caldera cycles and further silicic volcanism. Sapper (1925) was the first to suggest the lake lies in a collapse basin, and Weyl (1955) recognized that Ilopango was the source of all the Tierra Blanca units. A German team of geologists, in collaboration with the Ministry of Public Works of El Salvador, produced a geologic map of El Salvador (Weber and Wiesemann, 1978). Hart and Steen-McIntyre (1983) and Hart (1981) studied the TBJ eruption in detail, determining that Ilopango was the source and had erupted $\sim 18 \text{ km}^3$ DRE of tephra. The TBJ deposit

consisted of two phases, with each phase beginning with a less evolved, less vesicular magma with a higher phenocryst content and becoming more evolved, more vesicular and less phenocryst-rich over time. This suggested to Hart (1981) that the chamber was stratified, and due to its unique chamber geometry, the lower depths of the chamber were the first to be tapped, migrating towards the more evolved magma. During the course of geothermal exploration projects, CEL (1992) refined the stratigraphy and defined three additional units stratigraphically beneath TBJ, informally named TB2, TB3 and TB4. These eruptions have been temporally constrained to the last 56.9 \pm 2.8/-2.1 ka (Rose *et al.*, 1999). Dull *et al.* (2001) reported new AMS ages on new samples of TBJ and reassessed the previously dated samples to determine a revised age of A.D. 420 \pm 20.

Sample Preparation and Analytical Techniques

Lava samples were collected from domes which were being quarried, as well as from outcrops exposed in 2001 due to a series of earthquakes. Pumice samples were collected from primary tephra fall units in order to best represent original magma chemistry. Twenty-seven petrographic thin sections were prepared from rock samples collected in the study area. Careful examination of each sample was made with a petrographic microscope to characterize phenocryst assemblages and textures, and to select unaltered, uncontaminated samples for whole-rock geochemical analysis and $^{40}\text{Ar}/^{39}\text{Ar}$ radiometric age dating. Phenocryst and groundmass percentages were

calculated from total rock volume. When available, polished thin sections were used to determine the compositions of opaque minerals.

From the thin sections, 21 samples were chosen for whole rock analysis. The samples selected were crushed in a steel jaw crusher to produce small rock fragments < 1 cm. After grinding, samples CM196-01 and CM224-01 were hand-picked under a binocular microscope to separate out heterogeneities due to magma mingling. All samples were then powdered in an alumina shatterbox and divided into aliquots of 25 g.

Major and trace element analyses was performed using X-ray fluorescence (XRF) spectrometry methods. X-ray fluorescence of whole rock powders was carried out with a Philips PW2440 4 kW automated XRF spectrometer system at the Geochemical Laboratories, McGill University, Canada, by Tariq Ahmedali and Glenna Keating. Major elements (Si, Ti, Al, Fe, Mn, Mg, Ca, Na, K, P) and trace elements (Ba, Ce, Co, Cr, Ni, Sc, and V) were analyzed on 32-mm diameter fused beads and trace elements (La, Ga, Nb, Pb, Rb, Sr, Th, U, Y, Zr) were analyzed on 40-mm diameter pressed powder pellets. Calibrations were prepared using between 15 to 40 International Standard Reference Materials (Govindaraju, 1994). The overall precision (i.e. sample preparation and instrument analysis) is within 0.5% relative, and the instrument precision is within 0.3% relative. Accuracy for SiO₂ is within 0.5% and for all other major elements within 1%. For trace elements accuracy is within 5%. Replicates of internal standard UTR-2 were submitted and compared to previously determined results, and samples CM170-01 and CM195-01 were submitted twice each showing good replication (Table 3.1). Major elements are

reported as wt.% oxides and trace elements as ppm. Analyses are reported as 100% anhydrous, total Fe is expressed as FeO*, and BaO is recalculated to Ba.

TABLE 3.1 WHOLE-ROCK GEOCHEMISTRY REPLICATES

Sample	UTR-2 ¹	UTR-2	ABC-2	ABC-3	ABC-4	CM170-01	170-A	CM195-01	195-A
wt.%									
SiO ₂	74.16	73.30	73.89	73.79	73.75	69.31	69.19	70.60	70.77
TiO ₂	0.24	0.25	0.23	0.23	0.24	0.32	0.32	0.30	0.31
Al ₂ O ₃	10.44	10.54	10.43	10.50	10.44	14.88	15.09	15.16	14.97
Fe ₂ O ₃	4.43	4.83	4.61	4.62	4.63	3.06	2.92	2.64	2.74
MnO	0.09	0.09	0.09	0.10	0.09	0.11	0.11	0.11	0.11
MgO	0.05	0.26	0.14	0.14	0.14	0.82	0.89	0.76	0.79
CaO	0.18	0.51	0.20	0.20	0.21	2.99	3.07	2.9	2.82
Na ₂ O	5.52	5.39	5.51	5.54	5.52	4.28	4.39	4.43	4.61
K ₂ O	4.39	4.25	4.42	4.42	4.42	2.24	2.24	2.23	2.26
P ₂ O ₅	0.01	0.01	0.02	0.02	0.02	0.11	0.11	0.11	0.11
LOI	0.32	0.49	0.50	0.47	0.48	1.79	1.89	0.88	0.66
Total	99.83	99.92	100.04	100.03	99.94	99.88	100.23	100.12	100.15
ppm									
BaO	N.D.	0	0	0	21	1110	1154	1202	1242
Ce	179	180	190	187	189	33	0	34	17
Co	0	0	0	0	0	0	10	0	0
Cr ₂ O ₃	0	95	75	93	76	16	22	17	0
La	79	66	66	68	73	12	0	0	0
Ni	3	52	0	3	0	21	0	0	0
Sc	0	0	0	0	0	12	0	0	0
V	0	18	0	0	0	40	0	21	0
Ga	33	32	33	33	32	15	15	14	14
Nb	91	57	57	57	57	3	4	3	4
Pb	25	26	20	20	20	8	7	3	8
Rb	137	136	134	134	133	51	48	50	51
Sr	1	1	0	0	0	317	317	304	300
Th	17	19	18	19	19	0	0	0	0
U	4	5	5	5	5	5	5	5	5
Y	121	121	113	112	113	21	17	18	18
Zr	1174	1046	1049	1048	1047	155	156	160	163

Notes: N.D. = not determined; ABC-X = UTR-2

¹Stix et al., 1995

To build a robust data set I choose incompatible elements as tracers and compared my data to those of previous studies. To understand the magmatic evolution of silicic systems, enrichment of the incompatible elements provides the best proxy of evaluation. Under this premise, I used major elements and trace elements Ba, Rb, Sr and Zr as tracers for magma evolution at both Ilopango Caldera

and for the regional comparison of Central American silicic centers. I only chose datasets of others where these trace elements had been determined and where the sample was clearly identified.

From the petrographic sections, two samples (CM170-01 and CM163-01) with crystalline groundmass were chosen for $^{40}\text{Ar}/^{39}\text{Ar}$ geochronology and submitted to Dr. Andrew Calvert at the United States Geological Survey, California, U.S.A. Since the phenocrysts generally exclude potassium and can include nonradiogenic argon, groundmass was separated from crushed rock magnetically. Groundmass concentrates were cleaned with deionized water in an ultrasonic bath and handpicked for purity. Separates were irradiated in the central thimble of the USGS TRIGA reactor in Denver, Colorado for 2 hours. The J neutron-flux parameter for each sample packet was determined from Taylor Creek sanidine (TCR-2). TCR-2 sanidine is a secondary mineral standard calibrated at 27.87 Ma against the primary standard, SB-3 biotite, a 162.9 ± 0.9 Ma mineral whose age was determined using first-principles calibrations (Lanphere and Dalrymple, 2000). Monitors were run using the continuous argon-ion laser system attached to the MAP 216 mass spectrometer (Dalrymple, 1989) at the USGS-Menlo Park. Groundmass unknowns were step heated using a low-blank resistance furnace with a molybdenum crucible controlled by an infrared pyrometer. Reactive gases were removed by two SAES AP-10 getters and argon isotopes were measured with the MAP spectrometer. Measured ratios were corrected for instrumental blanks, mass discrimination, abundance sensitivity, decay and reactor-derived interfering isotopes. Errors reported at the 1σ level.

Sample CM250-01, lab sample number WW4157, was submitted to the Center for Accelerator Mass Spectrometry (CAMS), Lawrence Livermore National Laboratory, Livermore, California, for ^{14}C age analysis. The sample was processed at the ^{14}C Laboratory of the U.S. Geological Survey in Reston, Virginia. The $\delta^{13}\text{C}$ value was -25 according to the methodology of Stuiver and Polach (1977). The quoted age is in radiocarbon years (BP) using the Libby half-life of 5568 years.

Rock Descriptions

Lava domes and intracaldera lavas

There is a compositional range of basaltic-andesite to rhyolite lava domes, as well as basaltic cinder cones contained within the topographic rim of the Ilopango Caldera. I eliminated some samples due to alteration but was able to successfully analyze three groups: 1) a closely spaced group of domes in the north-northwest, 2) Islas Quemadas, erupted in 1880 and located in the center of the caldera and 3) a closely spaced group in the south-southeast part of the caldera (Fig. 3.2). While in the field, I was able to sample the most evolved domes within the caldera with the exception of the southern dome named Cerro Tepeulo.

Figure 3.2 Intracaldera topographic map of Ilopango showing area of study.
Modified from Instituto Geográfico Nacional (1981, 1984) and Weber and
Wiesemann (1978).

Northern Lavas

The northern lavas are comprised of two distinct domes on the mainland and an island named Isla Chacagaste (Fig. 3.2). The domes are presently being quarried which allowed observation of cross-sections through the domes, as well as obtain fresh samples for geochemistry. The two domes are approximately 500 to 700 m apart, while Islas Chacagaste is located approximately 500 km south. The tallest dome rises to an elevation of ~600 m a.s.l. or 150 m above lake level. The island is approximately 30 to 40 m above lake level and extends in a northerly direction below the lake surface according to the bathymetry map (Instituto Geográfico Nacional, 1981).

Northeast Lava Dome The rock of the northeast lava dome is a grey, friable rhyolite displaying flow banding, perlitic textures and inclusions of mafic rock. Phenocrysts make up 10 to 12 % of the rock by volume and are set in a crystalline matrix. Located closest to the Corinto Club, this dome is the larger of the two northern lava domes. While difficult to observe the dome shape, there appears to be a central, altered section, which is orange in color with vertical lava dikes. The lava dikes are defined by perpendicular cooling joints. The central orange section grades laterally into grey rock which displays subvertical flow bands. Laterally flanking the dome is a brecciated zone comprised of angular blocks of dome rock up to 8 m across which are hosted in a finer grained matrix. Portions of the gray, unaltered lava exhibit

perlitic texture and contain rounded, mafic inclusions up to 5 cm in diameter. Overlying the northeast dome is a white fall-out deposit identified as TB4 (J. Vallance, personal communication, 2002).

Petrography The rock of the northeast dome is hiatal porphyritic with a phenocryst assemblage of plagioclase > hornblende > orthopyroxene ≥ opaque oxides in a microlitic groundmass. Plagioclase occurs as subhedral to anhedral phenocrysts 0.06 to 3 mm in length. Irregularly shaped, large and clear glass inclusions, referred to from now on as LAC inclusions, following Halsor (1989), are present in plagioclase phenocrysts demonstrating embayed edges and overgrowth rims are common (Fig. 3.3A,B). Plagioclase is observed as inclusions in hornblende phenocrysts. Hornblende crystals form subhedral to euhedral, prismatic to needle shaped phenocrysts ranging from 0.3 to 3.9 mm in length. Hornblende displays light brown to dark brown pleochroism in plane light suggesting a more iron-rich composition. Many hornblende phenocrysts have melt channels similar to LAC texture within the crystal (Fig. 3.4A). Hornblende occurs commonly as discrete crystals, and less commonly intergrown with orthopyroxene and as inclusions in orthopyroxene (Fig. 3.4B). Orthopyroxene occurs as subhedral to anhedral more equant phenocrysts than the hornblende 0.1 to 1.6 mm. The orthopyroxene phenocrysts are present as discrete crystals and cumulo porphyritic with plagioclase, hornblende and opaque phenocrysts. Opaque phenocrysts occur commonly as discrete crystals and cumulo porphyritic with plagioclase and hornblende phenocrysts,

Figure 3. 3 Photomicrograph of plagioclase phenocrysts from the northeast lava dome demonstrating LAC texture. A) Plagioclase phenocryst demonstrating LAC texture and embayed edges. Note the plagioclase fragments and the trachytic groundmass microlites of plagioclase. B) Plagioclase phenocryst demonstrating LAC texture and an overgrowth rim. Note plagioclase fragment with an absence of LAC texture and the presence of embayed edges. Photomicrograph taken in crossed polars, field of view 2 mm.

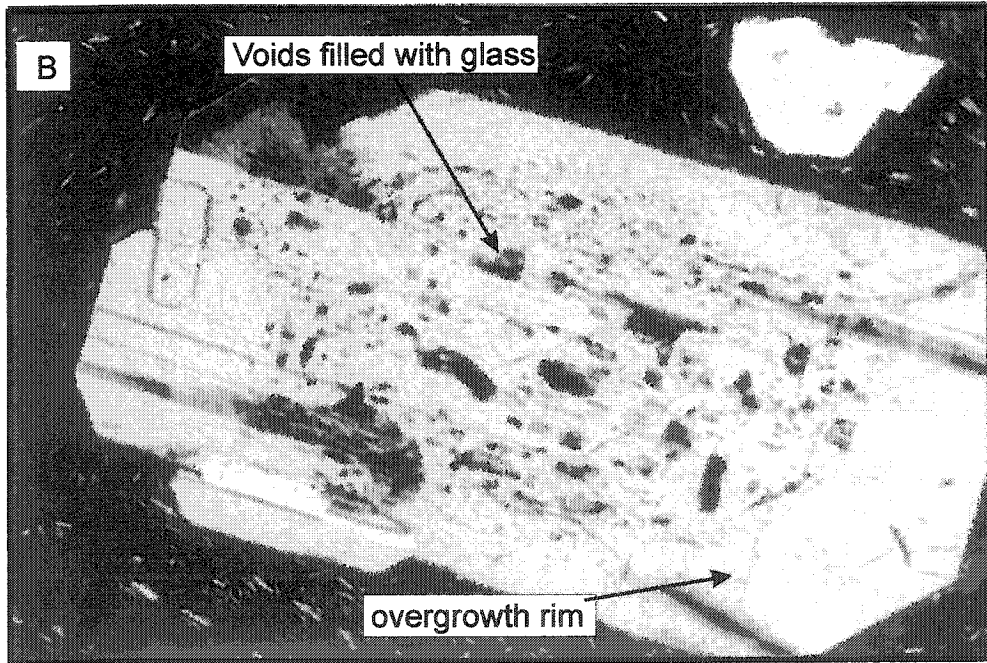
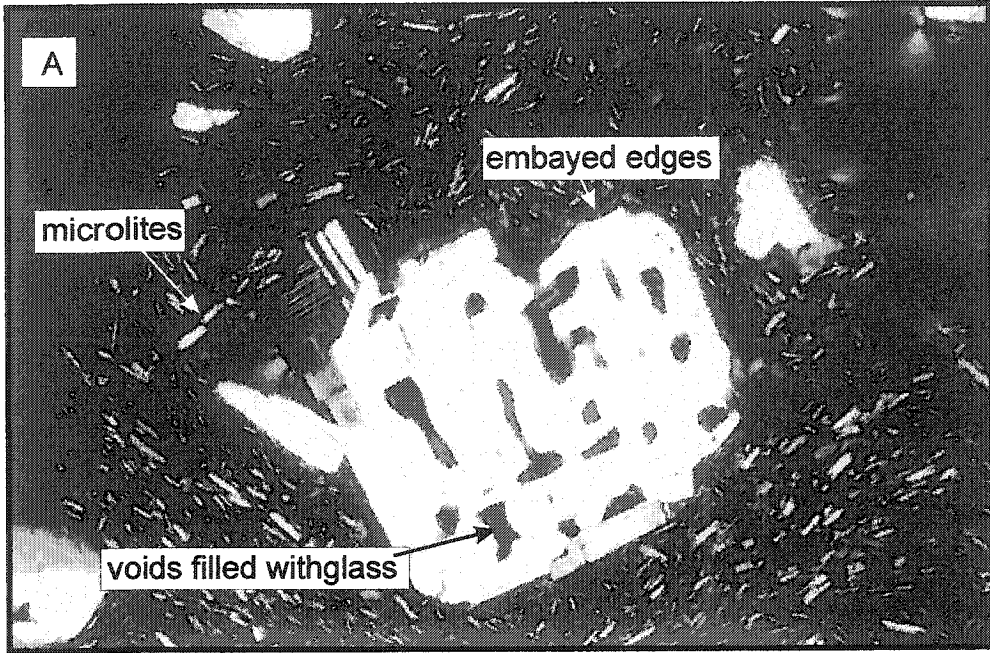
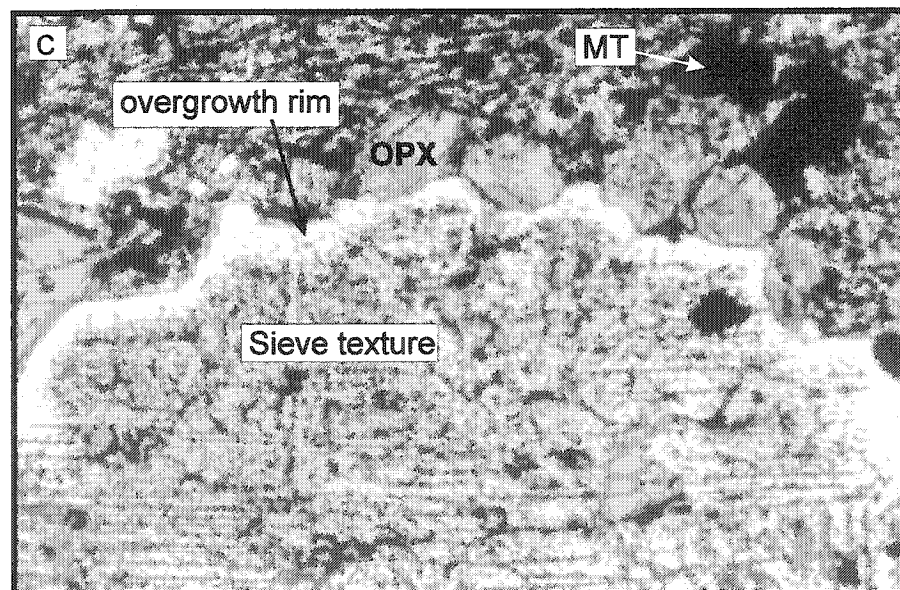
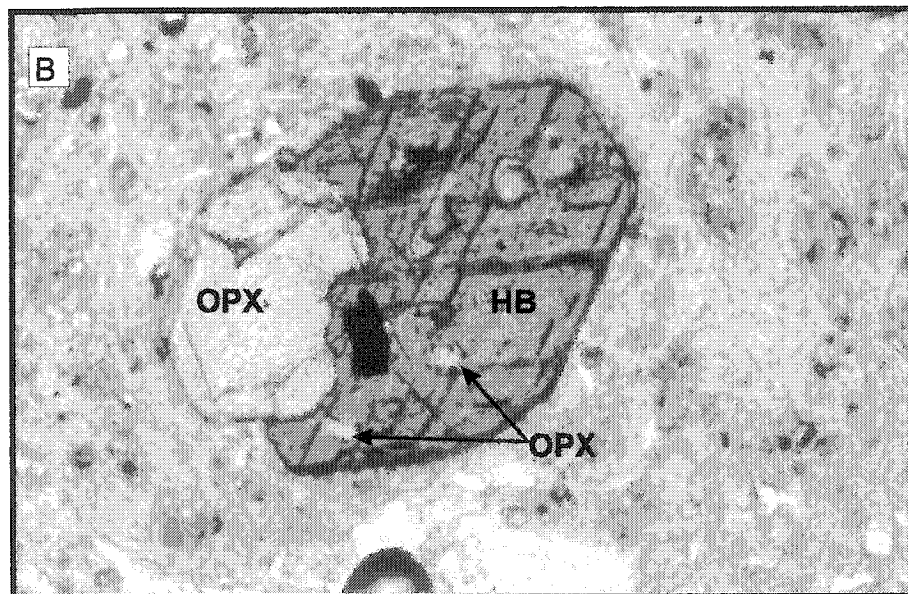
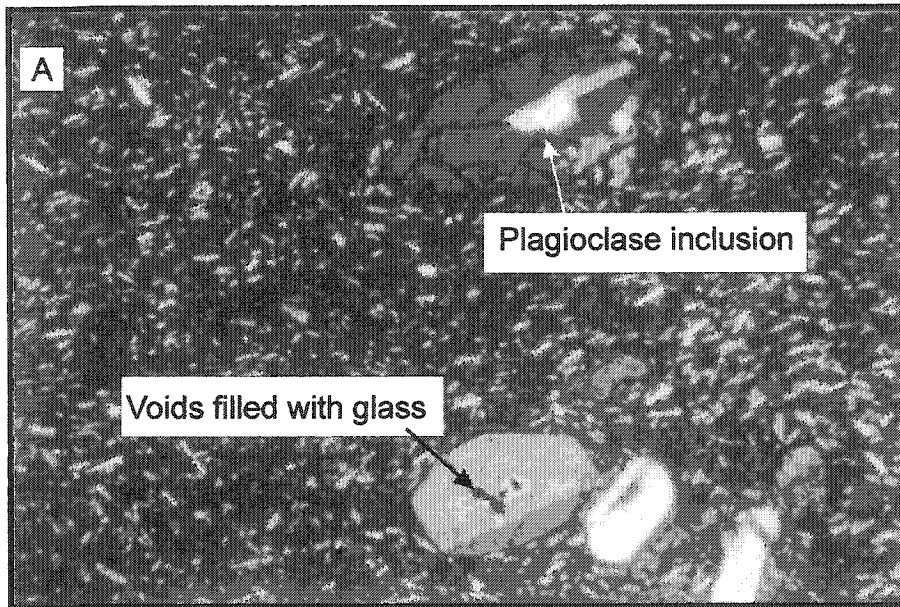


Figure 3.4 Photomicrograph of phenocryst textures represented by the northeast lava dome. A) Subhedral to euhedral prismatic hornblende phenocrysts with plagioclase inclusions and demonstrating LAC like voids. B) Phenocryst relationships demonstrated by hornblende (HB) and orthopyroxene (OPX) phenocrysts which are intergrown and orthopyroxene inclusions in the hornblende. C) Sieve textured plagioclase with an overgrowth of plagioclase found as a phase in the mafic inclusion of the northeast lava dome. The overgrowth rim appears to be squeezing between the euhedral orthopyroxene phenocrysts, suggesting that the orthopyroxene crystals were there previous. Note the groundmass is comprised of plagioclase and hornblende microlites. Photomicrograph taken in plain light, field of view 2 mm.



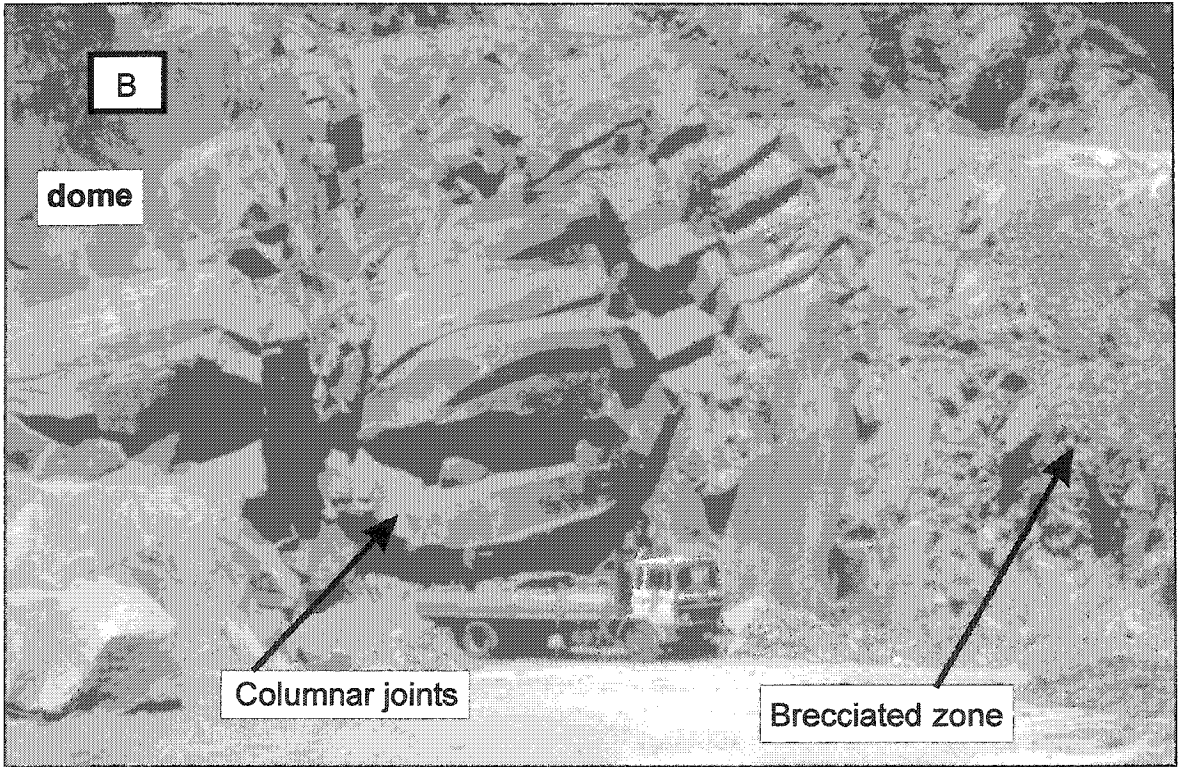
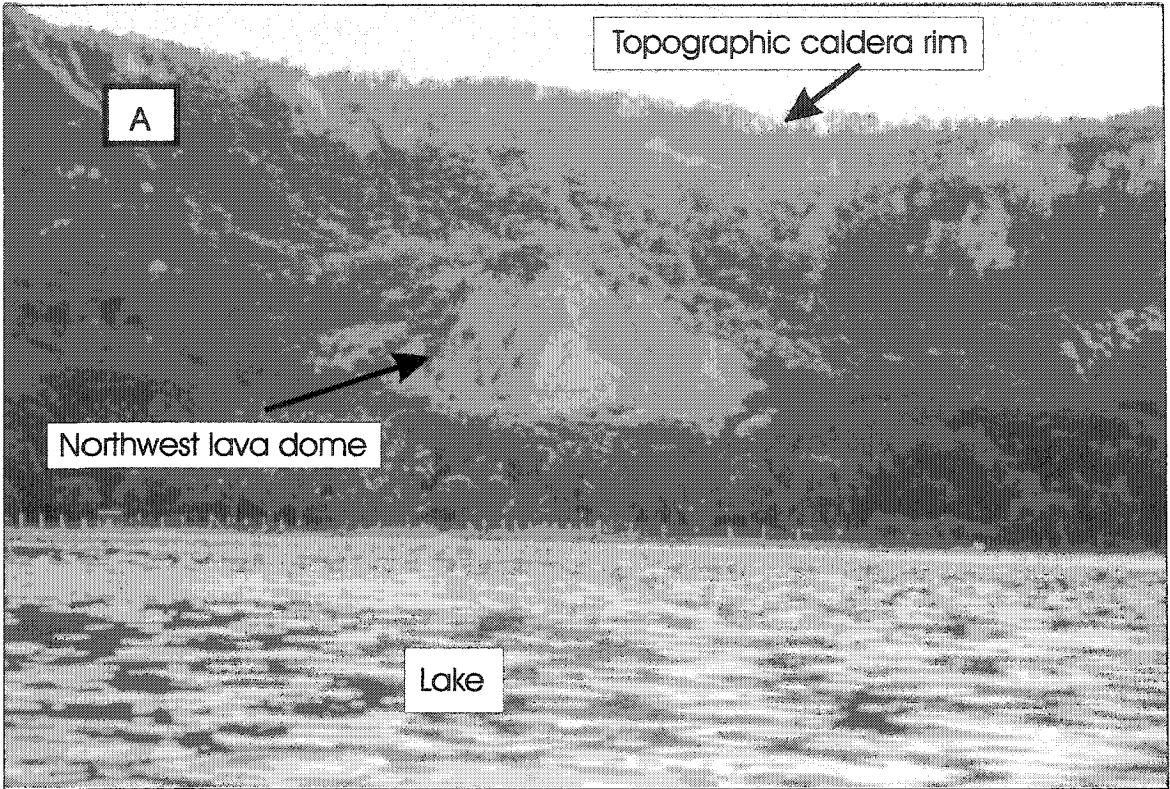
and occur less commonly as inclusions in plagioclase and hornblende. The groundmass comprises ~90 % of the rock by volume, containing 25 to 30 vol.% of plagioclase microlites and 70 to 75 vol.% light colored glass. The plagioclase microlites display a trachytic flow alignment. Vesicles are irregular in shape and comprise < 5 vol.% of the rock.

Hiatal, porphyritic mafic inclusions are a minor component of the northeast lava dome, comprising 1 to 2 % of the dome volume. Within these inclusions, phenocrysts make up 25 to 30 % by volume and are set in a microlite-rich, glass-poor groundmass. The phenocryst assemblage comprises plagioclase > orthopyroxene > clinopyroxene > opaque minerals. Plagioclase occurs as subhedral to anhedral phenocrysts 0.3 to 3.5 mm in length with tabular shapes, displaying central sieve textures and overgrowth rims (Fig. 3.4C). Orthopyroxene occurs as subhedral to anhedral, equant to lath shaped phenocrysts 0.7 mm in length. Clinopyroxene occurs as subhedral to anhedral phenocrysts commonly 0.4 mm in length commonly cumulo porphyritic with plagioclase, orthopyroxene and opaque minerals. Opaque crystals are typically rectangular in shape and occur on the order of 0.1 mm in length. The groundmass comprises 70 to 75 % of the inclusion by volume, containing approximately 55 to 60 vol.% plagioclase and hornblende needles in approximately 10 to 15 vol.% light colored glass. The mafic inclusions appear to be a minor component of the northeast lava dome, comprising 1 to 2 % of the dome volume. Vesicles are spherical and comprise < 5 vol.% of the rock.

Northwest Lava Dome The rock of the northwest lava dome is a gray, friable rhyolite. Phenocrysts make up 10 to 15 % of the rock by volume and are set in a glassy groundmass. Flow banding, columnar jointing and perlitic textures occur, but mafic inclusions were not observed. The northwest lava dome is the smaller of the two and located the farthest west. The northwest dome exhibits high-aspect-ratio lava dome morphology (Fig. 3.5A) with quaquaversal flow banding defining dome shape. Horizontally-oriented columnar joints with perlitic texture occur perpendicular to subvertical flow banding. The columnar joints appear to grade into a brecciated zone comprised of angular lava fragments and a matrix of finer material (Fig. 3.5B).

Petrography The rock of the northwest lava dome is hiatal porphyritic with a phenocryst assemblage of plagioclase > orthopyroxene > opaque minerals in a microlitic groundmass. By contrast with the northeast lava dome, hornblende is not observed. Plagioclase occurs as subhedral to anhedral phenocrysts 0.3 to 2.1 mm in length. Plagioclase phenocrysts commonly have embayed edges, and less commonly exhibit LAC textures and no sieve texture is observed. Normal oscillatory zoning is common with cores approximately An_{37} and rims approximately An_{25} . Glomeroporphyritic texture of plagioclase is common. Orthopyroxene occurs as subhedral to anhedral phenocrysts equant to blade shaped averaging 0.4 mm in length, more commonly cumulo porphyritic with plagioclase and less commonly as discrete crystals. The opaque minerals occur as subhedral to anhedral phenocrysts, equant in shape and typically 0.1 mm in length. The groundmass comprises

Figure 3.5 Photographs of the northwest lava dome. A) High-aspect morphology of the northwest lava dome in front of the topographic northern rim of the caldera. Dome approximately 500 m above lake level. B) Columnar joints perpendicular to the high aspect dome morphology. Flatbed quarry truck and man in red shirt for scale.



approximately 85 to 90 % of the total rock by volume, with plagioclase microlites displaying trachytic texture and occupying approximately 15 vol.%, and clear glass occupying approximately 70 vol.% of the total groundmass. Vesicles are elongated and comprise < 5 vol.% of the rock.

Islas Chacagaste The Islas Chacagaste lava is also a gray, friable rhyolite. Located directly south of the northwest lava dome, Islas Chacagaste is comprised of lava with an upper erosion surface marked by a soil layer and thick vegetation. Phenocrysts make up 10 to 15 % of the rock by volume and are set in a glassy groundmass. Subvertical flow bands are observed, but a dip direction was not obtained.

Petrography Islas Chacagaste lava is hiatal porphyritic with a phenocryst assemblage of plagioclase > orthopyroxene > opaque minerals in a microlitic groundmass. It therefore appears related to the northwest lava dome, also lacking hornblende. Plagioclase occurs as subhedral to anhedral phenocrysts 0.9 to 2.2 mm in length and less commonly as discrete crystals. Oscillatory zoning is observed, but reliable extinction angles were not obtained to determine compositional changes. LAC textures are common in the larger plagioclase phenocrysts, which occur as glomeroporphyritic clusters. Orthopyroxene occurs as subhedral to anhedral phenocrysts equant to blade shaped 0.3 mm in length, and is commonly cumulo- porphyritic with plagioclase and opaque phenocrysts. The opaque crystals occur as subhedral to anhedral phenocrysts 0.1 mm in length. Typically blocky to slightly rounded, the opaque phenocrysts are commonly found in cumulo- porphyritic

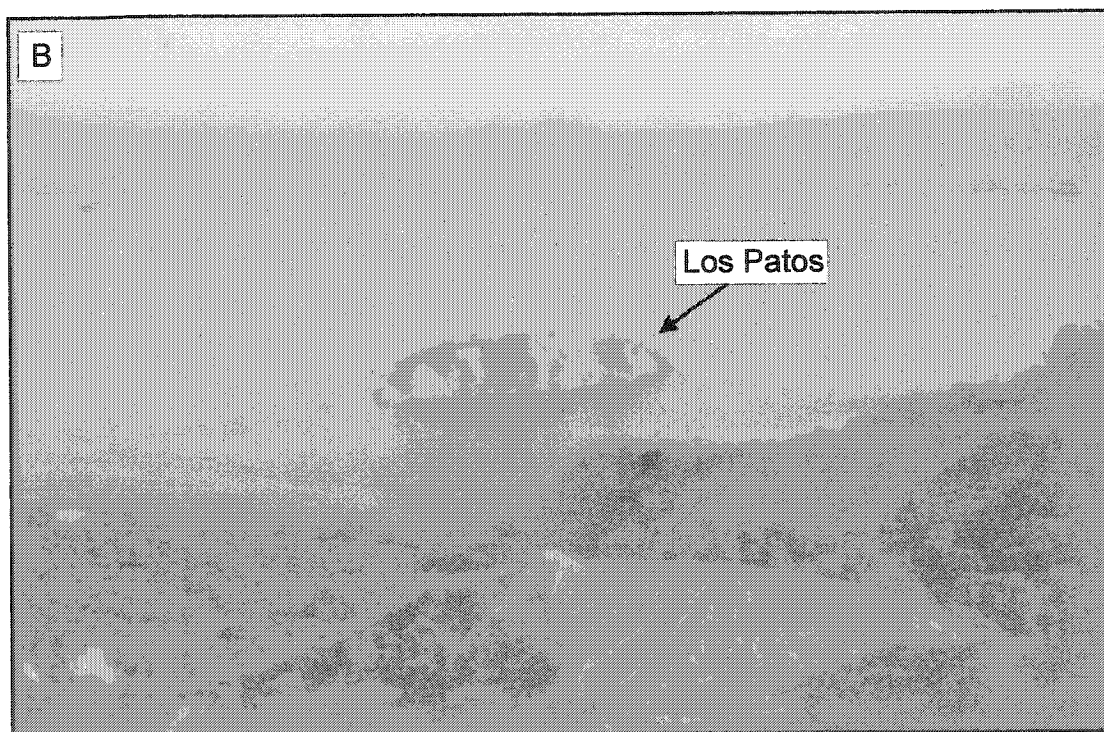
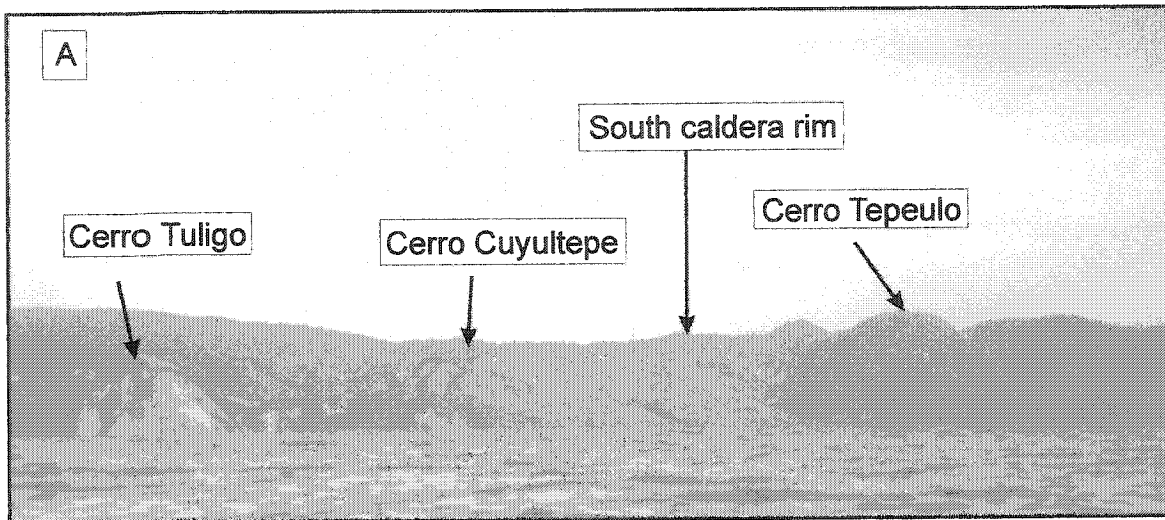
clusters and discrete crystals, and less commonly as inclusions in plagioclase. The groundmass comprises approximately 85 to 90 % of the total rock by volume, with trachytic plagioclase microlites making up approximately 5 vol.% and clear glass making up approximately 80 vol.% of the groundmass. Vesicles are elongated and comprise 5 to 10 vol.% of the rock.

Southern Lavas

In the southern part of the caldera, lava domes are comprised of Cerro Tuligo, Cerro Cuyultepe and an island named Isla Cerro Los Patos (Fig. 3.6). Located on the southwest side of Lake Ilopango, Cerro Cuyultepe and Cerro Tuligo are approximately 1 km apart, while Isla Cerro Los Patos is located approximately 1 km north of Cerro Cuyultepe. Cerro Cuyultepe rises approximately 250 m above lake level, Cerro Tuligo rises approximately 130 m above lake level and Isla Cerro Los Patos rises approximately 40 m above lake level at the time of this study.

Cerro Tuligo The rock of Cerro Tuligo is a grey, flow banded rhyolite with phenocrysts making up 15 to 20 % of the total rock by volume. This dome is the southeasternmost lava sampled. Cerro Tuligo demonstrates high-aspect dome morphology as observed in (Fig. 3.6A). As a result of the February 2001 earthquake, landslides defaced Cerro Tuligo, providing water access to fresh samples.

Figure 3.6 Photograph of South Lava Domes. A) Cerro Tuligo is defaced and rock is exposed, Cerro Cuyultepe in the middle and Cerro Tepeulo is the farthest to the west (right side of photograph). Cerro Tepeulo was not sampled. B) A photo of Cerro Los Patos demonstrating island shape and proximity to shore.



Petrography The rock of Cerro Tuligo is hiatal porphyritic with a phenocryst assemblage comprised of plagioclase > hornblende > orthopyroxene ≥ opaque minerals. Plagioclase occurs as subhedral to anhedral phenocrysts 0.3 mm to 1 mm in length. Oscillatory zoning is observed with cores of An₄₅ and more calcic rims of An₅₅. These same phenocrysts commonly exhibit LAC texture with embayed phenocryst edges.

Hornblende crystals form prismatic to needle-like subhedral to anhedral phenocrysts 0.4 to 1.9 mm in length. Hornblende displays light brown to dark brown pleochroism in plane light and occurs as discrete and cumulo porphyritic crystals with plagioclase and opaque phenocrysts. Some hornblende grains have a growth rim of opaque minerals. Orthopyroxene occurs as subhedral to anhedral phenocrysts 0.2 mm to 0.5 mm in length, exhibiting pale green to pale pink pleochroism in plane light. Orthopyroxene is found as inclusions in hornblende and appears to be intergrown with hornblende. Magnetite crystals occur as subhedral to euhedral phenocrysts 0.1 mm in length. Magnetite is less commonly found as inclusions in plagioclase and hornblende phenocrysts and more commonly occurs as discrete crystals or is cumulo porphyritic as previously mentioned. The groundmass comprises approximately 75 to 80 % of the rock by volume. Trachytic plagioclase needles make up 25 to 30 vol.% of the groundmass, and clear glass makes up 45 to 50 vol.%. Vesicles are elongated and comprise <5 vol.% of the rock.

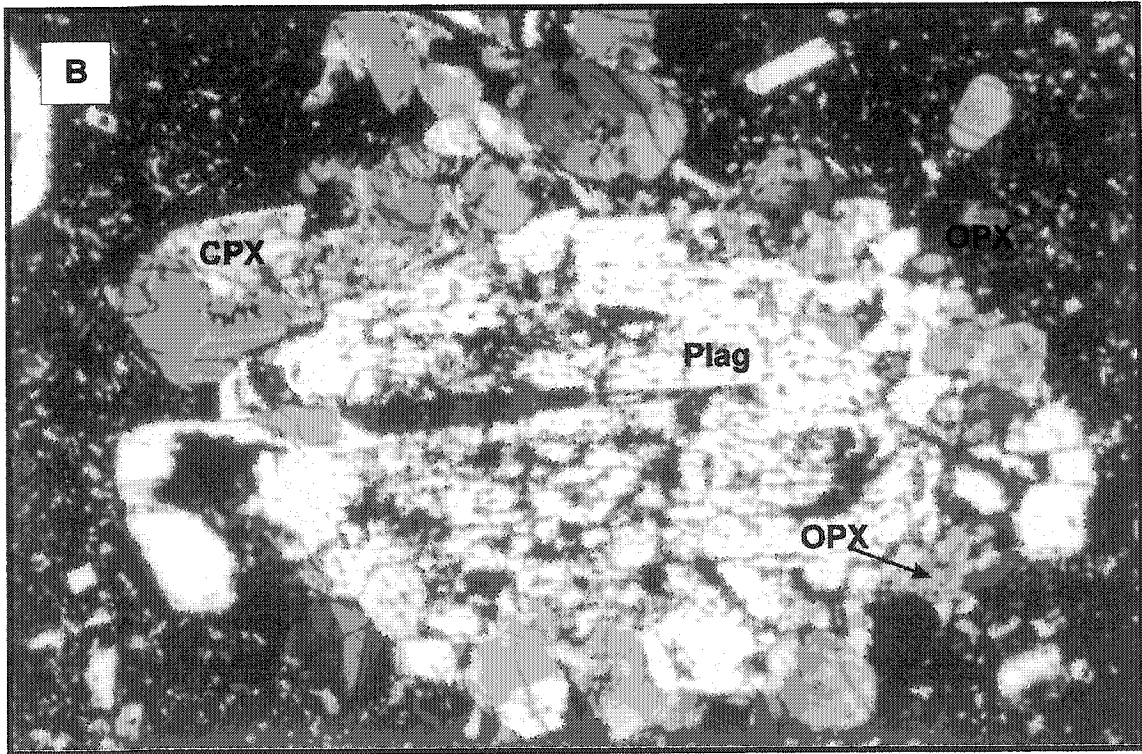
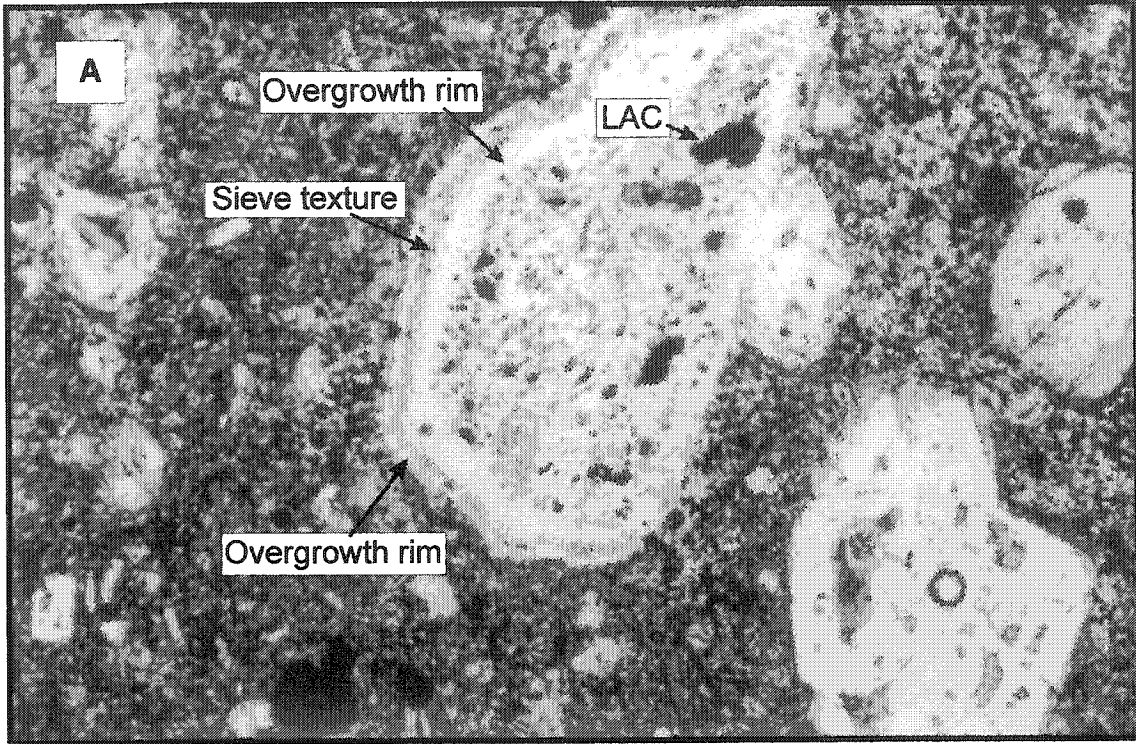
Cerro Cuyultepe The rock of Cerro Cuyultepe is a grey andesite with a pinkish tinge with phenocrysts making up 30 to 40 % of the rock by volume. This dome is

southwesternmost lava sampled. Cerro Cuyultepe demonstrates high-aspect dome morphology as observed in (Fig. 3.6A).

Petrography Cerro Cuyultepe lava is hiatal porphyritic with a phenocryst assemblage of plagioclase > clinopyroxene > orthopyroxene ≥ opaque crystals. Plagioclase occurs as subhedral to anhedral phenocrysts 0.5 mm to 1 mm in length. LAC texture is observed commonly with overgrowth rims and sieve textured edges (Fig. 3.7A). Plagioclase is commonly glomeroporphyritic with orthopyroxene, clinopyroxene and opaque minerals (Fig. 3.7B). Clinopyroxene occurs as equant to prismatic subhedral to anhedral phenocrysts 0.5 mm to 1 mm in length commonly with opaque overgrowth rims. Orthopyroxene occurs as subhedral to anhedral equant grains 0.3 to 0.5 mm in length commonly with opaque overgrowth rims and as microinclusions in orthopyroxene. Magnetite occurs as discrete phenocrysts up to 1 mm and as microphenocryst inclusions in plagioclase and pyroxene. Magnetite occurring as discrete crystals exhibits replacement by hematite, whereas magnetite inclusions are pristine, suggesting some secondary alteration has taken place. The groundmass comprises approximately 10-15 vol.% plagioclase microlites exhibiting pilotaxitic texture and approximately 15 vol.% glass. Vesicles are irregular in shape comprising 1 to 2 vol.% of the rock.

Isla Cerro Los Patos The rock of Isla Cerro Los Patos is a grey, friable rhyolite with phenocrysts making up 10 to 15 % of the rock by volume. Isla Cerro Los Patos is

Figure 3.7 Photomicrograph of phenocryst textures found in Cerro Cuyultepe. A) Plagioclase phenocrysts with inner LAC textures surrounded by an overgrowth rim of plagioclase, with sieve textured edges followed by another overgrowth rim. This may suggest two different episodes of reservoir disequilibrium. B) Plagioclase phenocryst with inner LAC textures glomeroporphyritic with clinopyroxene (CPX) and orthopyroxene (OPX) in a glassy microlitic groundmass. Scale for both photomicrographs is 2 mm for field of view.



elongate in the north – south direction, and flow-banded lava is well defined, dipping 45° S to subvertically (Fig. 3.6, 3.8A).

Petrography Los Patos lava is hiatal porphyritic with plagioclase > hornblende > pyroxene > opaque minerals in a glassy, microlitic groundmass. Plagioclase occurs as subhedral to anhedral phenocrysts 0.2 to 0.7 mm in length. The larger plagioclase phenocrysts have LAC textures and embayed edges, but sieve textures are not observed. Plagioclase with oscillatory zoning (Fig. 3.8B) was observed, but reliable extinction angles were not obtained to determine compositional changes. Glomeroporphyritic textures were common. Hornblende occurs as needle shaped subhedral to anhedral phenocrysts 0.07 mm to 0.3 mm in length, commonly with opaque overgrowth rims. Orthopyroxene occurs as equant to lath shaped, subhedral to anhedral phenocrysts 0.1 mm in length. Orthopyroxene is observed primarily as cumulo porphyritic with plagioclase and opaque phenocrysts. Opaque minerals are observed mainly as discrete phenocrysts and as inclusions in plagioclase phenocrysts. The groundmass is comprised of approximately 5 vol.% trachytic plagioclase microlites and 80 vol.% glass. Vesicles are irregular in shape comprising <2 vol.% of the rock.

Islas Quemadas

Islas Quemadas, formed in 1880, is a subaqueous dome with an emergent tip located at approximately the center of the Ilopango caldera lake (Fig. 3.9A). The Islas

Figure 3.8 Photographs of Cerro Los Patos. A) Well-defined flow banded lava dipping 45° S. Approximately 40 m high. B) Photomicrograph of an oscillatory zoned plagioclase observed in Los Patos. Cracks are made during thin section preparation. Scale 2 mm for field of view.

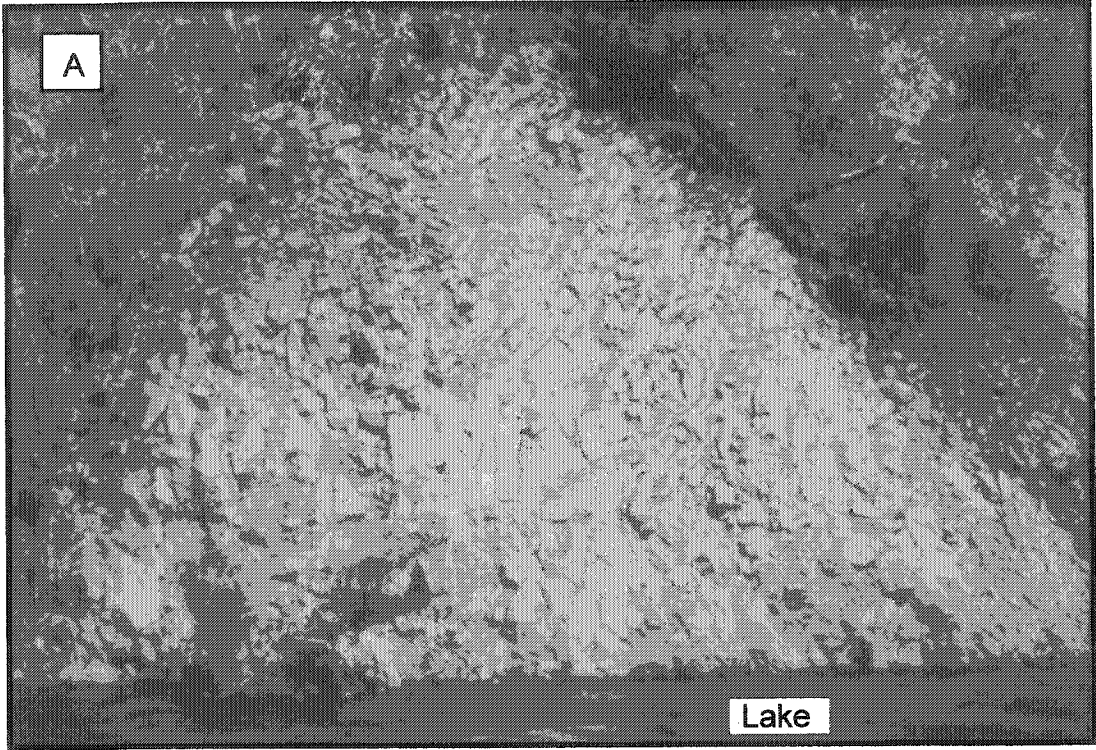
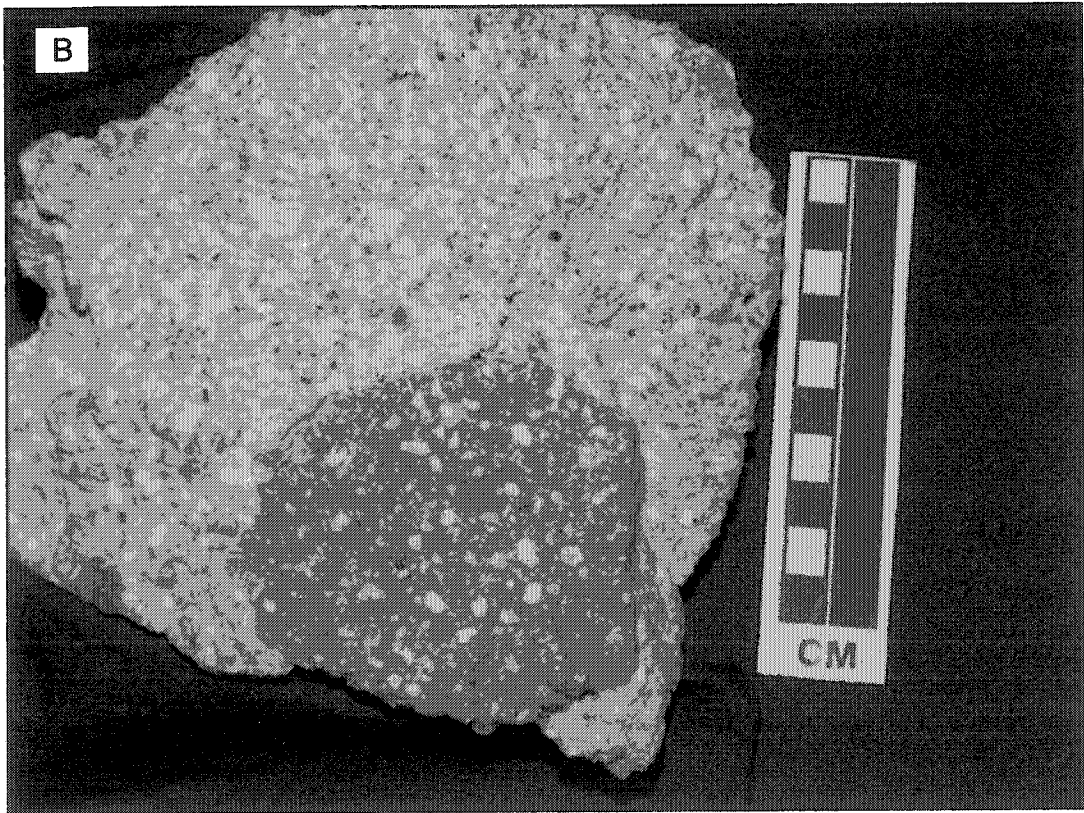


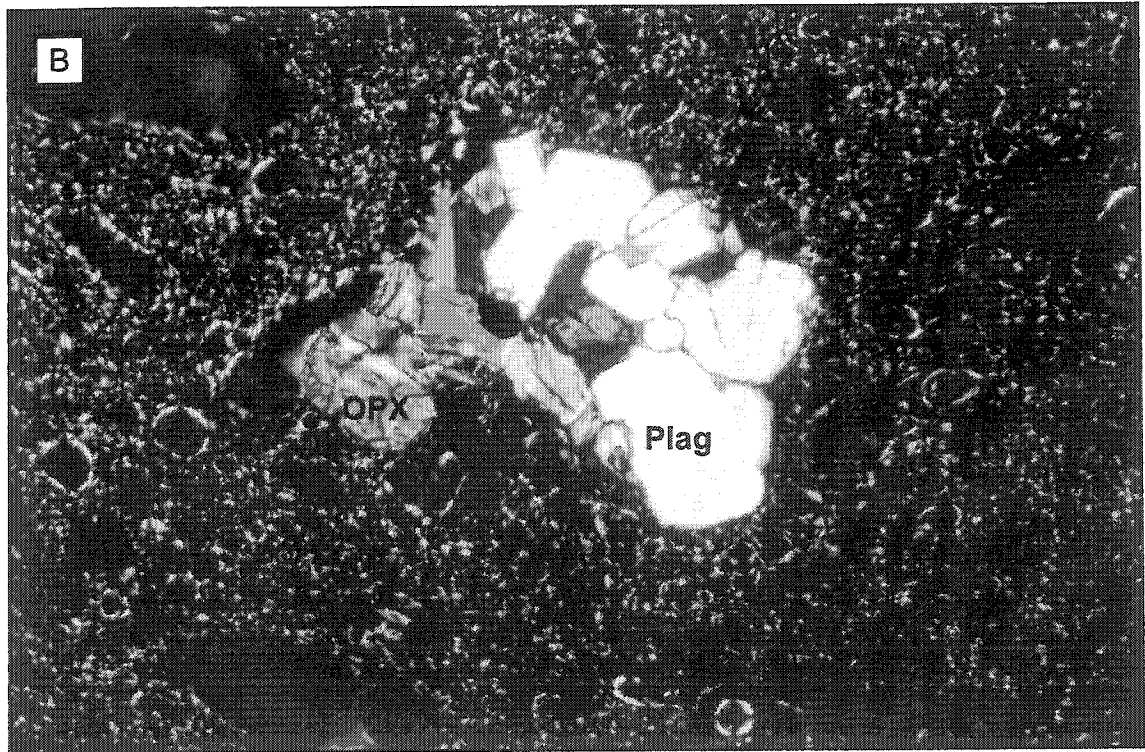
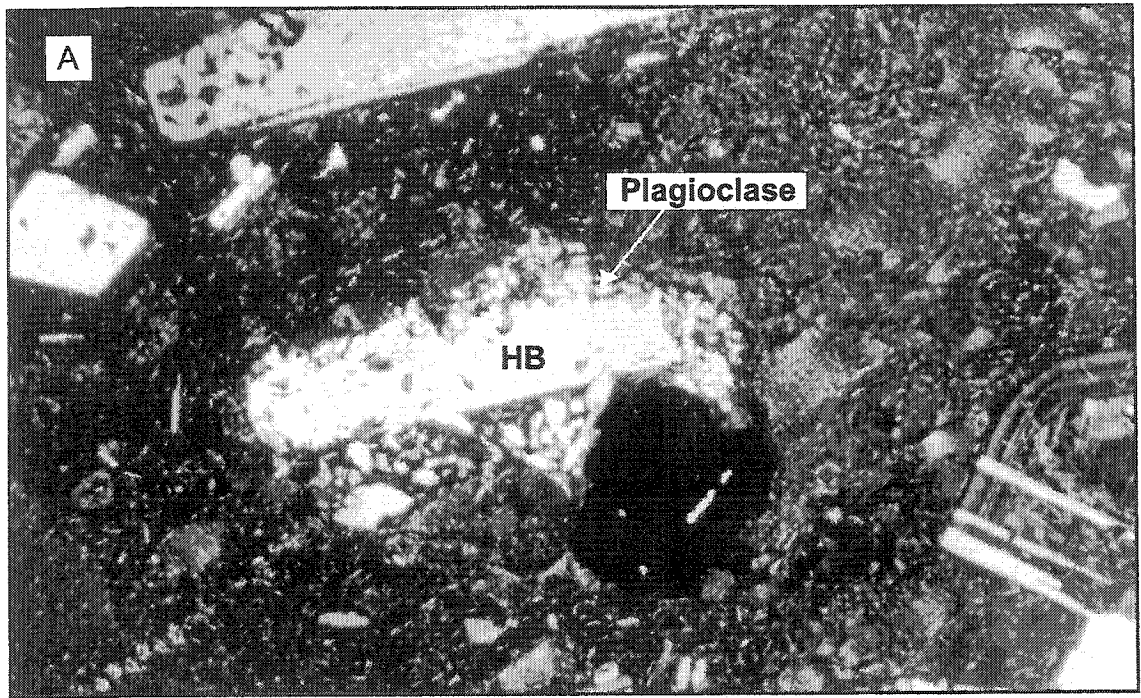
Figure 3.9 Photographs of Islas Quemadas. A) Islas Quemadas in the foreground. The defaced dome to the southwest is Cerro Tuligo. The caldera rim is in the middle ground and stratovolcano, San Vicente is observed in the background to the west. B) Photograph of the Islas Quemadas host dacite with a mafic enclave. Note the large plagioclase phenocrysts in both the host dacite and the mafic enclave.



Quemadas are expressed at the surface by two rock outcrops 3 to 5 m in height. The islands have been reduced in size since September 2002 due to earthquake activity (F. Thill, personal communication, 2003). The caldera lake is 240 m at its deepest point, thus the height of the Islas Quemadas is approximately 245 m (Instituto Geográfico Nacional, 1981). Islas Quemadas is 2 km long in the northeast-southwest direction and averages 1 km in width, with a volume of <1 km (Mooser *et al.*, 1958) The most striking feature about the Islas Quemadas is the mingling textures of two magmatic compositions. The Islas Quemadas host rock is dacitic with phenocrysts making up 20 to 25 % of the rock by volume, while the enclaves are basaltic andesite comprising 10 to 15 % of the rock by volume (Fig. 3.9B). The dacite is vesicular with large plagioclase phenocrysts. The mafic enclaves are subangular to subrounded in shape with visible olivine and plagioclase phenocrysts. Flow banding is not observed.

Petrography The dacitic host is hialal porphyritic with plagioclase > hornblende > orthopyroxene > opaque minerals in a glassy, slightly microlitic groundmass. The plagioclase occurs as subhedral to anhedral phenocrysts 0.1 to 3 mm in length. The phenocrysts have resorbed edges, some display a central LAC texture at the plagioclase core, while other plagioclase phenocrysts show a LAC textures towards the phenocryst edge mantled by a plagioclase rim. Sieve textures are observed as rims toward the phenocryst edge and are overgrown by a plagioclase rim. Hornblende occurs as subhedral to anhedral phenocrysts 0.1 to 2 mm in length. Phenocrysts are prismatic to lath-shaped many with coronas of plagioclase + orthopyroxene + magnetite (Fig. 3.10). Orthopyroxene occurs as subhedral to

Figure 3.10 Photomicrographs of phenocryst textures. A) Hornblende overgrown by a plagioclase corona. B) Tierra Blanca 4 (TB4) glomeroporphyritic texture comprised of plagioclase (Plag) and orthopyroxene (OPX). Scale is 2 mm for field of view.



anhedral phenocrysts 0.1 to 1.1 mm in length. Opaque minerals occur as subhedral to anhedral. Discrete phenocrysts of plagioclase, hornblende and opaque minerals are common, while less common are glomeroporphyritic clusters of plagioclase, hornblende, orthopyroxene and opaque minerals. The groundmass is comprised of approximately 65 to 70 vol.% pilotaxitic plagioclase microlites and 5 to 10 vol.% glass.

The Islas Quemadas mafic enclave is hiatal porphyritic basaltic andesite to andesite with plagioclase > olivine > orthopyroxene > opaque minerals ± clinopyroxene. The plagioclase occurs as subhedral to anhedral phenocrysts 0.1 to 3.5 mm in length. Phenocryst edges are commonly resorbed. Sieve texture is observed rimming phenocryst cores and then overgrown by a plagioclase overgrowth rim. Plagioclase is commonly cumulo porphyritic, and sieve texture zones exhibit a continuous rim outlining the entire cluster. LAC texture is less common. Olivine occurs as subhedral to anhedral phenocrysts up to 2 mm in length. Olivine commonly occurs as discrete phenocrysts and less commonly as cumulo porphyritic clusters with plagioclase. Orthopyroxene occurs mainly as discrete phenocrysts, but is also observed as cumulo porphyritic with plagioclase phenocrysts. Opaque minerals occur as subhedral to anhedral equant in shape more commonly as cumulo porphyritic clusters with plagioclase and less commonly as discrete phenocrysts. Opaque microphenocrysts occur as inclusions in plagioclase and orthopyroxene phenocrysts. The groundmass is comprised of approximately 70 to 75 vol.% pilotaxitic plagioclase and pyroxene microlites and 5 to 10 vol.% glass.

Pyroclastic units

San Agustín Block Unit - Pumice Breccia Two distinct facies define the San Agustín Block Unit: a basal fine ash layer and an overlying dacite pumice breccia. The pumice breccia is comprised of pumice clasts angular to ellipsoidal in shape, ranging in size from 0.02 to 3 m in width and < 1 % by volume of lava lithic fragments. The Pumice Breccia is found only inside the caldera and is traceable discontinuously around the lake, draping pre-existing topography with thicknesses ranging from 1 to 15 m. Magma mingling textures occur in the pumice breccia as rounded clots of more mafic compositions surrounded by the dacite and as planar bands alternating with the dacitic host.

Petrology The pumice breccia is hiatal porphyritic with plagioclase > hornblende > opaque minerals > orthopyroxene and vesicularites ranging from 49 to 87 % by volume. Plagioclase occurs as subhedral to anhedral phenocrysts 0.06 to 1.8 mm in length. Phenocryst edges appear to be embayed, while in other cases phenocrysts appear to have sharp edges, as if they are fragments. Some large phenocrysts display LAC texture. Hornblende occurs as subhedral to anhedral phenocrysts 0.1 to 1.3 mm in length and are prismatic to tabular in shape with inclusions of plagioclase. Hornblende is commonly cumulo porphyritic with plagioclase and opaque minerals. Opaque minerals occur as subhedral to euhedral equant shapes which are typically cumulo porphyritic as previously mentioned or as

microphenocrysts in hornblende. Aligned phenocrysts are common suggesting flow of magma.

Tierra Blanca 2 (TB2) Pumice from the TB2 airfall unit was observed outside the Ilopango caldera, reaching thicknesses of 10 to 20 cm where sampled and overlain by a paleosol layer. The pumice from TB2 is dacitic in composition with 5 to 7 vol.% phenocrysts comprising plagioclase > hornblende > opaque minerals > orthopyroxene ≥ apatite. Plagioclase occurs as subhedral to anhedral phenocrysts 0.2 to 1.4 mm in length. Phenocrysts display oscillatory zoning, but an angle of extinction was not obtained to determine core to rim compositional changes. Phenocryst edges are commonly embayed. No LAC texture or sieve textures are observed. Hornblende occurs as subhedral to euhedral phenocrysts prismatic in shape 0.16 to 1.2 mm in length. Opaque minerals are subhedral to anhedral and occur as discrete phenocrysts typically 0.2 mm in length. Orthopyroxene is a minor component observed to be approximately 0.2 mm in length and equant in shape. Apatite occurs as microlites. Vesicles are elongate in shape comprising 75 to 80 % by volume of the rock.

Tierra Blanca 4 (TB4) I observed the TB4 airfall unit both outside and inside the caldera. Outside the caldera TB4 was 1 to 2 m thick in the locations where sampled. Inside the caldera TB4 was 1 to 2 m thick above the northeast lava dome and 3 to 4 meters thick in a locality inside the caldera near the village of La Flor. The TB4 airfall unit is comprised of pumice and lithic fragments of lava. The pumice from TB4 is rhyolitic in composition with 3 to 5 vol.% phenocrysts of plagioclase > orthopyroxene ≥ opaque minerals > apatite. Plagioclase occurs as tabular to lath

shaped, subhedral to anhedral phenocrysts 0.1 to 0.6 in length. Phenocryst edges are embayed and occasionally fractured. No sieve or LAC textures are observed. Orthopyroxene occurs as equant grains 0.06 to 0.2 mm in length commonly cumulo porphyritic with plagioclase and less commonly as discrete phenocrysts (Fig. 3.10). Opaque minerals occur as microphenocrysts in the groundmass. Apatite occurs as microlites. Vecicles are irregular in shape comprising 80 to 85 vol.% of the rock.

Tierra Blanca Joven (TBJ) The following description is based on field observation by the C. P. Mann, but mostly on a description by Hart (1981) and Steen-McIntyre (1976). Pumice clasts are present as white pumice, grey pumice and pumice which is both white and grey. The phenocryst assemblage of the pumice clasts vary in percentage of plagioclase, hornblende, hypersthene and opaque minerals. Hart (1981) notes that hornblende is the dominant phase in the grey pumice and Steen-McIntyre (1976) recognized zircon, apatite and olivine phases. Honeycomb texture is observed in plagioclase. I observed the olivine phase in both the grey pumice and the white and grey mixed pumice clasts. The white pumice is highly vesiculated, whereas the vesicularity of the grey pumice is low. As the grey pumice approaches white, the vesicularity increases (Hart, 1981).

Results

Geochronology

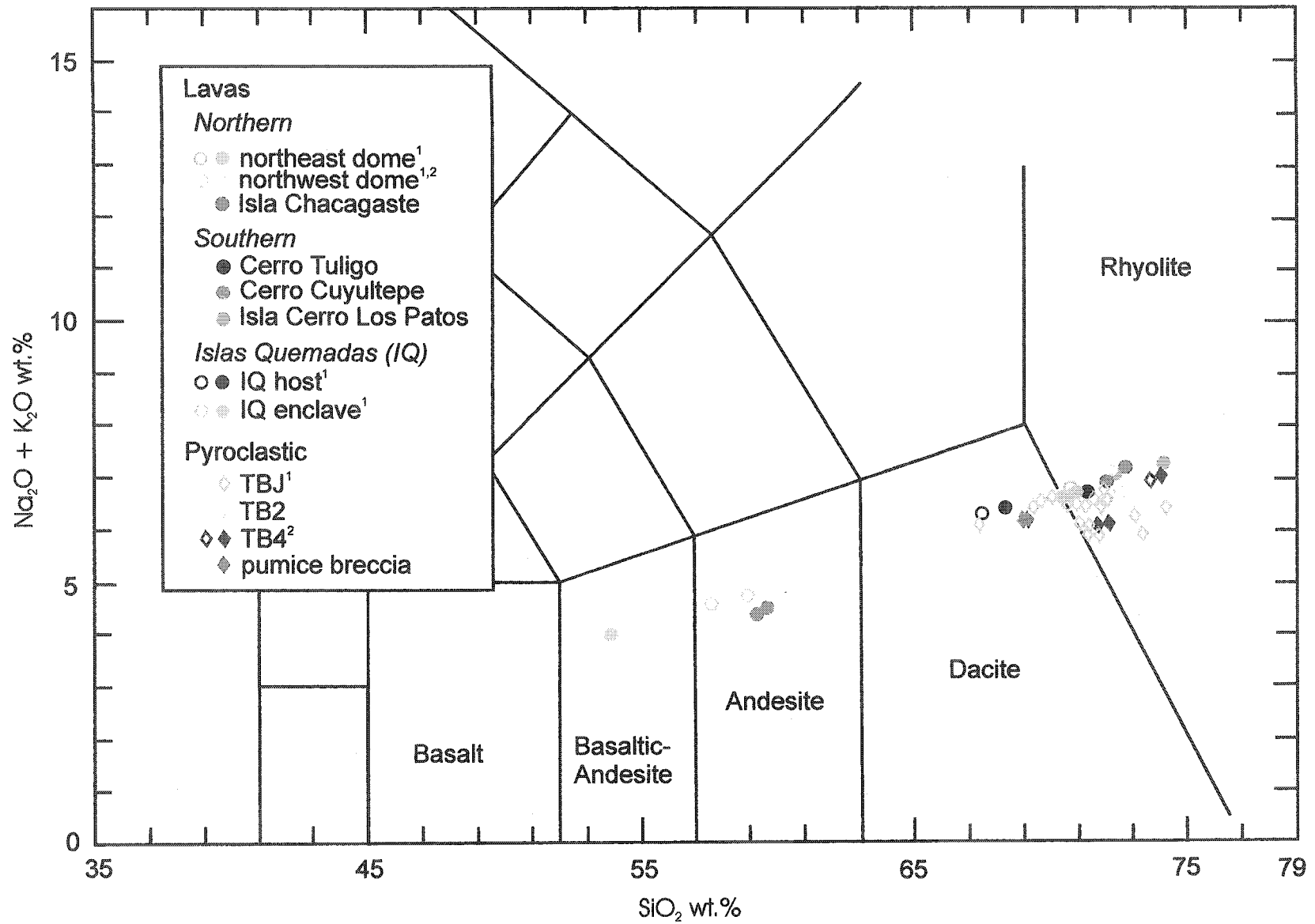
An additional ^{14}C age was determined on charred wood hosted a lacustrine unit below the San Agustín Block Unit. Mann *et al.* (*in press*) describes the sample location and field sampling techniques used. The radiocarbon contained in this sample was statistically indistinguishable from radiocarbon background standards, yielding a result of $>53,400$ y. B.P. This new value provides a new minimum limiting age on the San Agustín Block Unit.

The ages of two lava domes were determined by $^{40}\text{Ar}/^{39}\text{Ar}$ radiometric methods. Sample CM163-01, corresponding to the southwest andesite dome Cerro Cuyultepe, was dated at 359.3 ± 7.9 ka. Sample CM170-01, corresponding to the northeast rhyolite dome, was dated at 56 ± 1.9 ka. (Appendix 3.1; A. Calvert, personal communication, 2003).

Major and trace element data

Major and trace element concentrations for the Ilopango intracaldera lavas and extracaldera tephra are listed in Table 3.2 and Table 3.3. In general, the major-element data range from basaltic andesite (~ 54 wt.% SiO_2) to rhyolitic (~ 75 wt.% SiO_2) (Fig. 3.11; after Le Maitre, 1989) defining a calc-alkaline melt evolution trend

Figure 3.11. Whole-rock compositions from selected lavas and pyroclastic units erupted from Ilopango caldera on a SiO_2 vs. $\text{Na}_2\text{O} + \text{K}_2\text{O}$ classification diagram. All values are normalized to 100 wt.% anhydrous. Total Fe calculated as FeO^* . The open symbols represent data from ¹Carr and Rose (1987) and ²J. Vallance, unpublished (Appendix 3.2). In general, whole-rock compositions range from basaltic andesite to rhyolitic.



typical for calc-alkaline suites (Fig. 3.12; after Irvine and Barager, 1971; Carr *et al.*, 1982).

Harker Diagrams

Major element Harker variation diagrams of the Ilopango intracaldera lavas and Tierra Blanca units are shown in Fig. 3.13 and Table 3.2, 3.3. Compatible major elements such as TiO_2 , Al_2O_3 , FeO, MgO, and CaO and incompatible major elements such K_2O form linear arrays with a large compositional gap between 60 to ~67.5 wt.% SiO_2 . Smaller compositional gaps are observed at 69 wt.% SiO_2 and 73 wt.% SiO_2 . MgO, FeO*, CaO and TiO_2 show a steady decline with increasing SiO_2 . Al_2O_3 maintains a level of ~18 wt.% when silica is < 59.6 wt.% but then declines in Al_2O_3 from 16 to 14 wt.% when silica is >68 wt.%.

In general, three groups emerge from the major element data. The first group (~ 54 to 60 wt.% SiO_2) is comprised of the less evolved Islas Quemadas mafic enclave and the southwest andesite dome of Cerro Cuyultepe. The second group (~ 68 to 74 wt.% SiO_2) includes the Islas Quemadas host dacite, TB2 and the Pumice Breccia facies of the San Agustín Block Unit, the northeast dome, northwest dome, Isla Chacagaste, Isla Cerro Los Patos, the southeast dome Cerro Tuligo and the TB4 tephra. The third group is considered to be TBJ. TBJ ranges from ~67 to 74 wt.% SiO_2 , bridging the compositional gaps at 69 wt.% SiO_2 and 73 wt.% SiO_2 .

Figure 3.12 AFM diagram of selected lavas and pyroclastic units erupted from the Ilopango caldera demonstrating a calc-alkaline trend. Dashed line separates the tholeiitic field from the calc-alkaline field. Legend is the same as Figure 11. All values are normalized to 100 wt.% anhydrous. Total Fe calculated as FeO*. Open symbols represent data acquired from ¹Carr and Rose (1987) and ²J. Vallance, unpublished (Appendix 3.2).

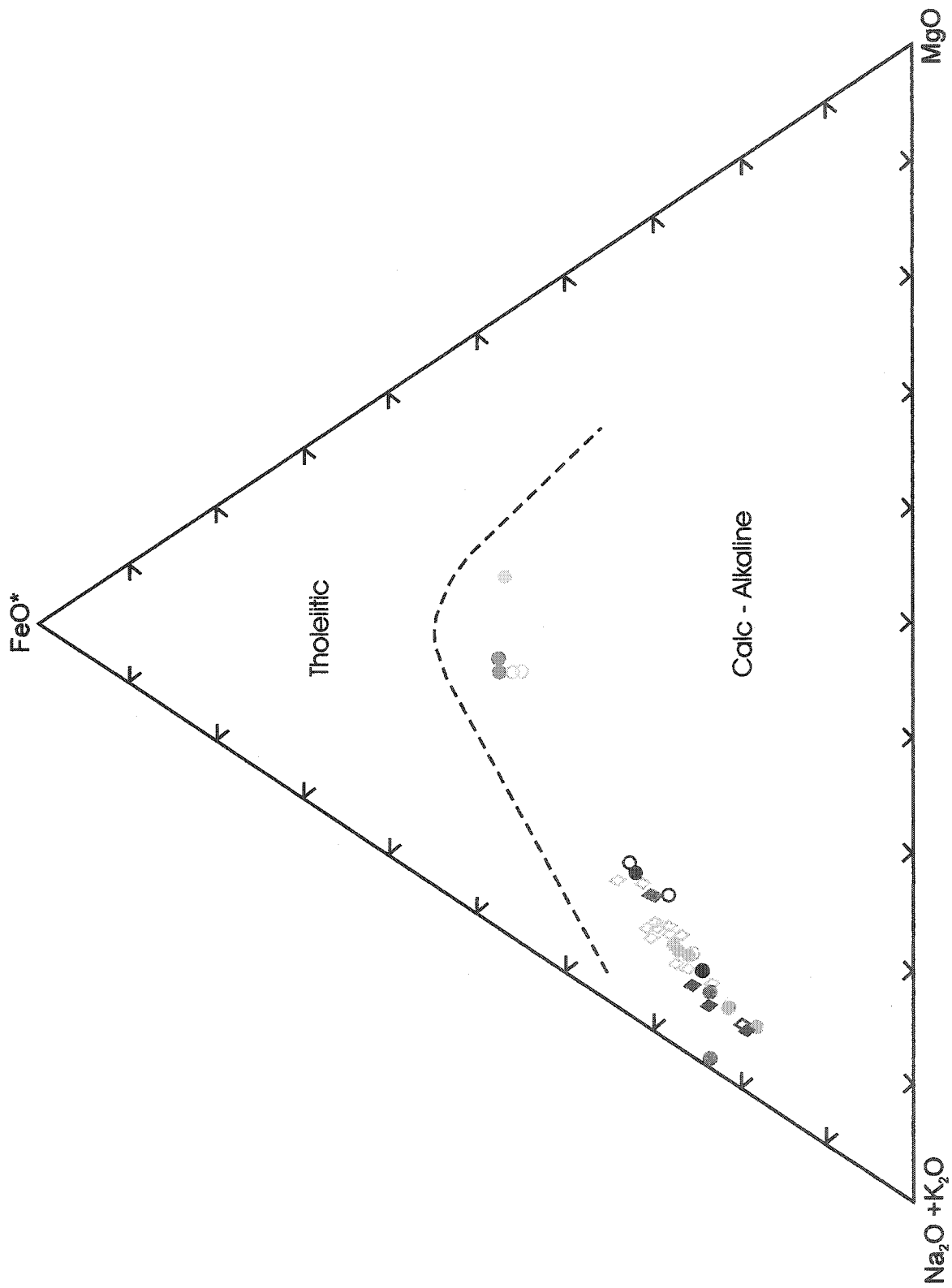


Figure 3.13 Major element Harker variation diagrams of selected Ilopango lavas and pyroclastic units. A) SiO₂ vs. Al₂O₃. B) SiO₂ vs. FeO*. C) SiO₂ vs. CaO. D) SiO₂ vs. K₂O. All values are normalized to 100 wt.% anhydrous. Total Fe calculated as FeO*. Open symbols represent data acquired from ¹Carr and Rose (1987) and ²J. Vallance, unpublished (Appendix 3.2).

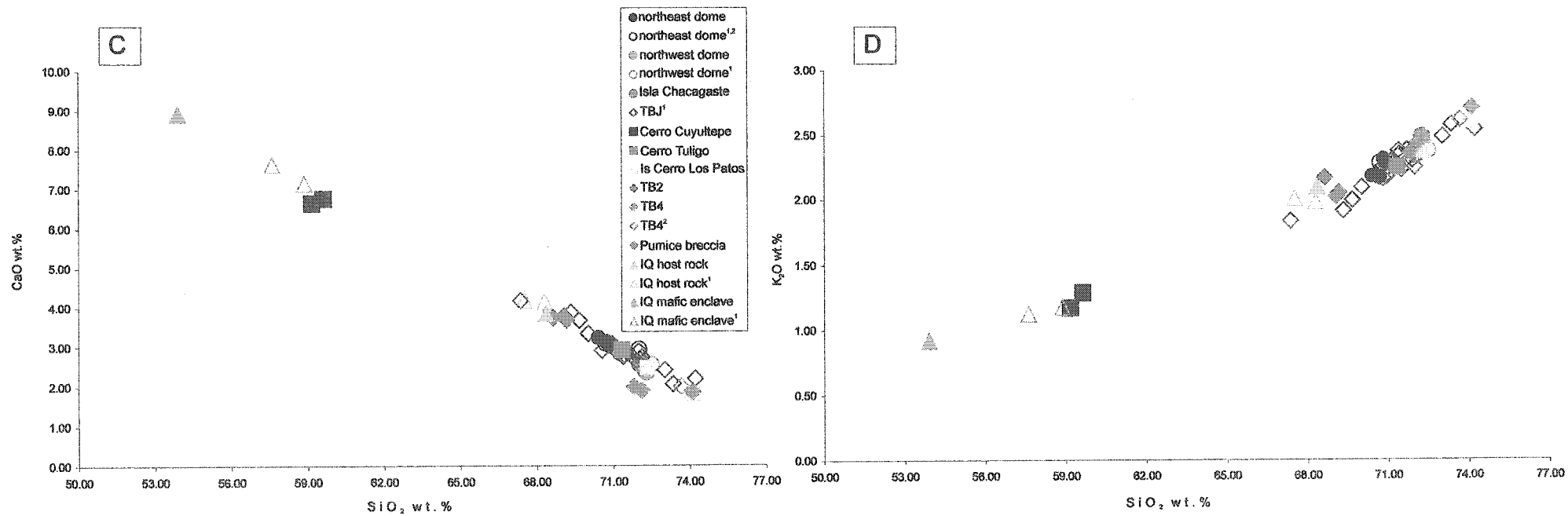
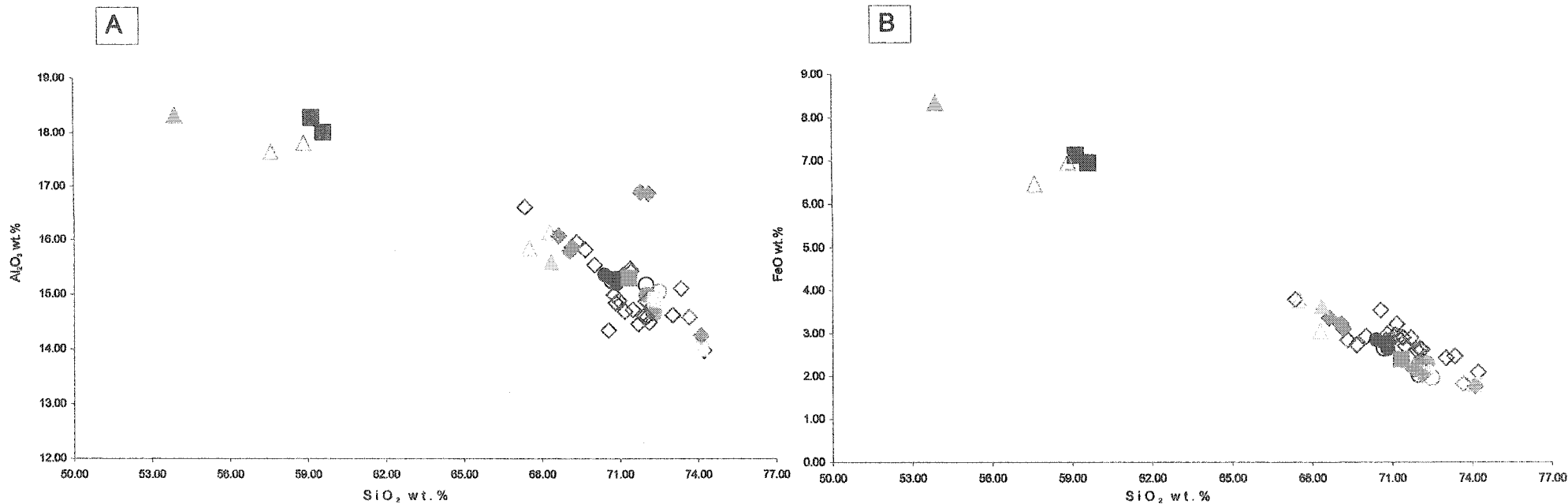


Table 3.2 WHOLE ROCK GEOCHEMISTRY OF ILOPANGO LAVAS AND PYROCLASTIC UNITS

Dome	Northeast	Northeast	Northeast	Northeast	Northwest	Chacagaste	Chacagaste	Tuligo	Cuyultepe	Cuyultepe	Los Patos	Los Patos
UTM	0493615 E 0287092 N	0493398 E 0287023 N	0493180 E 0287140 N	0493645 E 0287145 N	0492718E 0287408 N		0492663 E 0286699 N		0497663 E 0279476 N	0497617E 0279551N	1509355E 0280558N	
Sample	CM168-01	CM169-01	CM170-01	CM224-01	CM216-01	CM181-01	CM223-01	CM195-01	CM194-01	CM183-01	CM151-01	CM184-01
Rock	Rhyolite	Rhyolite	Rhyolite	Rhyolite	Rhyolite	Rhyolite	Rhyolite	Rhyolite	Bas - andesite	Bas- andesite	Rhyolite	Rhyolite
Wt.%												
SiO ₂	69.32	70.03	69.31	69.11	71.72	70.46	70.50	70.60	58.32	57.60	73.85	71.72
TiO ₂	0.33	0.33	0.32	0.32	0.30	0.30	0.29	0.30	0.63	0.68	0.27	0.27
Al ₂ O ₃	15.15	15.18	14.88	15.23	14.56	14.68	14.40	15.16	17.61	17.79	13.97	14.79
Fe ₂ O ₃	3.14	3.08	3.06	3.33	2.53	2.51	2.40	2.64	7.55	7.70	2.00	2.28
MnO	0.11	0.10	0.11	0.13	0.11	0.10	0.10	0.10	0.15	0.15	0.09	0.10
MgO	0.85	0.85	0.82	1.19	0.70	0.62	0.66	0.76	3.19	3.39	0.54	0.61
CaO	3.21	3.13	2.99	3.55	2.53	2.52	2.35	2.90	6.63	6.48	1.82	2.46
Na ₂ O	4.41	4.42	4.28	3.98	4.68	4.48	4.57	4.43	3.12	3.11	4.68	4.67
K ₂ O	2.15	2.15	2.24	1.97	2.41	2.29	2.43	2.23	1.26	1.14	2.60	2.35
P ₂ O ₅	0.11	0.11	0.11	0.13	0.10	0.11	0.10	0.11	0.12	0.12	0.05	0.14
LOI	1.18	0.69	1.79	3.73	0.48	1.89	2.01	0.88	1.41	1.86	0.12	0.55
Total	99.96	100.07	99.91	102.67	100.12	99.96	99.81	100.11	99.99	100.02	99.99	99.94
ppm												
BaO	1099	1105	1110	1181	1284	1192	1280	1202	1181	816	1383	1263
Ce	17	0	33	28	29	22	50	34	28	16	46	21
Co	0	0	0	0	0	0	0	0	0	22	0	0
Cr ₂ O ₃	27	17	16	0	16	0	32	17	0	0	15	18
La	0	12	12	13	0	0	0	0	0	0	0	15
Ni	7	15	21	0	0	0	3	0	0	0	0	0
Sc	0	0	12	0	0	0	0	0	0	20	0	0
V	44	39	40	39	16	23	20	21	39	110	15	14
Ga	15	14	14	15	14	15	15	14	15	19	13	15
Nb	3	2	3	3	3	2	2	3	3	0.60	4	3
Pb	8	8	7	3	8	8	8	2	3	5	8	3
Rb	51	52	50	49	52	53	53	50	49	23	55	52
Sr	323	320	317	306	268	287	287	304	306	356	216	275
Th	1	1	0	0	0	0	0	0	0	2	1	1
U	5	5	4	5	5	5	5	4	5	4	5	4
Y	20	21	20	18	20	22	22	17	18	22	19	19
Zr	156	157	155	157	174	166	166	160	157	113	175	165

TABLE 3.3 WHOLE ROCK GEOCHEMISTRY OF ILOPANGO LAVAS AND PYROCLASTIC UNITS

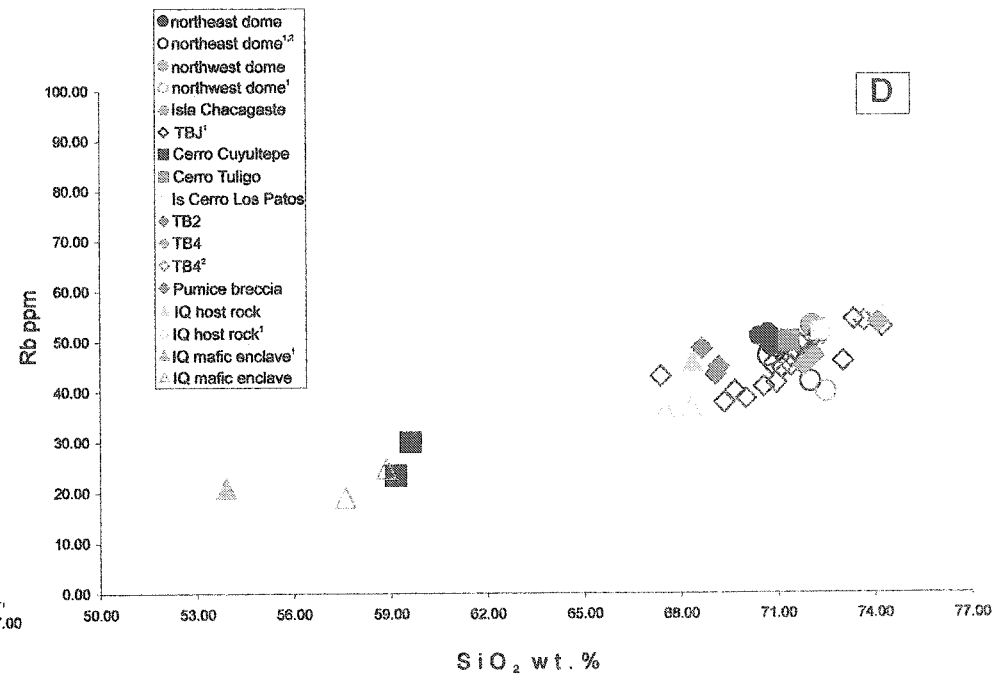
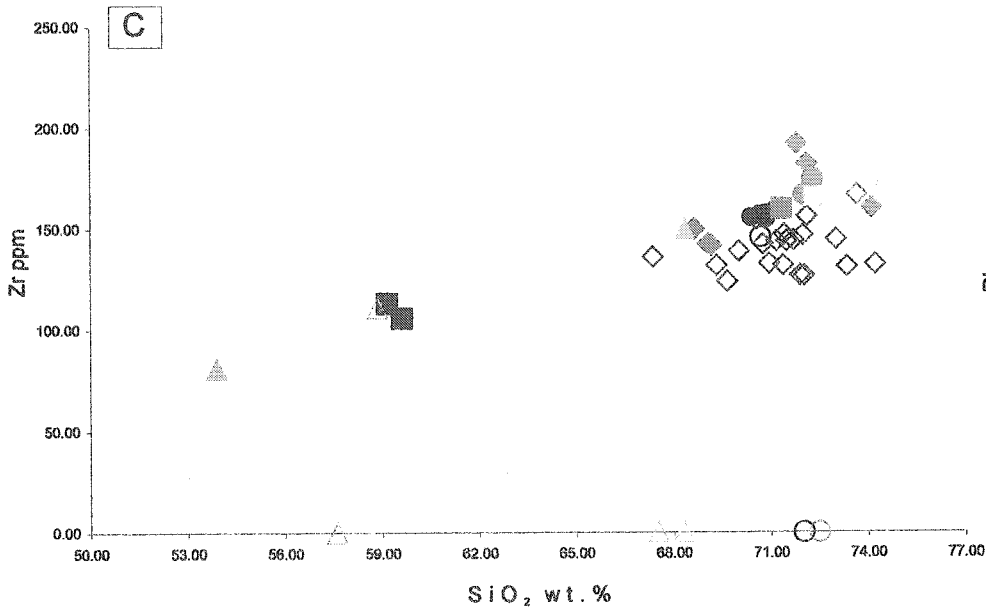
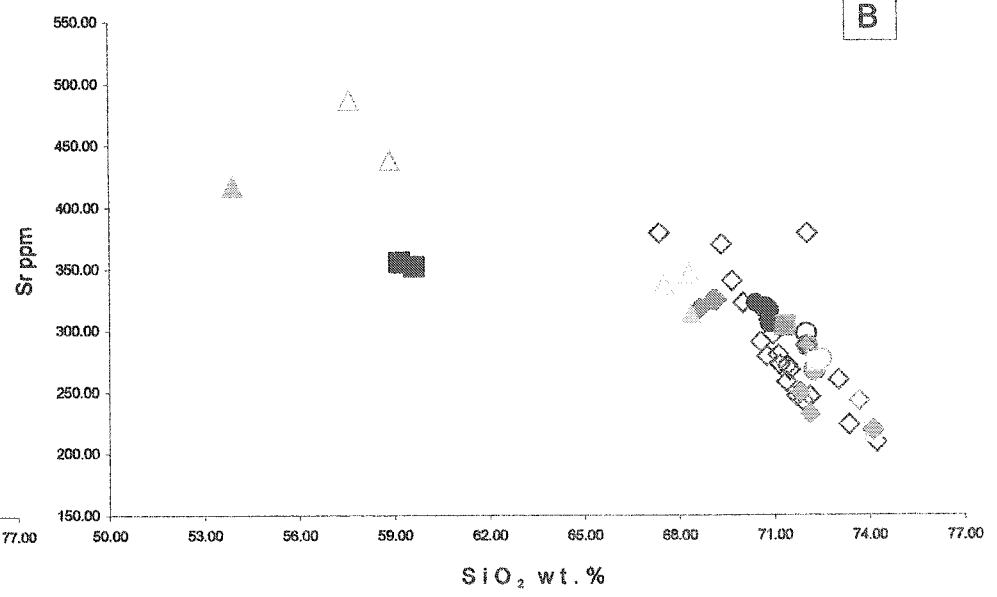
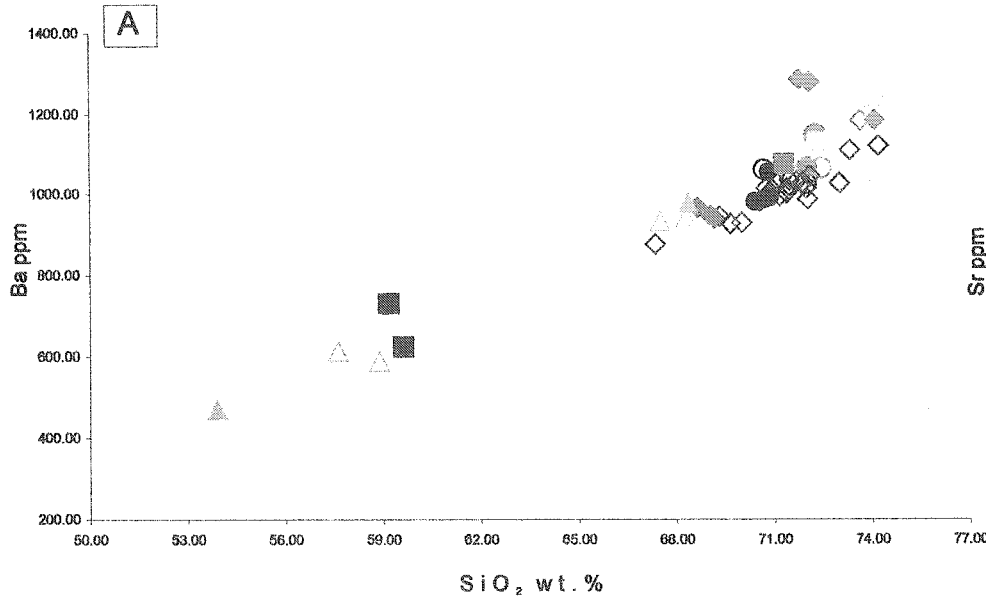
Unit UTM	Quemadas	Quemades	TB2	TB4	TB4	TB4	SABU-PBf 0499558 E 0286851 N	SABU-PBf 0498198 E 0287526 N
Sample Clast type	CM196-01i Basaltic-Andesite	CM196-01 Dacite	TB2-01 Dacite	CM226-01 Rhyolite	TB4p-01 Rhyolite	TB4-01 Pumice	CM261-01 Dacite	CM252-01 Dacite
Wt. %								
SiO ₂	53.39	67.74	66.03	70.96	67.19	67.34	66.49	66.31
TiO ₂	0.75	0.42	0.38	0.22	0.27	0.25	0.38	0.39
Al ₂ O ₃	18.15	15.47	15.48	13.65	15.81	15.75	15.22	15.23
Fe ₂ O ₃	9.18	4.02	3.61	1.89	2.26	2.12	3.47	3.33
MnO	0.16	0.12	0.12	0.09	0.10	0.09	0.13	0.13
MgO	5.39	1.41	1.13	0.49	0.48	0.42	1.15	1.19
CaO	8.84	3.83	3.62	1.79	1.88	1.79	3.66	3.55
Na ₂ O	3.05	4.26	3.95	4.17	3.53	3.48	4.03	3.98
K ₂ O	0.91	2.08	2.09	2.60	2.21	2.28	1.95	1.97
P ₂ O ₅	0.14	0.14	0.13	0.06	0.07	0.06	0.14	0.13
LOI		0.33	3.41	4.19	6.13	6.41	3.44	3.73
Total	99.96	99.82	99.95	100.11	99.93	99.99	100.06	99.94
ppm								
BaO	526	1095	1083	1322	1435	1428	1059	1053
Ce	0	27	33	32	31	26	0	26
Co	30	0	0	0	0	10	0	11
Cr ₂ O ₃	0	0	0	17	16	0	0	0
La	11	0	19	0	0	15	13	0
Ni	14	0	0	4	0	3	0	0
Sc	22	0	11	0	11	0	0	0
V	208	62	47	12	16	11	46	39
Ga	15	15	16	14	15	16	14	15
Nb	0	2	2	5	3	4	3	3
Pb	0	3	2	8	8	2	3	2
Rb	21	46	48	53	45	47	43	45
Sr	417	314	318	219	249	232	325	325
Th	2	0	0	0	0	0	0	0
U	3	4	4	5	5	5	4	4
Y	21	20	20	19	18	19	19	20
Zr	81	150	150	161	192	182	142	142

Notes: TB2 = Tierra Blanca 2; TB4 = Tierra Blanca 4; SABU = San Agustín Block Unit; PBf = Pumice Breccia facies.

Variation is observed in the TB4 tephra. TB4 ranges from 71.2 to 73.7 wt.% SiO₂. The lower silica (71.2 wt.% SiO₂) data point has 17 wt.% Al₂O₃ whereas the higher silica value plot has ~14 wt.% Al₂O₃. In the CaO vs. SiO₂ variation diagram, all the TB4 data plots at ~2 wt.% CaO. When considering the total alkali vs. SiO₂ variation diagram (Fig. 3.11) all TB4 data show lower alkali contents relative to the remainder of the Ilopango dataset.

Trace element abundances are listed in Table 3.2 and Table 3.3 and variation for selected elements is illustrated in Figure 3.14 using Harker variation diagrams. Ba, Rb, and Zr are incompatible and become more enriched with increasing silica, while Sr is compatible, becoming depleted with increasing silica. V also shows a decrease with increasing SiO₂ (Table 3.2,3.3). Variations for Nb, Th, Ni, Cr, Ce and La are not clear, but Co and Sc appear to decrease with increasing SiO₂. Y does not show much variation and appears to be buffered between 17 and 24 ppm with no clear change in concentration as silica varies. In general, the three groups observed in the major element Harker variation diagrams are supported by the trace element data. The first group (~ 54 to 60 wt.% SiO₂) comprised of the Islas Quemadas mafic enclave and Cerro Cuyultepe has the lowest concentrations of Ba, Rb, Zr and highest concentrations of Sr. The second group (~ 68 to 74 wt.% SiO₂), comprised of the Islas Quemadas host rock, TB2 and the Pumice Breccia facies of the San Agustín Block Unit, northeast dome, northwest dome, Cerro Tuligo, Isla Chacagaste and Isla Cerro Los Patos exhibits an increase in Ba, Rb, Zr and slightly lower concentrations of Sr than group 2.

Figure 3.14 Minor element Harker variation diagrams of selected Ilopango lavas and pyroclastic units. A) SiO₂ vs. Ba. B) SiO₂ vs. Sr. C) SiO₂ vs. Zr. D) SiO₂ vs. Rb. All values are normalized to 100 wt.% anhydrous. Total Fe calculated as FeO*. Open symbols represent data acquired from ¹Carr and Rose (1987) and ²J. Vallance, unpublished (Appendix 3.2).



The Islas Chacagaste, Isla Cerro Los Patos and northwest dome lavas consistently show overlap in the Ba, Rb, Zr and Sr trace element diagrams. The TB4 tephra (71.2 to 73.7 wt.% SiO₂) has the highest concentrations of Ba and Zr. The third group, comprised only of TBJ shows a range of trace elements overlapping the groups >67 wt.% SiO₂.

Interpretation of the data

Origin of the rock suite

The combined major and trace element dataset suggests chemical variations as a result of fractional crystallization. For major elements, the observed decreases in Al₂O₃, CaO, FeO* and MgO with increasing silica content, and corresponding increases in total alkalis and K₂O, are consistent with fractional crystallization processes of plagioclase, pyroxene and Fe-Ti oxides during the transition from basaltic andesite to andesite to dacite to rhyolite (Gill, 1981). These phenocrysts occur in all lavas with plagioclase > orthopyroxene ≥ opaque minerals ± hornblende and in the pyroclastic units TBJ and TB4 with plagioclase > orthopyroxene ≥ opaque minerals ± hornblende.

For trace elements, the values correlate closely with major element contents, and in some cases there is a variation in the modal percentage of phenocrysts (Fig. 3.15). For example a decrease in Sr and Ca is observed as the lavas become more silica-rich, and in the case of Isla Cerro Los Patos there is also a decrease in modal

plagioclase relative to the northeast dome (Fig. 3.16A, 3.15). V correlates with a decrease in Ti, but the opaque minerals are generally found close to the same modal percentage (Fig. 3.16B, 3.15). Elemental variation is observed in the pyroclastic units, but the modal percentages of the phenocrysts do not vary significantly. For example TB4 is depleted in Sr relative to TB2 and the Pumice Breccia, but the modal phenocryst percentage of plagioclase is approximately the same.

Normative mineralogy

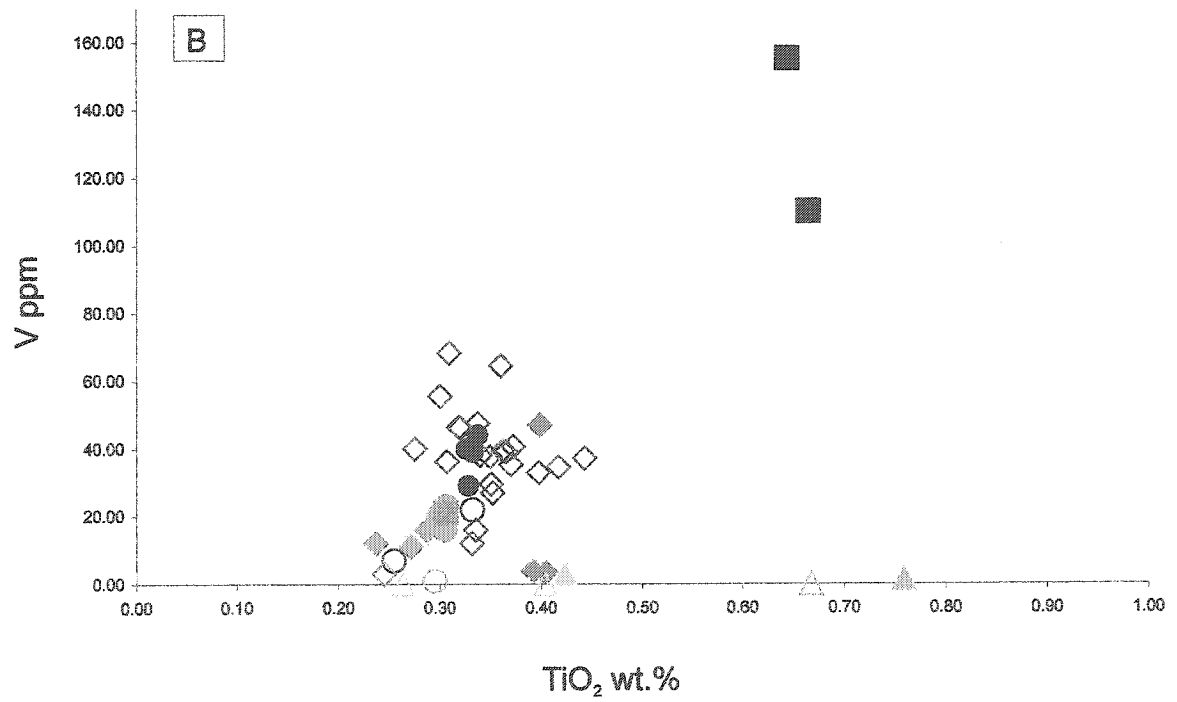
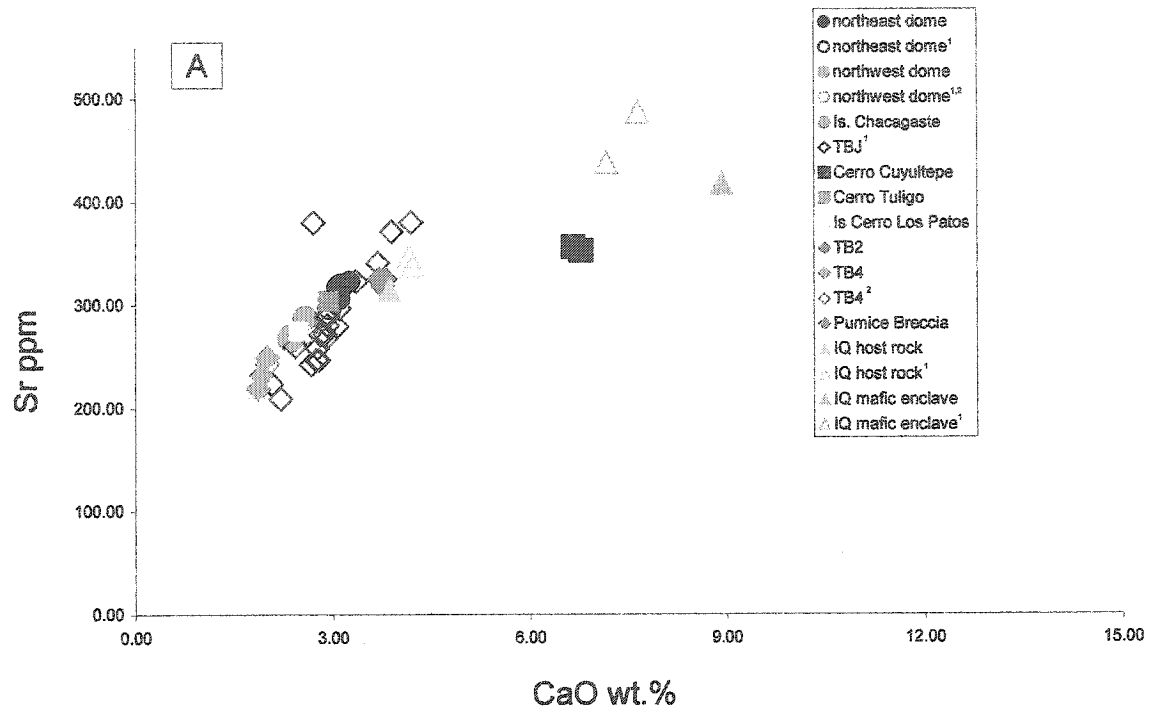
To further test the origin of the rock suite and to try and constrain the phases steering magma evolution, the normative minerals were calculated using Mesonorm (Mielke and Winkler, 1979) and compared with the modal mineralogy. In the case of the lavas, the samples were grouped based on presence of modal hornblende (Appendix 3.3) The norm calculation indicates that plagioclase > quartz > orthopyroxene > opaque minerals \geq hornblende in both the group with hornblende and the group without hornblende. In the case of the pyroclastic units, the normative mineralogy was the same as the lavas with plagioclase > quartz > orthopyroxene > opaque minerals \geq hornblende. The normative mineralogy is in agreement with the modal mineralogy except that hornblende appears to play a minor role, whereas in the modal proportions hornblende is generally \geq orthopyroxene and the normative calculation indicates the presence of quartz, which is not observed in the modal percentage.

Figure 3.15 Compiled modal phenocryst percentages observed in selected Ilopango lavas and pyroclastic units. ¹Hart (1981) and Steen-McIntyre (1976)

	Olivine	Plagioclase	Hornblende	OPX	CPX	Opaques	Magnetite	Hematite	Apatite
<u>North lavas</u> Northwest dome		○		X		X			X
Northeast dome		○	X	X		X			X
Northeast dome <i>inclusion</i>		□	X	X	X	X			
Isla Chacagaste		○		X		X			
<u>South lavas</u> Cerro Tuligo		○	X	X		X	X		
Cerro Cuyultepe		□		X	○	X	X	X	X
Cerro Los Patos		X	X	X		X			
<u>Islas Quemadas</u> IQ dacite		⊙	X	X		X			X
IQ enclave	X	⊙	X	X					
<u>Pyroclastic</u> TB2		X	X						X
TB4		X	X	X		X			X
Pumice breccia		X	X						
TBJ'	—	—	—	—		—			

X 0 to 5 % ○ 5 to 10 % ⊙ 10 to 15 □ >15 % — Modal % unknown

Figure 3.16 Variation diagrams showing elemental concentrations, which are compared to modal phenocryst observations. A) CaO vs. Sr. B) TiO₂ vs. V. All values are normalized to 100 wt.% anhydrous.



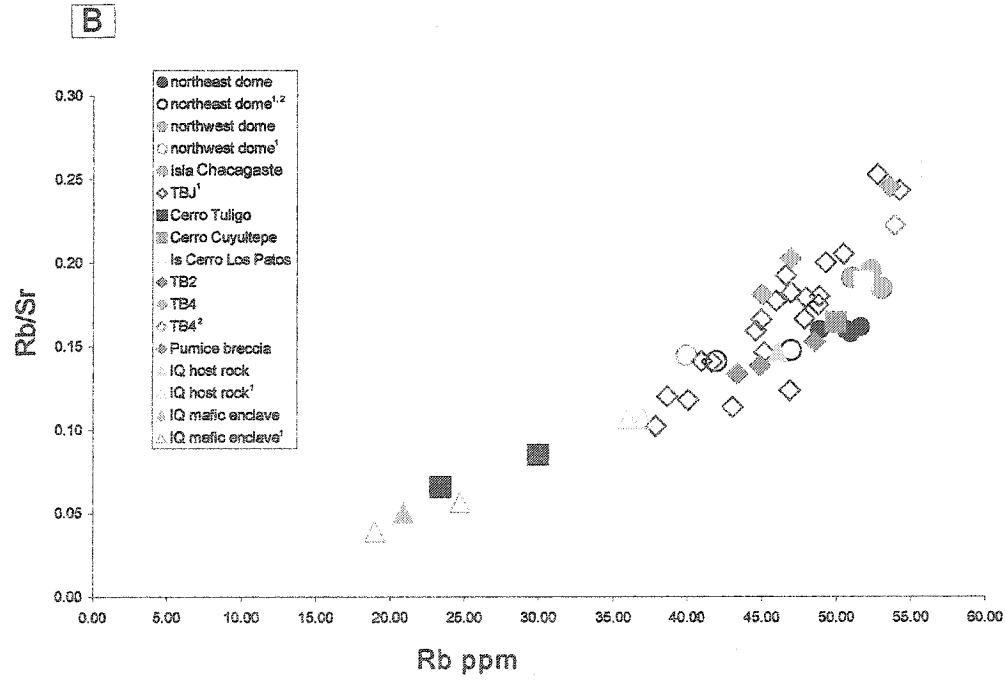
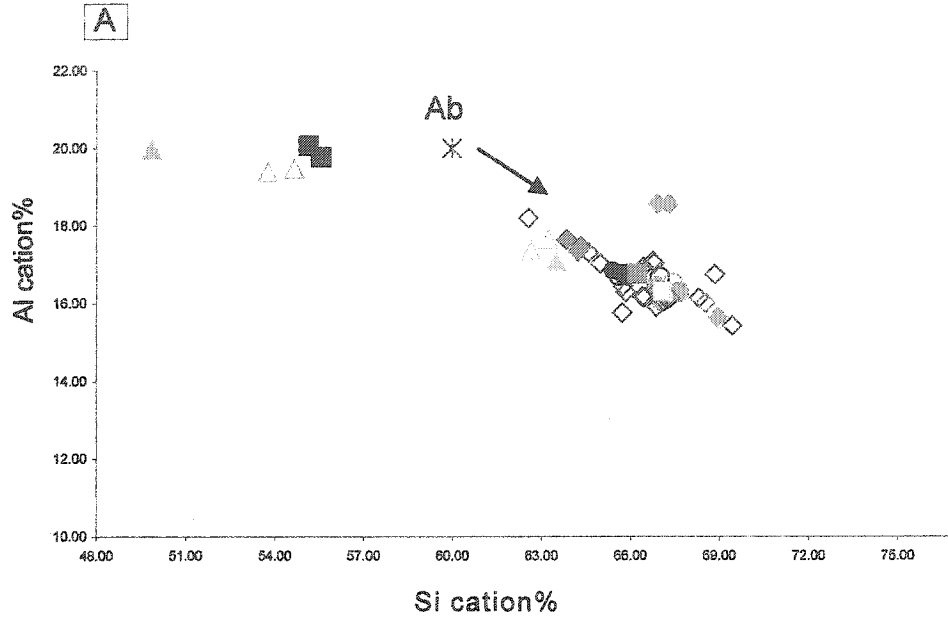
Cation diagrams

Cation – cation variation diagrams were used to discriminate the fractionating phases. Considering the major phases calculated from the normative and observed in the modal percentage, cation-cation variation diagrams helped to constrain the phenocrysts controlling crystal fractionation.

Plagioclase To test plagioclase fractionation, Si vs. Al was used and an ideal albite phenocryst ($\text{NaAlSi}_3\text{O}_8$) was used as a proxy (Fig. 3.17). The silicic rocks (≥ 62.7 SiO_2 wt.%) decrease away from albite (Ab) with increasing silica (Fig. 3.17A). On a Rb vs. Rb/Sr variation diagram, Rb becomes enriched in the melt relative to Sr over time, suggesting that Sr is being consumed by a fractionating phase (Fig. 3.17B). On a Sr vs. Ca variation diagram both become depleted (Fig. 3.16A). These signatures are typical indicators of plagioclase fractionation (Gill, 1981).

Mafic phases At least three mafic phases are considered to be undergoing crystal fractionation: orthopyroxene, hornblende and opaque minerals. The calculated normative mineralogy suggests that orthopyroxene and opaque minerals are major fractionating phases, while the modal percentages include hornblende. In order to extract the fractionating phases, a plot of Fe vs. Mg cation wt.% was constructed with ideal phenocryst compositions of enstatite (MgSiO_3), orthoferrosilite (FeSiO_3), hornblende endmembers and magnetite (FeFe_2O_4). . Although I was unable to get a clear indication which mafic phase was steering magma evolution at the different

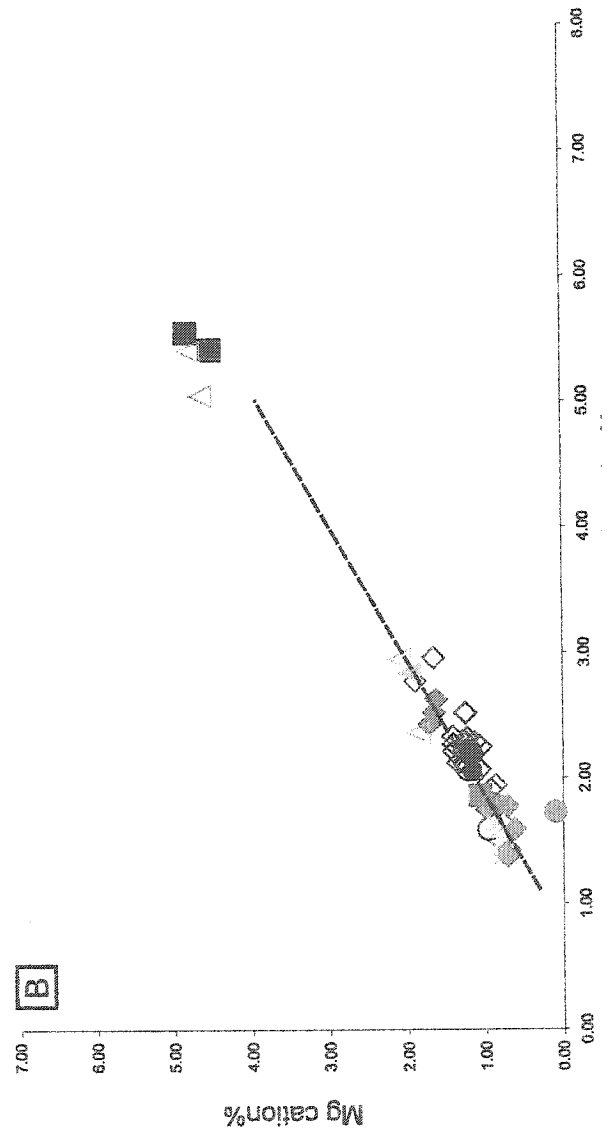
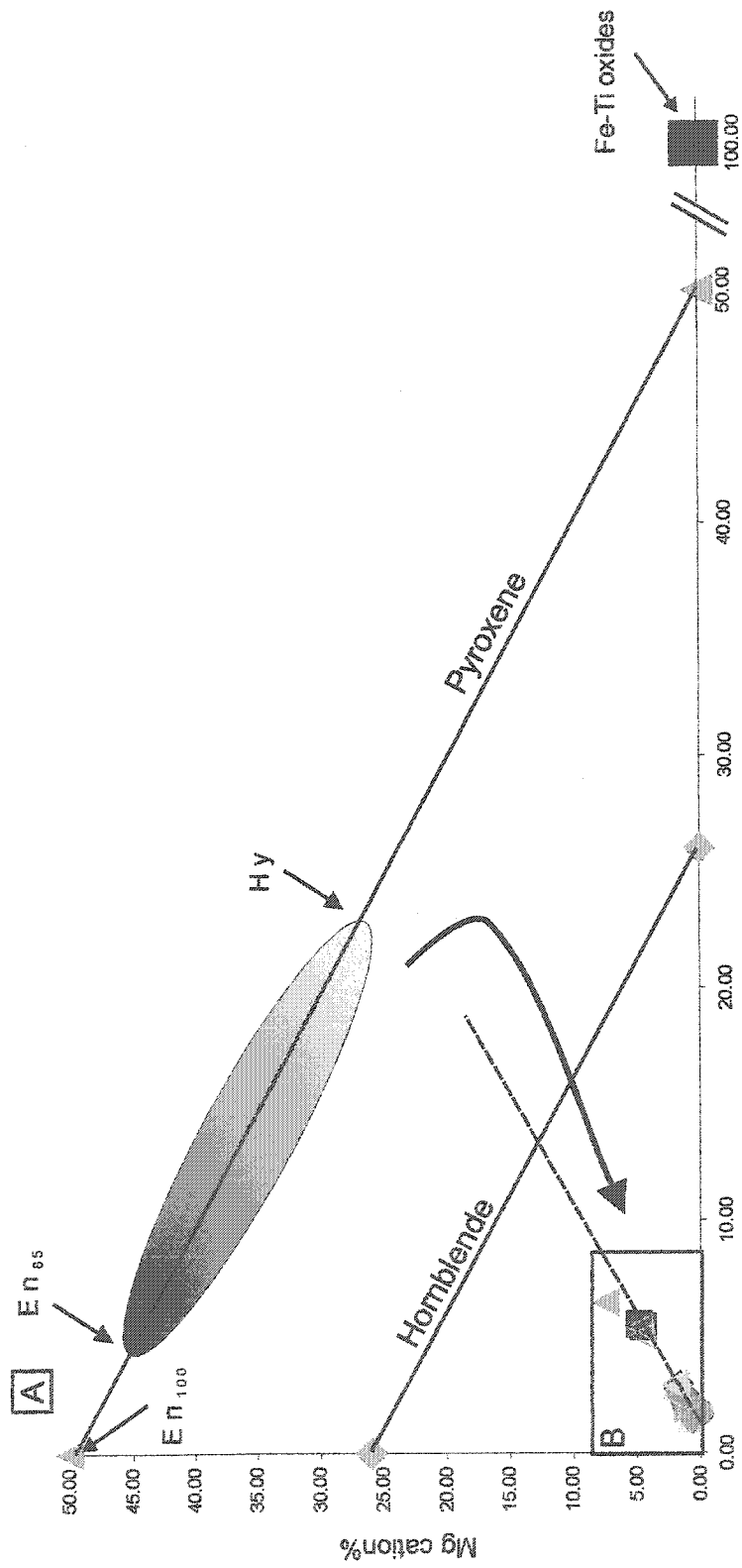
Figure 3.17 Variation diagrams considering plagioclase fractionation. A) Silica vs. aluminium in cation units, Albite (Ab) is used as an ideal phenocryst. B) Rb vs. Rb/Sr. All values are normalized to 100 wt.% anhydrous



stages, I was able to model a hypothetical case using optical properties of the minerals, petrography and the normative mineralogy.

Figure 3.18 is a suggested model for evolution of the mafic phases. The grey shaded area is the suggested composition of orthopyroxene expected to crystallize in an andesitic melt (Gill, 1981). In the northeastern dome and Cerro Tuligo, inclusions of orthopyroxene in hornblende suggest that the pyroxene was the first to crystallize. The thick, black line with an arrow is a hypothetical line of fractional crystallization beginning with the suggested orthopyroxene compositions. As orthopyroxene begins to fractionate, the melt becomes depleted in Mg and enriched in Fe. Eventually opaque minerals such as magnetite and ilmenite begin to crystallize, the melt becomes depleted in Fe and begins to move towards the hornblende field. Figure 3.19 demonstrates a negative correlation between Zr and Ti. Ti, considered a compatible element, is becoming depleted as Zr increases, suggestive of fractionation of magnetite (Cox et al., 1979). Hornblende is typically produced at the expense of orthopyroxene due to variables such as increased P_{H_2O} , increased alkali content or decrease in temperature (Cox et al., 1979). Phenocryst relationships in the northeast dome and Cerro Tuligo, demonstrate that orthopyroxene nucleated first followed by hornblende and both may have crystallized together for a period of time. Overgrowth rims on hornblende found in the Islas Quemadas host dacite also suggest a change in reservoir conditions. The presence of hornblende in most of the lavas and TBJ, TB2, TB4 and the Pumice Breccia, suggests that these rocks may have experienced one or a combination of these changes.

Figure 3.18 Hypothetical model for evolution of the mafic phases based on the modal mineralogy and the normative mineralogy using Fe vs. Mg cation%. A) Black arrow represents hypothetical path of crystal fractionation. Ideal phenocryst endmembers of hornblende (diamonds), pyroxene (triangles) and Fe-Ti oxides (black box) are plotted for comparison. Field of pyroxene based on Gill (1981). Note change of scale for Fe cat %. B) Inset from A. Magnified corner of A with a suggested path of fractionation using a best-fit line (dashed line). Legend the same as Fig. 17.



Rayleigh fractionation

Rayleigh fractionation modeling was done to test crystal fractionation by considering the evolution of the dacites and rhyolites by crystallization from the more mafic endmembers in the study area. I constrained the samples to those of known ages in stratigraphic order. For the first run, I used the Islas Quemadas dacitic host as the liquid, and basaltic andesite to andesite enclave as the parent. For the second run, I used the rhyolitic northeast dome, dated at 56 ± 1.9 ka and the basaltic-andesite dome, Cerro Cuyultepe, dated at 359.3 ± 7.9 ka. I calculated a D_{bulk} for various fractions of melt (F) using, $C_L/C_o = F^{(Kd-1)}$ where, C_L = liquid, C_o = parent, F = fraction of melt remaining and Kd = elemental partition coefficient (Appendix 3.4; Gill, 1981; Rollinson, 1993). I compared the results (CL) to element concentrations established by whole-rock analyses.

The first run compared the products of the 1880 dome growth. Trace element modeling results indicate that with 65 to 50 % crystallization from the basaltic-andesite parent would generate a fit for Rb, Sr, Zr and V with the host dacite. The trace elements suggest that the basaltic-andesite could be a primary melt to the dacitic host. The problem with this is that dacitic melt from the host dacite was observed in the mafic enclave, as well as crystal transfer of plagioclase phenocrysts from the dacitic host to the mafic enclave (Richer *et al.*, *in press*), therefore the comparable values could simply be an artifact of mixing rather than fractional crystallization.

The second run compared two domes found within the caldera. Trace-element modeling results indicate that with crystallization of 28 % from the basaltic-andesite parent would generate a fit for the strongly incompatible elements Ba and Zr, whereas crystallization of 51% generates a fit for Rb. The spread of values suggests that the northeast rhyolitic dome did not evolve from Cerro Cuyultepe in a closed-system reservoir.

Discussion

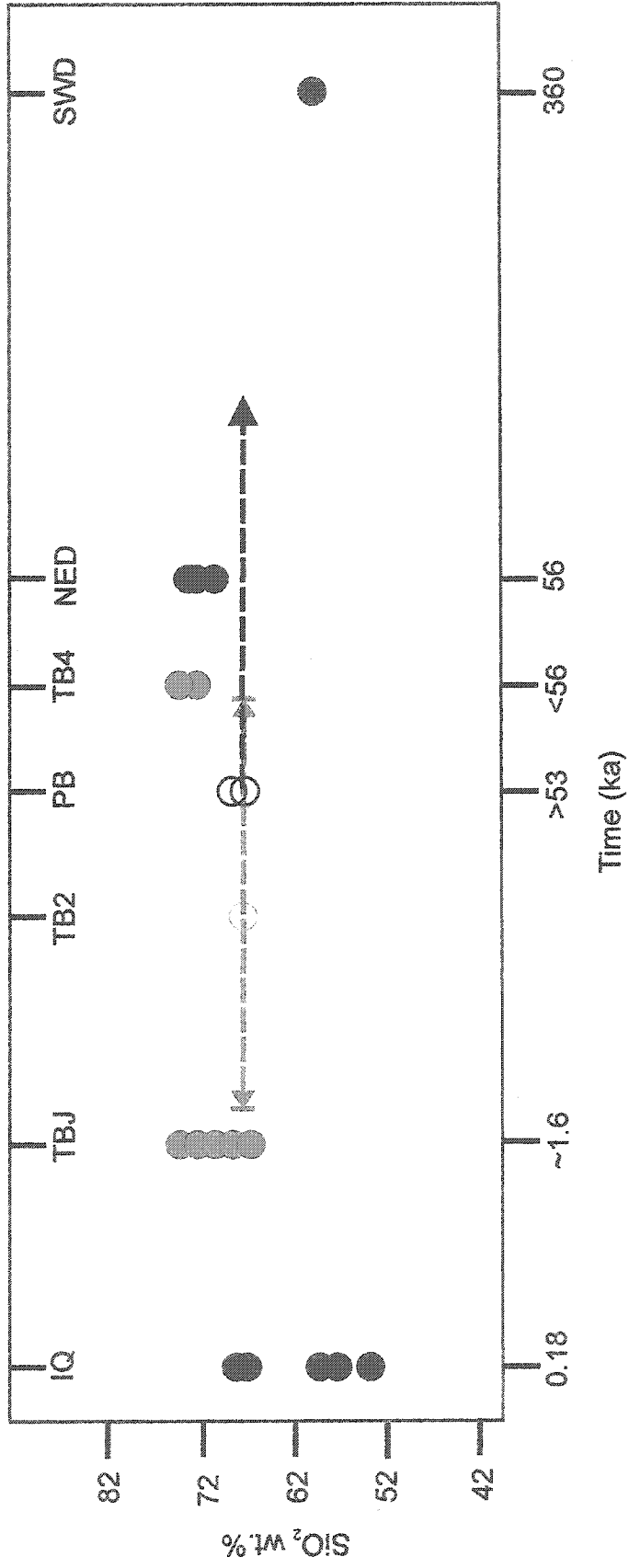
The overlap in the major element and trace element concentrations amongst the various lavas and pyroclastic units indicates that magma evolution at Ilopango Caldera is not a continued process directly related to a time factor, such as progressive differentiation caused by a closed-system crystallization process. The simplest explanation for the observed variations in magma composition is that a high-level magma reservoir (or reservoirs) experiences repeated injections of more mafic magma, which then undergoes fractional crystallization and is periodically tapped by eruptive processes.

The lavas erupted at Ilopango have SiO₂ contents ranging from ~54 to 75 %, with a compositional gap from 60 to 67 %. The ages of the lavas and pyroclastic units established by Ar-Ar dating methods, and relative ages established by ¹⁴C and stratigraphy, do not show a systematic enrichment or depletion in major element or trace element concentrations with time. For example, the Islas Quemadas dacitic dome erupted in 1880 is enriched in compatible major elements (e.g., Fe and Ca) and depleted in incompatible elements (e.g., Zr and Ba) compared to the older rhyolitic

dome in the northeast which was erupted ~56,000 years ago. The youngest pyroclastic unit, TBJ, erupted 1600 years ago and ranges from 67 wt.% SiO₂ to 74 wt.% SiO₂, overlapping lavas and pyroclastic units such as the Pumice Breccia and TB4, which are known to be older by stratigraphic relationships (Fig. 3.19). Magma replenishment and mingling/mixing processes appear to account for the observed chemical variations.

Phenocryst textures suggest melt disequilibrium conditions which can be attributed to an influx of a more mafic magma composition, the depressurization or the dehydration of the magma reservoir. Plagioclase phenocrysts in the northeast dome, Cerro Los Patos and Cerro Tuligo all exhibit LAC texture with embayed edges, suggesting either rapid growth during undercooling of the magma trapping melt (Halsor, 1989; Shelley, 1993) or similar textures, documented as honeycomb texture (Seaman, 2000; Damasceno *et al.*, 2002), are interpreted to be a result of resorption processes (Kuno, 1955; Gerlach and Grove, 1982). The embayed edges on some phenocrysts and higher An rims on LAC textured plagioclase phenocrysts suggest that perhaps an influx of hotter more calcic magma destabilized the plagioclase phenocrysts causing partial dissolution before the phenocryst had a chance to grow. Plagioclase phenocrysts found in Cerro Cuyultepe, the northwest dome, the Islas Quemadas dacite and the Islas Quemadas mafic enclave exhibit sieve textures with embayed edges, suggesting the dissolution of Na and replacement by Ca (Shelley, 1993; Seaman, 2000; Murphy *et al.*, 2000) again suggesting that reservoir was disrupted by influx of a more calcic-rich magma, depressurized or dehydrated. The more An rich overgrowth edges of plagioclase phenocrysts with sieve texture

Figure 3.19 Ilopango lavas and pyroclastic units represented on a Time vs. SiO_2 variation diagram. Blue solid dots represent Ilopango lavas with absolute age determinations (i.e. Ar/Ar dating), pink solid dots represent Ilopango pyroclastic units with relative age determinations (i.e. ^{14}C). TB2 (open pink circles) and pumice breccia (PB, closed black circles) represent pyroclastic units constrained by stratigraphy. The pink dashed line represents the depositional timeframe for TB2 and the black dashed line represents the depositional timeframe for the Pumice Breccia (PB). IQ = Islas Quemadas, TBJ (Tierra Blanca Joven, Dull et al., 2001), TB2 = (Tierra Blanca 2), PB = Pumice Breccia, TB4 = Tierra Blanca 4, NED = Northeast dome, SED = Southwest dome.



suggest the influx of a more calcic-rich magma. In some lavas the inclusions of orthopyroxene and intergrowth of hornblende and orthopyroxene suggests that reservoir conditions encouraging the crystallization of hornblende. Together these textures are indicative of an increase in temperature, possibly accompanied by a change in water pressure and a change in composition (Cox *et al.*, 1979). Recharge of a more mafic batch of magma would provide a mechanism by which to increase the temperature, introduce a more basic composition and likely cause the water pressure to change (Eichelberger, 1975; Tepley *et al.*, 2000).

If Ilopango were a closed magmatic system simply undergoing crystal fractionation, then an increase in silica, enrichment of incompatible elements and a decrease of compatible elements should be observed over time. However, there are instead decreases in silica, depletions in incompatible elements and enrichment of compatible elements with time, indicating that fluctuations in magma chemistry have occurred repeatedly over time.

There are two possible scenarios. The first is one shallow level reservoir, which experiences replenishment of a more mafic magma, undergoes fractional crystallization and periodically erupts. The second scenario is multiple shallow-level reservoirs in which magmas evolve independently with different residence times and experience occasional mafic replenishment. Based on the lack of data in support of multiple shallow-level reservoirs and the obvious existence of at least one, we suggest the first model is a reasonable scenario of the magmatic system beneath Ilopango. We propose that this reservoir is most likely a fractionating magma body that is occasionally recharged by magma of a more mafic composition. Once the more

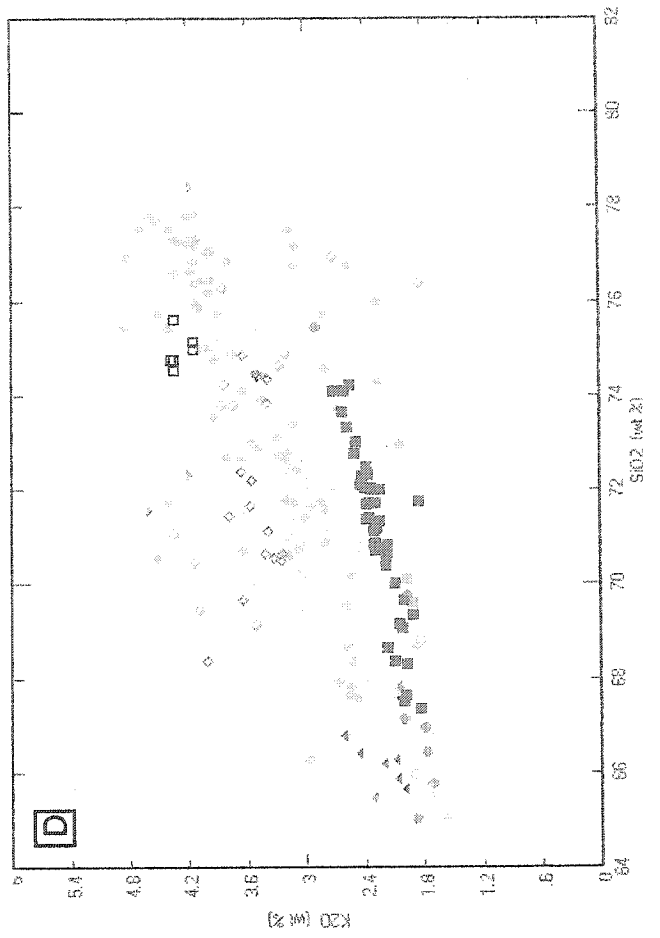
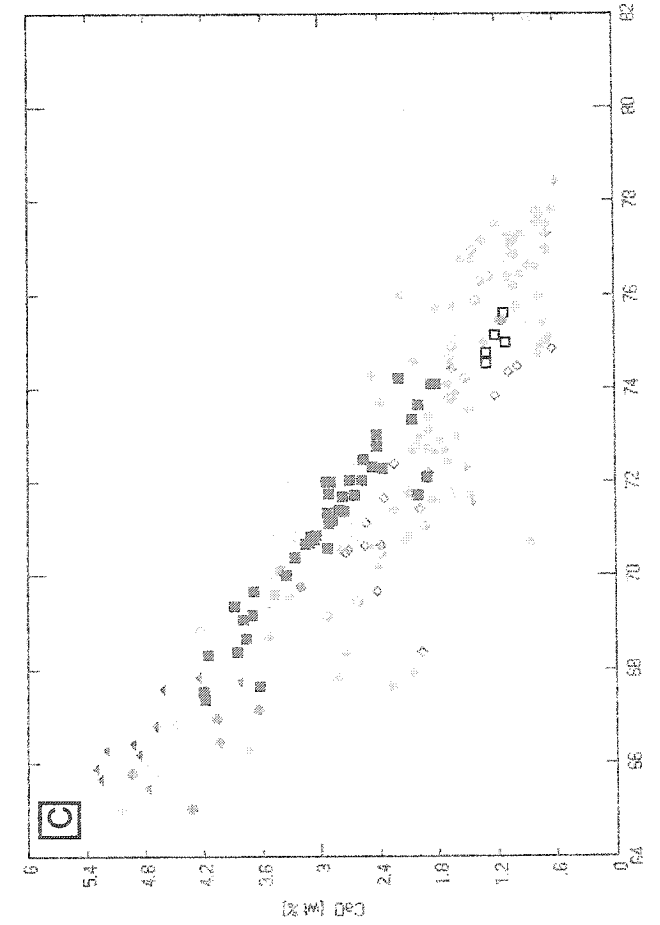
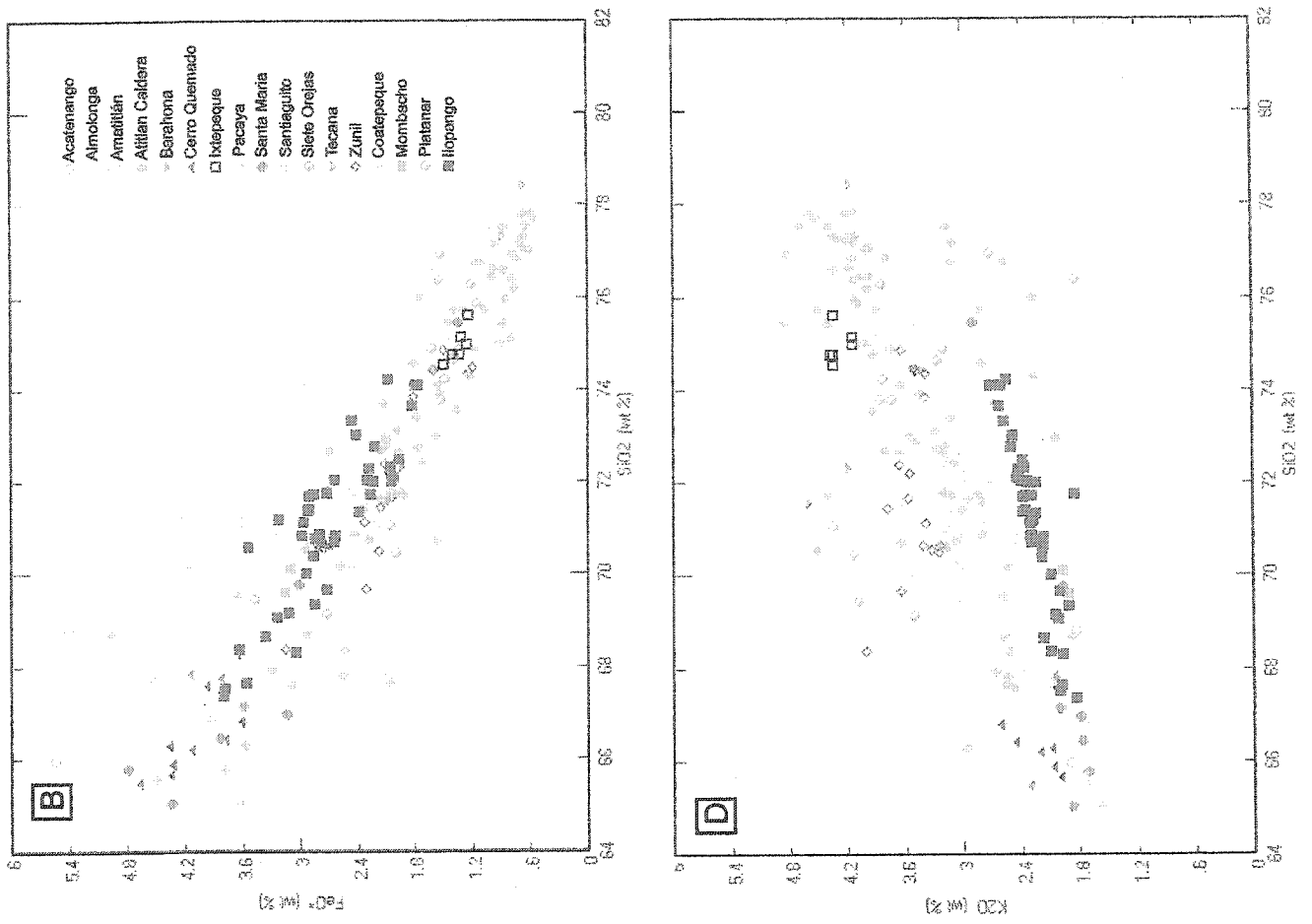
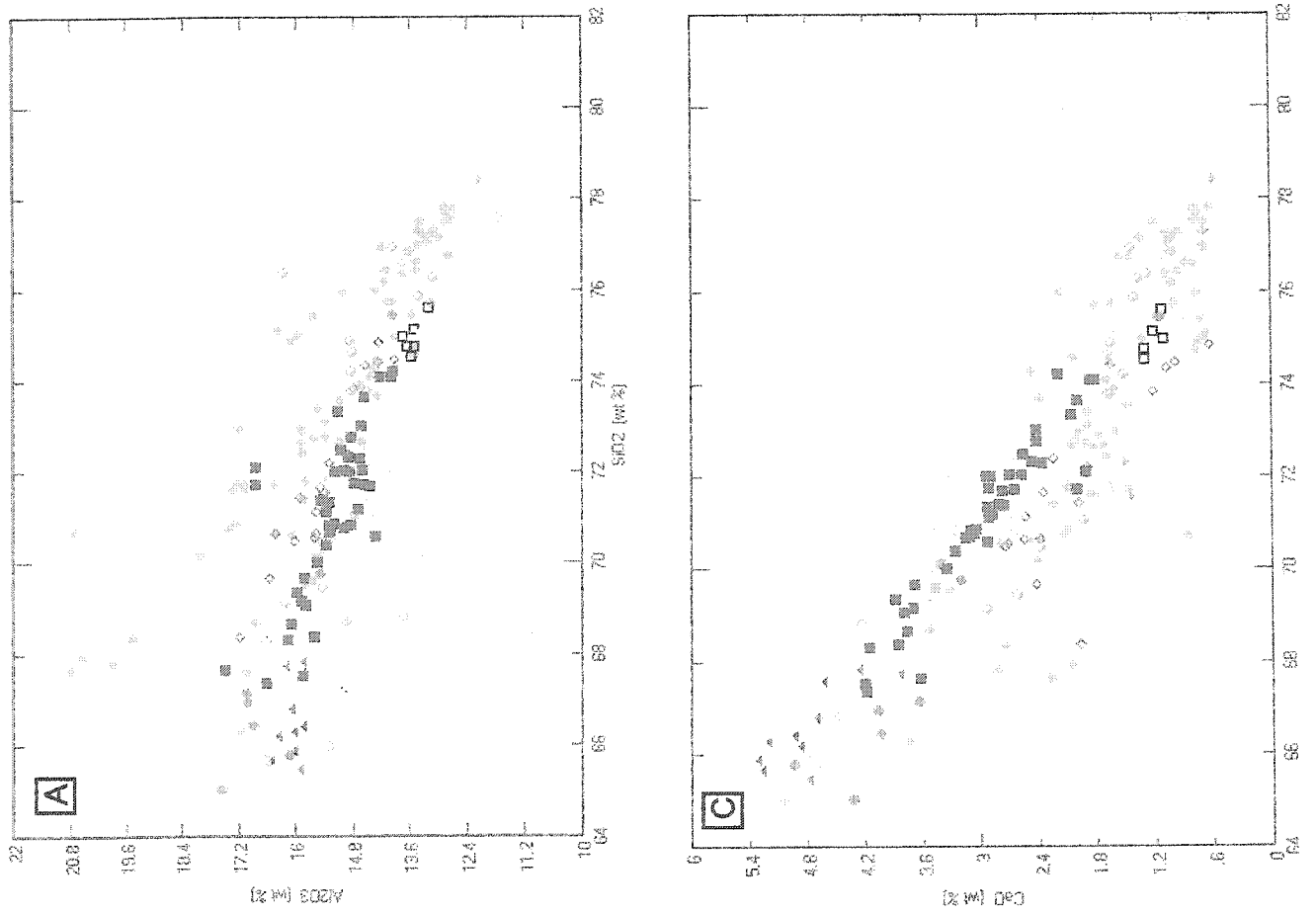
mafic magma intrudes the fractionating reservoir, disequilibrium occurs within the chamber, P_{H_2O} may increase, temperature will increase and resorption textures such as observed in the plagioclase phenocrysts are produced. Evidence for mafic mingling at Ilopango has been preserved in Islas Quemadas, the Pumice breccia facies of the San Agustín Block unit and TBJ (Hart, 1981; Richer *et al.*, *in press*; Mann *et al.*, *in press*). The mafic magma, as well as the resident magma, then undergo fractional crystallization, subsequently depleting the reservoir in incompatible elements and enriching it in compatible elements as observed.

Comparison of Ilopango with other Central American silicic centers

The Ilopango lavas and pyroclastic units are chemically distinct from other Central American silicic centers. The Ilopango volcanic rocks range from 67 to 74 wt.% SiO_2 , whereas silicic centers such as Atitlán, Ixtepeque, Platanar, Zúñil and Coatepeque are more evolved with values ranging from 66 to 82 wt.% SiO_2 . On the other hand, silicic centers such as Apoyeque, Santiaguito, Acatango, Cerro Quemado, Apastapeque and Santa María range from 65 to 67 wt.% SiO_2 , and are slightly less evolved than Ilopango. In general, Ilopango falls into the middle and clearly overlaps in SiO_2 with Barahona, Almolonga, Mombacho and Amatitlán.

Major element Harker variation diagrams are shown in Figure 3.20. At similar SiO_2 values, Ilopango has lower K_2O and higher CaO relative to other high-silica rhyolite silicic centers such as Atitlán, Zúñil and Ixtepeque, whereas silicic centers such as Mombacho and Santa María plot on the same linear array as Ilopango

Figure 3.20 Major element Harker variation diagrams representing major silicic centers in Central America. A) SiO_2 vs Al_2O_3 . B) SiO_2 vs FeO^* . C) SiO_2 vs. CaO . D) SiO_2 vs. K_2O . All values are normalized to 100 wt.% anhydrous. Total Fe calculated as FeO^* . Note data for comparison obtained from Carr and Rose, (1987).

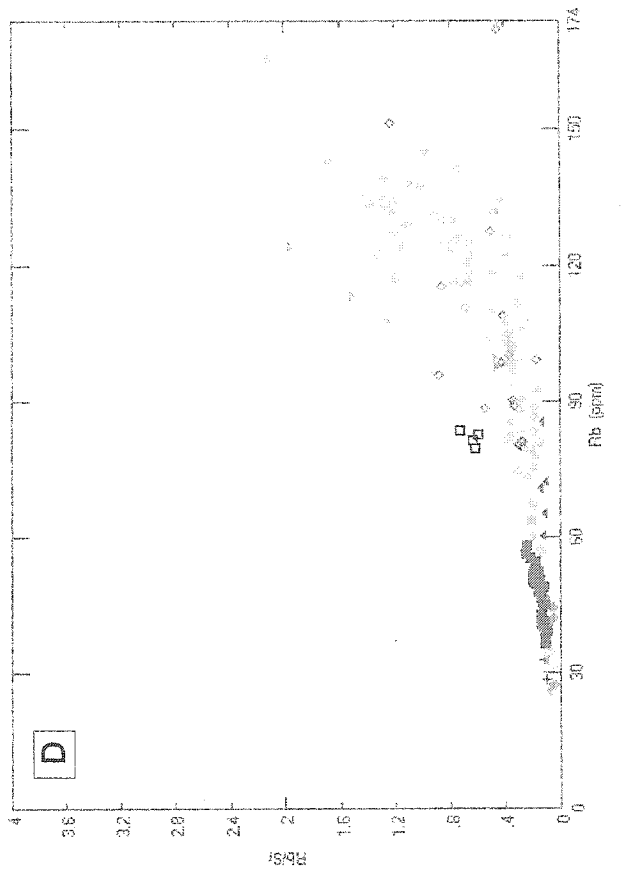
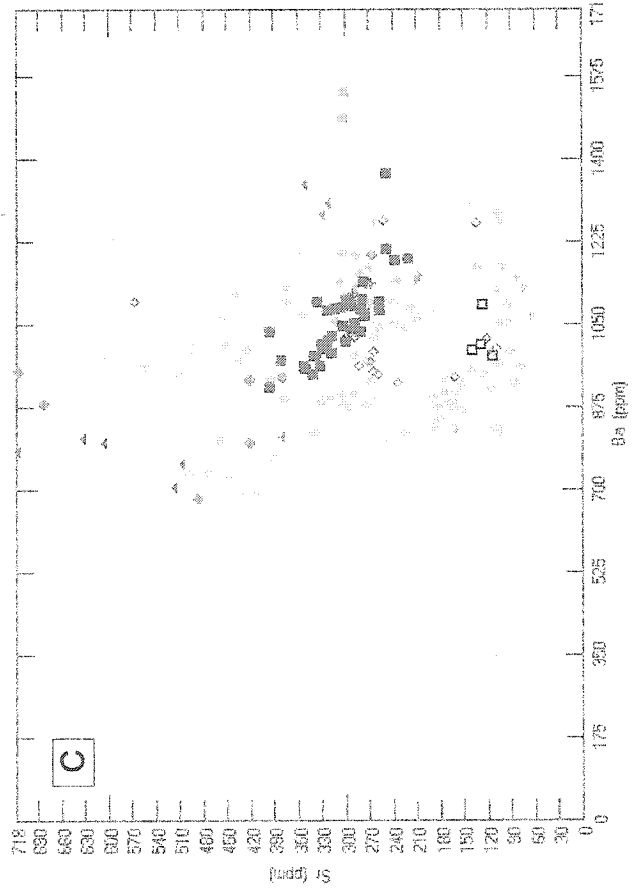
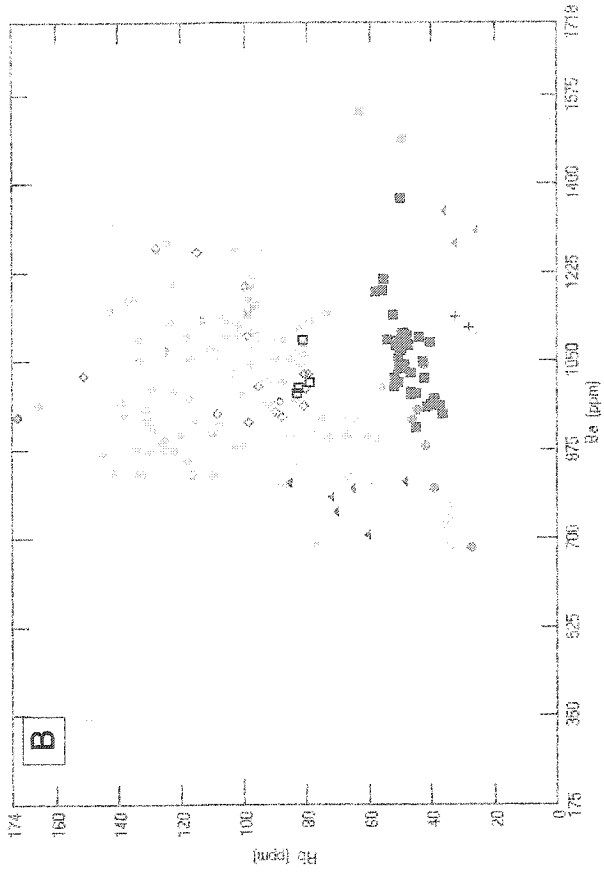
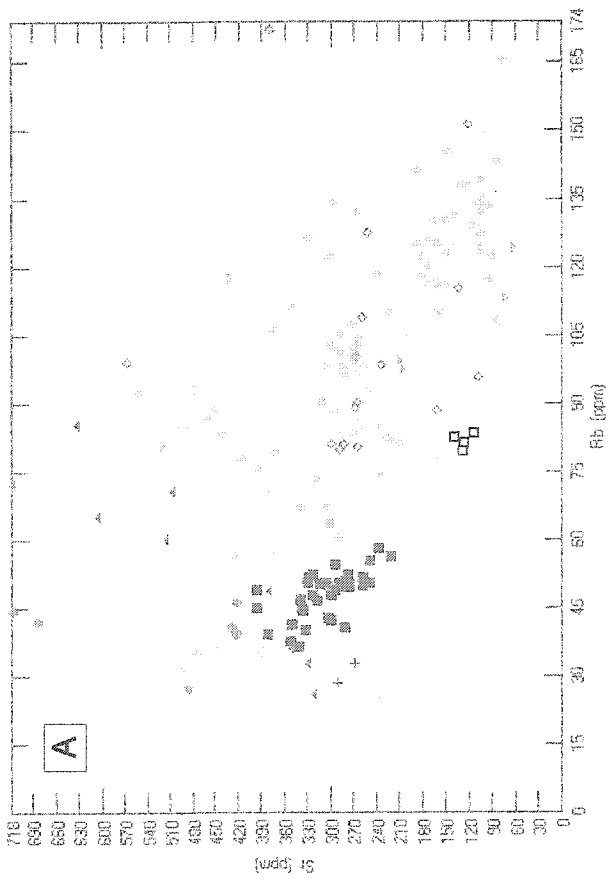


- Acatepango
- Almolonga
- Amatitlán
- Atitlán Caldera
- Barahona
- Cerro Quienado
- Mtepeque
- Pacaya
- Santa María
- Santiago
- Siete Orejas
- Tecana
- Zúñil
- Coatepeque
- Montebacho
- Platamar
- Hopongo

and overlap in K_2O and CaO concentrations (Fig. 20C, 20D). Santiaguito plots on the same linear array as Ilopango, at the low-silica end. When comparing FeO^* , Atitlán, Zuñil and Ixtepeque fall along the same linear array as Ilopango, but with lower FeO concentrations, whereas Mombacho and Santa María overlap, although Santa María extends to slightly higher FeO concentrations with lower SiO_2 . Santiaguito plots with higher FeO^* relative to Ilopango (Fig. 20B). When considering Al_2O_3 , the silicic centers fall along the same linear array except for Atitlán, which has slightly higher Al_2O_3 at similar SiO_2 . Ixtepeque is slightly depleted in Al_2O_3 relative to Ilopango, whereas Zuñil is comparable in Al_2O_3 concentration at similar SiO_2 . Santa María and Mombacho overlap in Al_2O_3 with Ilopango at similar SiO_2 concentrations, but Santa María is less evolved. Santiaguito is similar in Al_2O_3 concentrations to Ilopango at the low silica end of the Ilopango array (Fig. 20A).

Trace element Harker variation diagrams are shown in Figure 3.21. When comparing Rb vs. Sr, Ilopango is depleted in Rb and enriched in Sr relative to Ixtepeque, Zuñil, Atitlán, and Amatitlán, whereas it exhibits similar concentrations to Mombacho and is slightly more evolved than Santa María, Santiaguito and Acatenango (Fig. 3.21A). When comparing Ba vs. Rb, the silicic centers clearly plot with similar Ba concentrations, but Ilopango, Santa María, Santiaguito and Acatenango are lower in Rb, suggesting they are less evolved than centers such as Atitlán, Zuñil and Ixtepeque (Fig. 3.21B). Mombacho plots with similar Rb but has slightly higher Ba. When comparing Ba vs. Sr, Sr is considered to be a compatible

Figure 3.21 Trace element Harker variation diagrams representing major silicic centers in Central America. A) Rb vs. Sr. B) Ba vs. Rb. C) Ba vs. Sr. D) Rb vs. Rb/Sr. All values are normalized to 100 wt.% anhydrous. Note data for comparison obtained from Carr and Rose, (1987). Legend same as Figure 20.



element, and the less evolved compositions should have higher Sr concentrations as is observed in Ilopango, Santiaguito, Acantenango and Santa María. Mombacho also has similar Sr concentrations but slightly higher Ba (Fig. 3.21C). Considering the trace element variation diagrams as a whole, Ilopango, Santiaguito, Acantenango and Santa María are less evolved than the silicic centers of Atitlán, Amatitlán, Ixtepeque and Zúñil.

To understand the evolution of Ilopango relative to the other silicic centers, crystal fractionation was considered. A variation diagram of Rb vs. Rb/Sr was constructed to test fractionation of plagioclase (Fig. 3.21D). As Sr is partitioned into plagioclase and Rb is excluded, the melt becomes more enriched in Rb and the Rb/Sr ratio increases. Compared to Atitlán, Amatitlán and Zúñil, Ilopango is less enriched in Rb relative to Sr. This observation suggests that either the parental melt of the other silicic centers was more enriched in Rb than at Ilopango, or these silicic systems are generally more evolved than Ilopango.

In summary, Ilopango is less evolved compared to other high-silica rhyolite silicic centers in Central America. This suggests three possibilities: 1) The source of the Ilopango magmas is less evolved. 2) The Ilopango reservoir experiences proportionately greater replenishment of a more mafic magma, both changing the composition of the melt and potentially triggering eruptions before the magma has had sufficient time to evolve to the extent of the other centers. 3) Atitlán, Amatitlán, and Zúñil experience a greater crustal contribution, resulting in higher K_2O and Rb concentrations.

The Ba concentrations of the Central American silicic centers may be a subduction indicator (Patino et al, 2000). The similar concentrations of Ba for the different centers suggest that magmas erupting at the silicic centers have a parent composition with a similar Ba concentration. Ba is often concentrated in marine sediments (Cox *et al.*, 1979), suggesting that the source of high Ba in the erupted magmas may be a subducting slab and according to Ba at least, the “subduction input” for the different centers is about the same.

Conclusions

The lavas and pyroclastic rocks at Ilopango follow a calc-alkaline trend and range in composition from basaltic andesite (~ 54 wt.% SiO₂) to rhyolitic (~ 75 wt.% SiO₂). Above 65 wt.% SiO₂, the mineral assemblage of the intracaldera lavas is plagioclase > orthopyroxene ≥ opaque minerals ± hornblende. The pyroclastic rocks, such as TBJ, TB4 and the Pumice breccia, are all above 65 wt.% SiO₂ and have a mineral assemblage of plagioclase > hornblende ≥ orthopyroxene ≥ opaque minerals, except for TB2 which lacks orthopyroxene. Major element and trace element data, combined with the known stratigraphy, indicate the evolution of magmas at Ilopango in not a progressive process such as closed-system crystallization, but rather a combination of crystal fractionation and replenishment by a more mafic magma composition. Magma replenishment and mingling/mixing processes are suggested due to the presence of mafic enclaves and banding of a more mafic composition, as well as plagioclase phenocryst features such as LAC textures, sieve textures and embayed edges. A model is proposed whereby the magmatic evolution of Ilopango is

the result of a shallow level reservoir which experiences repeated replenishment of a more mafic magma, undergoes fractional crystallization and periodically erupts. Comparison of major and trace element data to other Central American silicic centers suggests that Ilopango is less evolved than Atilán, Amatitlán, Iztepeque and Zúñil, but is comparable in composition to Santa María, Santiaguito, and Acantenango. The less evolved nature of Ilopango may be the result of mafic magma replenishment and differences in crustal composition or thickness, or both.

Acknowledgements

We extend our gratitude to the Fundación de Amigos del Lago de Ilopango, especially Ernesto Freund, Jeannette Monterrosa and Fred Thill, for their help with logistics while in El Salvador. Many thanks to Carlos Pullinger of the Servicio Geológico division of the Servicio Nacional de Estudios Territoriales, for taking the time to familiarize us with the outer caldera deposits. We are forever indebted to our new friends at San Agustín, especially Natividad Rauda and his family, for their patience while in the field and acceptance of C.P.M and M.R. into their village and homes. We thank Chris Harpel of the Cascades Volcano Observatory for his help tracking down elusive references. We are most grateful to Mike Carr and Bill Rose for use of whole-rock data from their Central American database. We thank Andy Calvert from the United States Geological Survey for the Ar/Ar age determinations. This project was funded by a bursary awarded through the Canadian Bureau of International Education by the Canadian International Development Agency to C.P.M., by a research grant from the Natural Sciences and Engineering Research

Council of Canada to J.S., and by National Science Foundation Grant EAR-9903291 to J.V.

References

- Carr, M.J., Feigenson, M.S., and Bennett, E.A., 1990, Incompatible element and isotopic evidence for tectonic control of source mixing and melt extraction along the Central American arc: Contributions to Mineralogy and Petrology, v. 105, p. 369-380.
- Carr, M.J., Rose, W.I., and Stoiber, R.E., 1982, Central America, *in* Thorpe, R.S., ed., Andesites: John Wiley and Sons, New York, p. 149-166.
- Carr, M.J., and Rose, W.I., 1987, CENTAM-a database of analyses of Central American volcanic rocks: Journal of Volcanology and Geothermal Research, v. 33, p. 231-252.
- Carr, M.J., and Stoiber, R.E., 1977, Geologic setting of some destructive earthquakes in Central America: Geological Society of America Bulletin, v. 88, p. 151-156.
- Carr, M.J., and Stoiber, R.E., 1990, Volcanism, *in* Dengo, G., and Case, J.E., eds., The Caribbean region: Boulder, Colorado, The Geology of North America, v. H, p. 375-391
- CEL, 1992, Desarrollo de los recursos geotérmicos del area centro-occidental de El Salvador. Prefactibilidad geotérmica del area de Coatepeque: Comisión Ejecutiva Hidroelectrica del Rio Lempa Reconocimiento Geotérmico, Internal Report, p. 1-104.

- Cox, K.G., Bell, J.D., and Pankhurst, R.J., 1979, The interpretation of igneous rocks: Becaes and London, London, 450 p.
- Dalrymple, G.B., 1989, The GLM continuous laser system for $^{40}\text{Ar}/^{39}\text{Ar}$ dating: description and performance characteristics: U.S. Geological Survey Bulletin, Open-file report B 1890, p. 89-96.
- Damasceno, D., Scoates, J.S., Weis, D., Frey, F.A., and Giret, A., (2002), Mineral Chemistry of midly alkalic basalts from the 25 Ma Mont Crozier section, Kerguelen Archipelago: Constraints on phenocryst crystallization environments: *Journal of Petrology*, v. 43, n. 7, p. 1389-1413.
- Demets, C., 1990, Current plate motions: *Geophysical Journal International*, v. 101, n. 2, p. 425-478.
- Dengo, G., Bohnenberger, O., and Bonis, S., 1970, Tectonics and volcanics along the Pacific marginal zone of Central America: *in Lateinameika*, *Geologische Rundschau*, v.59, n. 3, p. 1215-1232.
- Dull, R., Southon, J., and Sheets, P., 2001, Volcanism, ecology and culture: a reassessment of the Volcán Ilopango TBJ eruption in the southern Maya realm: *Latin American Antiquity*, v. 12, p. 25-44.
- Eichelberger, J. C., 1975, Origin of andesite and dacite: evidence of mixing at Glass Mountain in California and at other circum-Pacific volcanoes: *Geological Society of America Bulletin*: v. 86, p. 1381-1391.
- Gerlach, D. C. and Grove, T. L., 1982, Petrology of Medicine Lake Highland volcanics: characterization of endmembers of magma mixing, *Contributions to Mineralogy and Petrology*, v. 80, p. 147-159.

- Gill, J., 1981, *Orogenic Andesites and Plate Tectonics*: Springer-Verlag, Berlin-Heidelberg, Germany, 390 p.
- Goodyear, W.A., 1880, Earthquake and volcanic phenomena. December 1879 and January 1880 in the Republic of Salvador, Central America, *Star and Herald*, p. 56.
- Govindaraju, K., 1994, 1994 compilation of working values and sample description for 383 geostandards: *Geostandards Newsletter*, v. 18, p. 1-158.
- Halsor, S.P., 1989, Large glass inclusions in plagioclase phenocrysts and their bearing on the origin of mixed andesitic lavas at Tolimán Volcano, Guatemala: *Bulletin of Volcanology*, v. 51, p. 271-280.
- Halsor, S.P., and Rose, W.I., 1991, Mineralogical relations and magma mixing in calc-alkaline andesites from Lake Atitlán, Guatemala: *Mineralogy and Petrology*, v. 45, p. 47-67.
- Hart, W.J.E, 1981, The Panchimalco tephra, El Salvador, Central America [unpublished M.Sc. thesis]: New Brunswick, Rutgers University, New Jersey.
- Hart, W.J., and Steen-McIntyre, V, 1983, Tierra Blanca Joven tephra from the AD 260 eruption of Ilopango Caldera: *in* Sheets, P.D. ed., *Archeology and volcanism in Central America; the Zapotitan Valley of El Salvador*, University of Texas Press, Austin, p. 14-34.
- Instituto Geográfico Nacional "Ingeniero Pablo Arnoldo Guzmán", 1981, *América Central República de El Salvador Lago de Ilopango*: map SAL-LL1, scale 1:20,000, 1 sheet.

- Instituto Geográfico Nacional "Ingeniero Pablo Arnoldo Guzmán", 1984, República de El Salvador: maps 2356 I, 2357 II, 2457 III, 2456 IV scale 1:50,000, 4 sheets.
- Irvine, T.N., and Baragar, W.R.A., 1971, A guide to the chemical classification of the common volcanic rocks : Canadian Journal of Earth Sciences, v. 8, n. 5, p. 523-548.
- Kuno, H., 1950, Petrology of the Hakone Volcano and the adjacent areas: Geological Society of America Bulletin, v. 61, p. 957-1020.
- Lanphere, M.A., and Dalrymple, G.B., 2000, First principles calibration of ^{38}Ar tracers; implications for the ages of $^{40}\text{Ar}/^{39}\text{Ar}$ fluence monitors: U.S. Geological Survey Professional Paper, Open file Report P1621, 10 p.
- Le Bas, M.J., Le Maitre, R.W., Streckeisen, A.L. and Zanettin, B., 1986, A chemical classification of volcanic rocks based on the total alkali-silica diagram : Journal of Petrology, v. 27, p. 247-250.
- Le Maitre, R.W., 1989, A classification of igneous rocks and a glossary of terms: Blackwell, Oxford, 193 p.
- Mann, C., Stix, J., Vallance, J., and Richer, M., *in press*, Subaqueous intracaldera volcanism, Ilopango Caldera, El Salvador, Central America, *in* Rose, W.I., Bommer, J.J., López, D.L, Carr, M.J., and Major, J.J., eds., Natural Hazards in El Salvador: Geological Society of America Special Paper.
- Mielke, P., and Winkler, H.G.F., 1979, An improved mesonorm calculation for granitic rocks: Neues Jahrbuch für Mineralogie, Monatshefte, p. 471-480.

- Molnar, P., and Sykes, L.R., 1969, Tectonics of the Caribbean and Middle America regions from focal mechanisms and seismicity: Geological Society of America Bulletin, v. 80, p. 1639-1684.
- Mooser, F., Meyer-Abich, H., and McBirney, A.R., 1958, Catalogue of active volcanoes of the world including Solfatara fields, Part VI, Central America: International Volcanological Association, Napoli, Italy.
- Murphy, M.D., Sparks, R.S.J., Barclay, J., Carroll, M. R., and Brewer, T.S., 2000, Remobilization of an andesite magma by intrusion of mafic magma at the Soufriere Hills Volcano, Montserrat, West Indies: Journal of Petrology, v. 41, n. 1, p. 21-42.
- Newhall, C.G., 1987, Geology of the Atitlan region, western Guatemala: Journal of Volcanology and Geothermal Research, v. 33, p. 23-55.
- Patino, L.C., Carr, M.J., and Feigenson, M.D., 2000, Local and regional variations in Central American arc lavas controlled by variations in subducted sediment input: Contributions to Mineralogy and Petrology, v. 138, p. 265-283.
- Peterson, P.S., and Rose, W.I., 1985, Explosive eruptions of the Ayarza calderas, southeastern Guatemala: Journal of Volcanology and Geothermal Research, v. 25, no. 3-4, p. 289-307
- Richer, M., Mann, C., and Stix, J., *in press*, Mafic magma injection triggering eruption at Ilopango caldera, El Salvador, Central America, *in* Rose, W.I., Bommer, J.J., López, D.L, Carr, M.J., and Major, J.J., eds., Natural Hazards in El Salvador: Geological Society of America Special Paper.

- Rollinson, H.R., 1993, Using geochemical data: evaluation, presentation, interpretation: Prentice Hall, England, 352 p.
- Rose, W.I., Conway, F.M., Pullinger, C.R., Deino, A., and McIntosh, W.C., 1999, An improved age framework for late Quaternary silicic eruptions in northern Central America: *Bulletin of Volcanology*, v. 61, p. 106-120.
- Sapper, K., 1925, Los volcanes de la America Central: Estudios sobre America y Espana, Extraserie, 116 p.
- Seaman, S.J., 2000, Crystal clusters, feldspar glomerocrysts and magma envelopes in the Atascosa Lookout lava flow, southern Arizona, USA: recorders of magmatic events: *Journal of Petrology*, v. 41, n. 5, p. 693-617.
- Sheets, P.D., 1979, Environmental and cultural effects of the Ilopango eruption in Central America, *in* Sheets, P.D., and Grayson, D.K., eds., *Volcanic activity and Human Ecology*, Academic Press, p. 525-564.
- Shelley, D., 1993, Igneous and metamorphic rocks under the microscope: classification, textures, microstructures and mineral preferred orientations: Chapman and Hall, London, England, 445 p.
- Steen-McIntyre, V., 1976, Petrography and particle size analysis of selected tephra samples from western El Salvador: A preliminary report: *in* Sheets, P., ed., *Ilopango volcano and Maya Protoclassic: University Museum Studies #9*, Southern Illinois University, p 68-79.
- Stix, J., Gauthier, G., and Ludden, J.N., 1995, A critical look at quantitative laser-ablation ICP-MS analysis of natural and synthetic glasses: *The Canadian Mineralogist*, v. 33, p. 435-55.

- Stoiber, R.E., and Carr, M.J., 1973, Quaternary volcanic and tectonic segmentation of Central America, *Bulletin of Volcanology*, v. 37, p 304-325.
- Stuvier, M., and Polach, H.A., 1977, Discussion; reporting of C-14 data: *Radiocarbon*, v.19, n. 3, p. 355-363.
- Stoiber, R.E. and Carr, M.J., 1973, Quaternary volcanic and tectonic segmentation of Central America: *Bulletin of Volcanology*, v. 37, p. 304-325.
- Tepley III, F.J., Davidson, Tilling, R. I., and Arth, J. G., 2000, Magma Mixing, Recharge and Eruption Histories Recorded in Plagioclase Phenocrysts from El Chichón Volcano, Mexico: *Journal of Petrology*, v. 41, n. 9, p. 1397-1411.
- Weber, H.S., and Wiesemann, G., 1978, Mapa geológico general de El Salvador: Instituto Geográfico Nacional de El Salvador, map San Salvador, scale 1:100,000, 1 sheet.
- Weyl, R., 1955, Beiträge zur Geologie El Salvadors: *Neues Jahrbuch Geologie und Paläontologie*, v 101, p. 12-38.
- Williams, H., and Meyer-Abich, H., 1955, Volcanism in the southern part of El Salvador with particular reference to the collapse basins of Lakes Coatepeque and Ilopango: *University of California Publications in the Geological Sciences*, v. 32, p. 1-64.
- Wunderman, R.L., and Rose, W.I., 1984, Amatitlán, an actively resurging cauldron 10 Km south of Guatemala city: *Journal of Geophysical Research*, v. 89, no. B10, p. 8525-8539.

Appendix 3.1

Hopango Dome $^{40}\text{Ar}/^{39}\text{Ar}$ Summary

Sample	Separate	Plateau Age (Ka)	Steps used (% ^{39}Ar)	Isochron Age (Ka)	MSWD	Total Gas Age (Ka)
163-01	Dacite Groundmass	359.3 ± 7.9	675-775°C (46%)	363.4 ± 8.3	15.4	375.4 ± 10.3
170-01	Dacite Groundmass	56.0 ± 1.9	750-1100°C (69%)	58.6 ± 5.4	1.1	54.3 ± 1.6

Appendix 3.2

Sample (JV) Date	SG1 19/05/2002	SG2A 19/05/2002
UTM	N13.70416 W89.05920	
Unit	Northeast Dome	TB4
wt.%		
SiO ₂	69.57	71.95
Al ₂ O ₃	15.03	14.26
TiO ₂	0.327	0.240
FeO	2.62	1.79
MnO	0.106	0.100
CaO	3.07	1.96
MgO	0.87	0.49
K ₂ O	2.25	2.56
Na ₂ O	4.46	4.26
P ₂ O ₅	0.108	0.064
Total	98.41	97.68
ppm		
Ni	4	5
Cr	0	0
Sc	7	6
V	22	6
Ba	1063	1184
Rb	47	54
Sr	319	243
Zr	146	167
Y	15	17
Nb	4.9	3.8
Ga	14	15
Cu	7	4
Zn	46	45
Pb	6	4
La	13	13
Ce	26	30
Th	4	3

Major elements are normalized on a volatile-free basis, with total Fe expressed as FeO.

"R" denotes a duplicate bead made from the same rock powder.

"†" denotes values >120% of our highest standard.

Appendix 3.3

(¹ Carr and Rose, 1987; ² J. Vallance, unpublished, Appendix 3.2)

Mesonorm calculation of mineral phases

W/O Hornblende

Sample #	Qz	Or	Ab	An	C	Hy	Mt	Il	Ap	Hbl	Total
CM216-01	28.34	14.35	39.90	11.09	0.22	4.73	0.56	0.57	0.24	0.00	100
¹ Carr IL-3	31.11	14.07	36.69	11.53	1.13	4.00	0.48	0.56	0.43	0.00	100
CM223-01	29.50	14.82	39.90	11.29	0.25	2.88	0.54	0.57	0.27	0.00	100
CM181-01	28.90	13.83	38.73	12.04	0.52	4.57	0.56	0.58	0.27	0.00	100
CM163-01	12.60	6.92	27.02	31.16	0.00	16.54	1.72	1.27	0.02	2.76	100
CM194-01	13.32	7.60	28.94	29.13	0.00	14.19	1.67	1.22	0.29	5.65	100

W/ Hornblende

CM168-01	26.31	12.90	37.88	15.41	0.00	5.87	0.89	0.64	0.26	0.04	100
CM169-01	27.02	12.62	37.73	14.94	0.16	5.77	0.68	0.63	0.26	0.00	100
CM224-01	27.37	13.68	37.02	14.60	0.26	5.52	0.84	0.62	0.29	0.00	100
CM170-01	27.47	13.53	37.01	14.42	0.25	5.76	0.68	0.62	0.27	0.00	100
¹ Carr IL-1	30.36	13.86	35.72	13.48	0.77	4.43	0.49	0.46	0.41	0.00	100
² JV SG1	26.34	13.50	38.33	14.40	0.00	5.36	0.64	0.64	0.26	0.53	100
CM151-01	31.17	15.41	39.72	8.73	0.27	3.62	0.44	0.53	0.12	0.00	100
CM184-01	26.80	14.00	39.83	11.38	0.43	4.19	0.50	0.54	0.33	0.00	100
CM196-01	23.39	12.39	36.34	15.94	0.00	6.34	0.88	0.80	0.33	3.58	100
¹ Carr IL-5	22.13	11.87	36.56	16.73	0.00	6.68	0.92	0.77	0.64	3.69	100
¹ Carr IL-6	22.72	11.70	37.72	16.87	0.00	5.21	0.74	0.50	0.41	4.14	100
CM195-01	28.12	13.31	37.86	13.60	0.45	5.04	0.58	0.58	0.26	0.00	100

Pyroclastic units

Sample #	Qz	Or	Ab	An	C	Hy	Mt	Il	Ap	Hbl	Total
CM261-01	25.51	11.96	35.40	17.90	0.17	7.18	0.78	0.75	0.34	0.00	100
CM252-01	25.89	12.14	35.11	17.47	0.42	7.12	0.76	0.77	0.32	0.00	100
¹ TBJ	25.02	12.83	34.73	17.71	0.49	7.31	0.82	0.75	0.34	0.00	100
¹ TBJ	28.36	13.19	37.42	13.58	0.06	5.78	0.86	0.86	0.29	0.00	100
¹ TBJ	24.85	11.32	38.17	16.67	0.00	4.87	0.69	0.65	0.32	2.47	100
¹ TBJ	26.98	13.27	37.49	14.32	0.03	6.21	0.69	0.69	0.32	0.00	100
¹ TBJ	25.56	12.38	38.51	15.74	0.00	5.92	0.71	0.67	0.27	0.24	100
¹ TBJ	27.21	12.79	37.58	14.13	0.00	6.29	0.72	0.68	0.32	0.28	100
¹ TBJ	28.86	13.31	36.03	13.76	0.00	4.58	0.54	0.58	0.22	0.10	100
¹ TBJ	29.14	13.45	35.29	13.33	0.49	6.47	0.78	0.71	0.34	0.00	100
¹ TBJ	25.02	11.80	36.49	16.28	0.00	4.99	0.86	0.61	0.29	1.87	100
¹ TBJ	27.23	12.91	36.28	13.32	0.00	7.81	0.86	0.84	0.34	0.41	100
¹ TBJ	29.98	14.19	35.86	12.73	0.37	5.29	0.64	0.69	0.28	0.00	100
¹ TBJ	37.43	15.26	28.09	9.99	3.21	4.73	0.60	0.59	0.10	0.00	100
¹ TBJ	29.97	14.10	34.54	12.99	0.41	6.25	0.70	0.76	0.30	0.00	100
¹ TBJ	32.32	14.08	31.07	13.02	2.09	5.82	0.71	0.67	0.25	0.00	100
¹ TBJ	22.65	10.85	36.29	19.99	0.24	7.97	0.92	0.79	0.30	0.00	100
¹ TBJ	35.20	15.05	33.05	10.33	1.01	4.11	0.51	0.52	0.23	0.00	100
¹ TBJ	32.80	13.59	30.63	12.51	1.55	7.37	0.89	0.61	0.25	0.00	100
¹ TBJ	34.12	14.72	32.06	11.26	1.57	4.83	0.59	0.57	0.28	0.00	100
¹ TBJ	31.01	13.60	32.42	13.60	1.59	6.12	0.72	0.63	0.30	0.00	100
¹ TBJ	32.56	13.88	30.61	13.26	2.08	6.01	0.70	0.64	0.26	0.00	100
TB4-p	34.55	13.94	31.87	9.46	4.85	4.25	0.55	0.55	0.18	0.00	100
TB4q	32.76	16.03	36.82	8.79	0.93	3.53	0.43	0.54	0.17	0.00	100
TB4	35.26	14.42	31.52	9.09	4.76	3.79	0.49	0.51	0.15	0.00	100
¹ JV SG2	32.29	15.48	36.90	9.55	1.09	3.64	0.44	0.47	0.14	0.00	100

Rayleigh Fractionation Spreadsheet

Kd values (Gill, 1981)

 D_{bulk}

(Rollinson, 1993)

Kd	OLIV	PLAG	CPX	OPX	HB	MT		RUN 1	RUN 2
RB	0.01	0.07	0.02	0.02	0.05	0.01	RB	0.05	0.05
SR	0.01	1.80	0.02	0.03	0.23	0.01	SR	0.96	1.24
BA	0.01	0.16	0.08	0.02	0.09	0.01	BA	0.11	0.12
ZR	0.01	0.01	0.25	0.10	0.40	0.40	ZR	0.17	0.07
HF	0.01	0.01	0.25	0.10	0.40	0.40	HF	0.17	0.07
NB	0.01	0.03	0.30	0.35	1.30	1.00	NB	0.51	0.17
TH	0.01	0.01	0.01	0.05	0.15	0.10	TH	0.06	0.02
NI	58.00	0.01	6.00	8.00	10.00	10.00	NI	4.76	7.21
CO	0.00	0.01	3.00	6.00	13.00	8.00	CO	5.01	1.66
CR	34.00	0.01	30.00	13.00	30.00	32.00	CR	13.13	8.53
V	0.08	0.01	1.10	1.10	32.00	30.00	V	11.89	3.05

134

Mineral percentages

Mineral percentages are based on modal percentages.

	RUN 1	RUN 2
OLIV	0.00	9.09
PLAG	50.00	68.18
CPX	0.00	4.55
OPX	12.50	9.09
HB	25.00	4.55
MT	12.50	4.76

Rayleigh Fractionation Spreadsheet

CL = Trace element concentration in liquid

Co = Trace element concentration in parent

F= Fraction of melt remaining

CM168-01 = northeast rhyolite dome

CM163-01 = basaltic andesite Cerro Cuyultepe

XRF data

Sample	CL	Co
	CM168-01	CM163-01
RB	51.00	23.40
SR	323.30	356.20
BA	984.00	731.33
ZR	155.80	113.10
HF	0.00	0.00
NB	3.20	0.60
TH	1.10	2.40
NI	8.90	0.00
CO	0.00	22.00
CR	27.00	0.00
V	44.00	110.00

F	0.10	0.35	0.39	0.44	0.49	0.50	0.55	0.56	0.57	0.60	0.63	0.65
---	------	------	------	------	------	------	------	------	------	------	------	------

RUN 1 CL

RB	184.52	56.42	50.93	45.44	41.04	40.26	36.79	36.17	35.57	33.88	32.36	31.41
SR	238.69	323.51	332.12	341.99	351.04	352.76	361.02	362.60	364.16	368.73	373.12	375.96
BA	3573.60	1186.70	1078.91	970.25	882.57	867.02	797.27	784.73	772.60	738.50	707.47	688.28
ZR	696.71	216.07	195.28	174.46	157.77	154.82	141.62	139.26	136.97	130.56	124.74	121.15
HF	0.00	0.00	0.00	0.00	0.00	0.00	0.00	0.00	0.00	0.00	0.00	0.00
NB	0.00	0.00	0.00	0.00	0.00	0.00	0.00	0.00	0.00	0.00	0.00	0.00
TH	132.38	38.99	35.08	31.19	28.08	27.53	25.09	24.65	24.23	23.05	21.97	21.31
NI	0.00	0.02	0.04	0.09	0.17	0.19	0.34	0.38	0.43	0.59	0.79	0.96
CO	6.55	14.99	16.10	17.44	18.72	18.97	20.21	20.45	20.69	21.40	22.10	22.57
CR	0.00	0.00	0.00	0.00	0.00	0.00	0.00	0.00	0.00	0.00	0.00	0.00
V	1.86	24.22	30.24	38.71	48.26	50.29	61.14	63.43	65.78	73.06	80.74	86.08

Rayleigh Fractionation Spreadsheet

CL = Trace element concentration in liquid
 Co = Trace element concentration in parent
 F = Fraction of melt remaining

CM196-01 = Islas Quemadas host dacite
 CM196-01i = Islas Quemadas mafic enclave

RUN 2

Sample	CL	Co
	CM196-01	CM196-01i
RB	46.10	20.90
SR	314.60	417.40
BA	980.74	471.12
ZR	150.00	81.00
HF	0.00	0.00
NB	2.70	0.00
TH	0.00	14.00
NI	0.00	14.00
CO	0.00	30.00
CR	0.00	0.00
V	62.00	208.00

F	0.10	0.49	0.50	0.55	0.56	0.57	0.60	0.63	0.65	0.70	0.72	0.75
---	------	------	------	------	------	------	------	------	------	------	------	------

RUN 2 CL

RB	207.95	46.04	45.17	41.26	40.56	39.89	37.99	36.27	35.21	32.82	31.96	30.74
SR	388.32	365.86	365.58	364.28	364.03	363.79	363.09	362.43	362.00	361.00	360.62	360.06
BA	5726.16	1383.57	1358.81	1247.86	1227.92	1208.65	1154.49	1105.23	1074.79	1005.91	980.89	945.75
ZR	769.06	204.82	201.40	186.04	183.27	180.59	173.04	166.15	161.89	152.20	148.67	143.71
HF	0.00	0.00	0.00	0.00	0.00	0.00	0.00	0.00	0.00	0.00	0.00	0.00
NB	1.87	0.85	0.84	0.81	0.80	0.79	0.77	0.75	0.74	0.72	0.71	0.69
TH	20.84	4.69	4.60	4.21	4.14	4.07	3.88	3.70	3.60	3.35	3.27	3.14
NI	0.00	0.00	0.00	0.00	0.00	0.00	0.00	0.00	0.00	0.00	0.00	0.00
CO	0.00	1.26	1.37	2.01	2.16	2.32	2.84	3.46	3.92	5.27	5.90	6.95
CR	0.00	0.00	0.00	0.00	0.00	0.00	0.00	0.00	0.00	0.00	0.00	0.00
V	0.00	0.05	0.06	0.16	0.20	0.24	0.42	0.72	1.01	2.26	3.07	4.79

Chapter 4

Conclusions

This study has attempted to provide a working stratigraphy of the intracaldera lavas and pyroclastic units at the Ilopango Caldera, as well as to determine the evolution of the Ilopango magmatic system over time. The results of whole-rock geochemistry and age determinations suggest that Ilopango is a long-lived silicic system with periodic fluctuations in magma composition over time.

1) The Ilopango intracaldera stratigraphy begins with a pyroclastic density current sequence, overlain by a lacustrine unit, in turn overlain by the San Agustín Block unit. This portion of the intracaldera stratigraphy is mostly subaqueously emplaced, and two ^{14}C ages acquired from the upper portion of the lacustrine unit suggest that a lake occupied the Ilopango caldera > 53,000 y. B.P.

2) The San Agustín Block unit, which is comprised of a basal fine ash layer and an overlying pumice breccia, is the result of an explosive to effusive subaqueous eruption. The eruption began with a gas-rich silicic magma making contact with external water, most likely lake water, resulting in a phreatomagmatic eruption. The next phase was more degassed, in which pumice clasts were quenched and spalled from the shedding carapace of a subaqueously growing dome. The San Agustín Block unit provides a distinct intracaldera marker horizon with which to base further studies.

3) The intracaldera lavas are basaltic andesite to rhyolite in composition.

The lavas above 65 wt.% SiO₂ are orthopyroxene hornblende bearing or hornblende bearing dacites to rhyolites. The pyroclastic units, TBJ, TB4 and the Pumice Breccia facies, are orthopyroxene hornblende bearing dacites to rhyolites, whereas TB2 is a hornblende dacite.

4) Geochemistry and Ar-Ar age determinations indicate that Ilopango is a long-lived silicic system undergoing crystal fractionation and replenishment of a more mafic composition.

5) Comparison of Ilopango to other Central American silicic centers indicates that Ilopango is less evolved than Amatitlán, Atitlán and Zuñil, but is similar in composition to Santiaguito, Acantenango and Santa María.

Ilopango Caldera is a long-lived silicic system that is a potential threat to people both globally and locally. The combination of periodic mafic recharge, combined with the presence of a lake, is a recipe for disaster. The mafic recharge is the motor by which the magmatic system is sustained, since the mafic magma provides heat and mass. This explains, in part, the very high frequency of catastrophic explosive eruptions at Ilopango. The presence of the caldera lake unquestionably enhances, the explosivity of the eruptions. Understanding the magmatic evolution of Ilopango through time, as well as the effusive and explosive nature of Ilopango eruptions, will aid scientists in predicting future eruptions and possibly minimizing future catastrophes.